Tampere University

RITAYAN BISWAS

Performance Evaluation of Ambient Backscattering Communication (AmBC) in Outdoor Environments

Tampere University Dissertations 916

Tampere University Dissertations 916

RITAYAN BISWAS

Performance Evaluation of Ambient Backscattering Communication (AmBC) in Outdoor Environments

ACADEMIC DISSERTATION
To be presented, with the permission of
the Faculty of Information Technology and Communication Sciences
of Tampere University,
for public discussion in the auditorium S2
of the Sähkötalo building, Korkeakoulunkatu 3, Tampere,
on 1 December 2023, at 12 o'clock.

ACADEMIC DISSERTATION
Tampere University, Faculty of Information Technology and Communication Sciences
Finland

Responsible supervisor and Custos
Professor
Jukka Lempiäinen
Tampere University
Finland

Pre-examiners
Professor
Mario Garcia-Lozano
Universitat Politecnica de Catalunya (UPC)
Spain

Professor
Michele Segata
University of Trento
Italy

Opponents
Professor
Ari Pouttu
University of Oulu
Finland

Professor
Michele Segata
University of Trento
Italy

The originality of this thesis has been checked using the Turnitin OriginalityCheck service.

Cover design: Roihu Inc.

ISBN 978-952-03-3183-2 (print)
ISBN 978-952-03-3184-9 (pdf)
ISSN 2489-9860 (print)
ISSN 2490-0028 (pdf)
http://urn.fi/URN:ISBN:978-952-03-3184-9

Carbon dioxide emissions from printing Tampere University dissertations have been compensated.

PunaMusta Oy – Yliopistopaino
Joensuu 2023

Dedicated to my parents, Jaydip and Rina.

PREFACE

This is a compound thesis based on the research work carried out during 2018-2022 at the erstwhile Department of Electronics and Communications Engineering, Tampere University of Technology, Tampere, Finland, and the Faculty of Information Technology and Communication Sciences, Tampere University, Finland.

Firstly, I would like to thank and express gratitude to my supervisor, Prof. Jukka Lempiäinen for giving me the opportunity to pursue a doctoral degree. It was a pleasure to work under his supervision. I have cultivated a lot of knowledge both on a personal and professional front over the years working under his watchful guidance.

I would also like to express my gratitude to the Academy of Finland for helping fund the initial stages of my doctoral studies when I was hired as a researcher for the WiFiUS project. I would also like to express my utmost gratitude to the University for providing me with funding for 4 years (2019-2022). The uninterrupted funding really helped me focus on the research work. I would like to thank Prof. Jukka Lempiäinen for the support when applying for University funding. I would also like to thank Prof. Jari Nurmi and the doctoral training network in electronics, telecommunications, and automation (DELTA) for the financial support in the registration and travel for different conferences. I would like to thank the secretaries Sari Kinnari, Taina Meriläinen, Alisa Myllynpää, and Terhi Salminen for their help regarding various administrative aspects. I would also like to express my utmost gratitude to Jari Salo for his help in the procurement of various devices. Finally, I would also like to thank the head of our department, Prof. Mikko Valkama for creating a wonderful working environment at the university.

I would like to thank my co-authors Joonas Säe and Mohammad Usman Sheikh for the valuable support they provided me right from the M.Sc. thesis days. They helped me immensely to adjust to the life of a doctoral student. I would especially like to thank Joonas for a lot of support during the initial days of my research. I would also like to thank Usman for his never-ending support during probably the toughest

phase of my research career. I would also like to thank my co-author Hüseyin Yiğitler for the deep understanding he gave me regarding challenging research topics. Also, a huge amount of gratitude is reserved for Prof. Riku Jäntti. I definitely feel that his support was one of the major reasons why I was able to complete my doctoral studies.

I would also like to thank Prof. Michele Segata and Prof. Mario Garcia Lozano for agreeing to examine my thesis. They provided me valuable feedback which enabled me to improve my thesis.

I would like to thank my friends both in India and Finland for their unwavering support throughout life. I would also like to express my appreciation towards Roman Kovalchukov, Daria Alekseeva, and Anna Gaydamaka for being such nice and kind friends to me. A special mention also goes to my friends Gaurav Naithani, Sajjad Nouri, and Nikita Tafintsev for their help and friendship from the beginning of my time at the University. I would also like to thank my office roommates Hans Jakob Damsgaard, Antoine Grenier, and Kaan Çelikbilek for some insightful conversations and coffee breaks that we shared together. Finally, I would like to thank my dear friend Victoria Shubina for her support and encouragement during the various stages of my doctoral studies.

Everything I achieve in life is incomplete unless I express my gratitude to my two pillars, my father and mother. Ever since my childhood, they have been there with me through all the good and especially the difficult moments. I would also like to thank my dear brothers Ritabrato and Ritajit for helping me stay motivated.

Last but certainly not least, I would like to thank my healer, Mother Nature for taking care of me when the going got really tough.

Tampere, September 2023
Ritayan Biswas

ABSTRACT

The demand for wireless communications surged in the past decade due to the massive number of devices requiring a connection to the internet. Although traditional wired communications provide a much more reliable connection, utilizing wires in specific deployment scenarios is improbable. The Internet of Things wireless communication is a concept where interrelated and interlinked devices and objects are connected to each other and the internet to collect information and respond intelligently to the end users. These "things" are deployed at a variety of locations with the objective of providing support for various use cases. Furthermore, the Internet of Things is envisioned to integrate everyday objects into the connected ecosystem. This has led to a significant increase in the amount of energy that will be required to power up these devices.

Modern battery technology involves the movement of electrons between the positive and negative electrodes. Thus, lithium-ion batteries need to be replaced as they degrade over time. However, different deployment scenarios of the Internet of Things render the regular maintenance of these devices impossible. Therefore, newer technologies need to be identified in order to provide energy and power to such devices.

Ambient backscattering communication utilizes ambient radio frequency signals to establish connection links between the transmitter, receiver, and backscatter devices. Radio frequency signals can originate from a variety of sources such as television and radio broadcasts, Wi-Fi signals, and cellular signals to name a few. Additionally, in ambient backscattering communication, the backscatter devices are able to harvest energy from the ambient signals and utilize them as the source of power for the backscatter devices.

This thesis focuses on the coverage, capacity, and interference aspects of ambient backscattering communication pertaining to different outdoor deployment scenarios. The main contributions to this thesis can be divided into three main parts.

Firstly, an analysis to determine the maximum coverage of ambient backscattering communication systems (operating in the mono-static and bi-static modes) was performed utilizing ambient FM radio signals. It was observed that in the bi-static mode of operation, about 44 dB (from the path loss) remained for the propagation of the signal between the backscatter device (located 30 km from the TX) and the RX. Additionally, in the mono-static mode of operation, the backscatter device could be located 14.5 km away utilizing the free space path loss equation. The achievable distance reduces with the decrease in the cross-section of the backscatter device.

Secondly, cellular signals were utilized to evaluate the achievable range of communication of mono-static ambient backscattering communication systems. It was observed that utilizing ambient Long-Term Evolution (LTE) signals (operating at a carrier frequency of 700 MHz) a communication link between the TX/RX and the backscatter device located a few hundred meters apart could be established. Additionally, an analysis was carried out to determine the applicability of 5G signals for ambient backscattering communication systems in the outdoor macro cell and small cell environments. It was concluded that very short-range communication distances could be established between the TX/RX and the backscatter device at 5G frequencies, especially at the millimeter-wave carrier frequency of 26 GHz. The achievable range of communication was heavily dependent on the cross-section of the backscatter device and the additional loss. Furthermore, a study was carried out to determine the impact of the cell load and the adjacent cell interference on the coverage of mono-static ambient backscattering communication systems. It was observed that there was a 44 percent decrease in the coverage in a heavily loaded cellular network in comparison with an unloaded network.

Finally, bi-static AmBC systems were studied utilizing sub-1 GHz ambient signals. It was observed that only the carrier frequency of 200 MHz was suitable for bi-static ambient backscattering communication. Subsequently, the need for the suppression of the direct path signal from the legacy source was studied and some interference suppression techniques were proposed. In addition, the impact caused by the presence of a second backscatter device in the environment was studied. It was observed that the second backscatter device caused the most interference when it was located close to the original backscatter device or the RX. The impact of the second backscatter device could be alleviated by positioning it one wavelength meter away from the first backscatter device or the RX.

CONTENTS

LIST OF PUBLICATIONS

P1 R. Biswas, J. Säe and J. Lempiäinen, "Power Budget for Wide Area Ambient Backscattering Communications," 2018 IEEE Vehicular Networking Conference (VNC), Taipei, Taiwan, 2018, pp. 1-6, doi: 10.1109/VNC.2018.8628465.

P2 R. Biswas, J. Säe and J. Lempiäinen, "Evaluation of Maximum Range for Backscattering Communications Utilising Ambient FM radio signals," 2022 International Balkan Conference on Communications and Networking (BalkanCom), Sarajevo, Bosnia and Herzegovina, 2022, pp. 142-146, doi: 10.1109/BalkanCom55633.2022.9900759.

P3 R. Biswas, J. Säe and J. Lempiäinen, "Maximum Receiver Harvesting Area of Backscatter Signals from Ambient Low-Frequency Mobile Networks," 2021 IEEE Global Communications Conference (GLOBECOM), Madrid, Spain, 2021, pp. 1-5, doi: 10.1109/GLOBECOM46510.2021.9685741.

P4 R. Biswas and J. Lempiäinen, "Assessment of 5G as an ambient signal for outdoor backscattering communications," Wireless Networks 27, 4083–4094 (2021), doi: 10.1007/s11276-021-02731-x.

P5 R. Biswas and J. Lempiäinen, "Sensitivity Analysis of Ambient Backscattering Communications in Heavily Loaded Cellular Networks," 2023 18th Wireless On-Demand Network Systems and Services Conference (WONS), Madonna di Campiglio, Italy, 2023, pp. 51-55, doi: 10.23919/WONS57325.2023.10062021.

P6 R. Biswas, M. U. Sheikh, H. Yiğitler, J. Lempiäinen and R. Jäntti, "Direct Pa-

th Interference Suppression Requirements for Bistatic Backscatter Communication System," 2021 IEEE 93rd Vehicular Technology Conference (VTC2021-Spring), Helsinki, Finland, 2021, pp. 1-5, doi: 10.1109/VTC2021-Spring51267.2021.9448755.

P7 R. Biswas, M. U. Sheikh, H. Yiğitler, J. Lempiäinen and R. Jäntti, "Interference Analysis of Bi-static Backscatter Communication System: Two Backscatter Devices," 2021 IEEE International Conference on RFID Technology and Applications (RFID-TA), Delhi, India, 2021, pp. 85-88, doi: 10.1109/RFID-TA53372.2021.9617234.

ABBREVIATIONS

3GPP	3rd generation project partnership
5G	Fifth generation
ADC	Analog to digital converter
AGC	Automatic gain control
AmBC	Ambient backscattering communications
BD	Backscatter device
CDF	Cumulative distribution function
CI	Cross interference
CoMP	Coordinating multipoint
D2D	Device-to-device
eMBB	Enhanced mobile broadband
FSPL	Free space path loss
IoT	Internet of Things
ITU	International telecommunications union
LoRa	Long range (IoT)
LOS	Line-of-sight
LTE	Long term evolution
LTE-700	Long term evolution (700 MHz)
LTE-A	Long term evolution advanced
NB-IoT	Narrowband IoT
NF	Noise figure

NFC	Near field communications
NLOS	Non line-of-sight
OFDM	Orthogonal frequency division multiplexing
OMA	Orthogonal multiple access
RCS	Radar cross section
RE	Radar equation
RF	Radio frequency
RFID	Radio frequency identification
RIS	Relective intelligent surfaces
RT	Ray tracing
RX	Receiver antenna
SI	Self interference
SIC	Successive interference canceller
SINR	Signal-to-interference-and-noise ratio
SIR	Signal-to-interference ratio
SNR	Signal-to-noise ratio
TX	Transmit antenna
URLLC	Ultra reliable low latency communications
WLAN	Wireless local area network

SYMBOLS

A_{OH}	Frequency dependent parameter for Okumura-Hata model
B_{OH}	Frequency dependent parameter for Okumura-Hata model
B	System bandwidth
C	Propagation slope
C_m	Area correction factor
G_r	RX antenna gain
G_t	TX antenna gain
L	Path loss due to Okukura-Hata
L_{LOS}	Line-of-sight loss
L_{NLOS}	Non line-of-sight loss
L_c	Cable loss
L_{d1}	Loss in the forward link
L_{d2}	Loss in the backscatter link
L_{suburban}	Additional loss in suburban environment
L_{urban}	Additional loss in urban environment
P	Location percentage
P_{LOS}	Probability of line-of-sight
P_i	Interference power
P_n	Thermal noise power
P_r	Received power
P_t	Transmission power
R	Range of radar
T	Temperature
λ	Wavelength
π	Pi
σ	Radar cross section
$a(h_{\mathrm{ms}})$	City size dependent function

d_1	Distance of forward link
d_{2D}	Distance of forward link between TX-BD from the base of the TX to the BD
d_2	Distance of backscatter link
d_{3D}	Distance of forward link between TX-BD from the top of the TX to the BD
d_{km}	Distance [km]
f	Frequency
f_{MHz}	Frequency [MHz]
h_{ms}	Height of mobile station
h_t	Height of TX
k	Boltzmann constant

1 INTRODUCTION

There is a huge demand for connectivity in modern society. This requirement is driven by the massive number of connected devices. The particular devices can range from personal handheld equipment and gadgets to sensors capable of measuring and monitoring different parameters. Due to various deployment scenarios, wireless communication technologies are required to support different types of devices.

1.1 Background and motivation

The Internet of Things (IoT) has accentuated the need for wireless communications because billions of connected devices share information utilizing the internet. These connected devices comprise autonomous vehicles capable of communicating with other objects and traffic signals in order to navigate freely in a modernized urban environment [27]. Additionally, the notion of smart cities was conceptualized based on the idea of a connected future where everything is connected over the internet to share and exchange information [35]. Furthermore, IoT is envisioned to be integrated with medicine and healthcare [39, 65], in addition to a variety of other use cases [40, 52]. Hence, this has led to a significant amount of energy required to power these billions of devices [4, 54]. Traditional lithium-ion batteries which are the most common in use degrade over time due to the continuous flow of electrolytes between the electrodes [47, 48]. Thus, the periodic replacement of the battery modules in the sensors or backscatter devices (BDs) is necessary till advanced battery technology is available. Therefore, the need to determine alternative technologies capable of powering these devices and enabling them to remain operational for the long term is of utmost importance.

Ambient backscattering communication (AmBC) is a technology that utilizes ambient radio frequency (RF) signals to provide connectivity between the TX/RX and BDs [64]. The ambient RF signals can originate from various sources such as

television and FM radio broadcasts, cellular and WLAN signals. Furthermore, prior research on AmBC technology indicates that the BDs have the capability to harvest energy from the ambient RF signals that impinge on them [34, 44, 67]. Therefore, AmBC eliminates the need for batteries and enables wireless communication with the BDs. The concept of AmBC was first introduced by the authors in [45] during the year 2013. The achievable communication range of AmBC was constrained by limited coverage based on previous research. The studies in articles [6, 38, 45] indicate achievable communication distances less than 10 m utilizing ambient TV broadcast and Wi-Fi signals, respectively.

1.2 Thesis objectives and scope

The objective of this thesis was to analyze the different aspects of backscattering communications such as coverage, capacity, and interference. These parameters were evaluated based on the different ambient RF signals at different outdoor deployment scenarios. Different operating modes of backscatter communications utilizing ambient signals were analyzed in the studies performed and are subsequently summarized in the thesis.

The coverage of AmBC systems was a restriction based on prior research [6, 38, 45]. Therefore, in order to maximize the achievable communication range low-frequency RF signals from FM radio broadcasts are utilized. FM radio signals are broadcast at a low frequency that enables a large range of communication. Furthermore, the analysis is carried out for AmBC systems operating in both mono-static and bi-static modes which have different use cases.

It was also noted that research utilizing ambient cellular signals for AmBC systems was few and far between. Hence, in the subsequent research, ambient cellular signals were leveraged in the simulations to determine the coverage and interference of mono-static AmBC systems. Long-term evolution (LTE) signals operating at the carrier frequency of 700 MHz were utilized to determine the maximum achievable range of communication in the urban macrocellular and suburban highway environments. Additionally, the applicability of 5G as an ambient signal for backscattering communication was studied. Finally, the adjacent cell interference and the effect of the network load on the coverage of AmBC systems were examined utilizing ambient LTE-700 and 5G signals.

Bi-static backscatter communication utilizing ambient RF signals is an interesting topic because useful information can be transferred to the end user from the BD. However, in prior research, the coverage and the impact of interference had not been studied in great detail. Therefore, the coverage of bi-static AmBC systems was studied at various sub-1 GHz frequencies in the urban microcellular environment. In addition, the interference caused due to the direct path signal was analyzed and certain methods to mitigate the effects were proposed. Subsequently, the capacity of bi-static AmBC systems was studied in the urban microcellular environment. Consequently, techniques to mitigate the impact of interference caused due to additional backscatter devices are also proposed.

1.3 Thesis contribution and structure

The main contributions to the thesis are listed as follows:

- The power budget for wide area AmBC is proposed to evaluate the coverage utilizing ambient FM radio signals [P1].
- The maximum range of mono-static AmBC systems utilizing ambient low-frequency FM radio signals is evaluated in [P2].
- The maximum communication range utilizing the lowest available cellular frequency (LTE-700) is evaluated for mono-static AmBC in [P3].
- The suitability of ambient 5G signals for mono-static backscattering communications is studied in the publication [P4].
- The effect of the adjacent cell interference on the coverage in a heavily loaded cellular network is studied in the publication [P5].
- Direct path interference suppression requirements from legacy networks in bi-static AmBC systems are studied in the publication [P6].
- The interference caused due to the presence of multiple backscatter devices in the environment is studied in [P7].

The publications [P1-P7] provide a more detailed explanation of the work carried out for this thesis. A summary of these publications is provided extensively in this thesis.

This thesis is structured into four main chapters. Chapter 2 provides insight into the concept of ambient backscattering communication and the previous research performed in this field. Ambient FM radio signals are utilized for the work done in publications [P1, P2]. Mono-static and bi-static modes of operation of AmBC were studied and summarized in Chapter 3. Ambient signals from mobile networks are utilized in the simulations performed in [P3-P5] for the mono-static mode of operation of AmBC. Chapter 4 provides a summary of the findings of the studies carried out in publications [P3-P5]. The bi-static mode of operation for AmBC utilizing sub-1 GHz ambient signals is studied in publications [P6, P7]. The findings of publications [P6, P7] are summarised in Chapter 5. The conclusions of the thesis are summarized in Chapter 6.

1.4 Author's contribution to the publications

The idea and concept of this thesis were formulated based on an Academy of Finland-funded project for wireless innovation between Finland and the United States (WiFiUS). The research was initiated in collaboration between the University of Houston, Aalto University, and the erstwhile Tampere University of Technology. The research topic was "Ambient re-scatter inspired machine type communication for heterogeneous IoT systems (CNS-1702850)" [70]. After the completion of the project, the author in collaboration with Prof. Jukka Lempiäinen continued performing research on this topic.

The author is the first author and main contributor in all the publications [P1-P7]. Prof. Jukka Lempiäinen initiated the discussion regarding publications [P1-P5] with the author. He also provided ideas and support during the research and writing phase for the publications [P1-P5]. D. Sc. Joonas Säe was the co-author and contributor to the publications [P1-P3] and provided some valuable ideas during the research phase and helped in proofreading the articles closer to the publication. The simulation of the research work and writing of the publication [P1] was performed by the author. The author presented the findings of the work at the Vehicular Networking Conference (VNC) in Taipei, Taiwan in December 2018.

The simulation and the writing of the publication [P2] were done by the author. The article was presented by D. Sc. Joonas Säe at the Balkan Conference on Communications and Networking (BalkanCom) in Sarajevo, Bosnia and Herzegovina in

August 2022. The work leading to the publication of [P3] and the final manuscript was prepared by the author. The findings of the work were presented by the author at the Global Communications (GLOBECOM) conference in Madrid, Spain in December 2021.

The author and Prof. Jukka Lempiäinen co-authored the articles [P4, P5]. The author performed the simulations and wrote the manuscript for publication [P4] and this was published in the Springer Wireless Networks Journal of Mobile Communication, Computation, and Information in August 2021. Prof. Lempiäinen provided invaluable feedback during the writing process of the journal. The simulation of the research work and the writing of the manuscript for publication [P5] were performed by the author. Publication [P5] was presented by the author at the Wireless On-demand Network Systems and Services (WONS) conference in Madonna di Campiglio, Italy in January 2023.

Prof. Riku Jäntti from Aalto University initiated and formulated the idea for the research performed in the publications [P6, P7] in discussion with the author and Prof. Lempiäinen. The author performed the simulations and writing for the publication [P6]. D. Sc. Mohammad Usman Sheikh helped the author validate the simulations and helped proofread the article closer to publication. D. Sc. Hüseyin Yiğitler provided valuable feedback during the simulation and writing of the publication [P6]. The findings of the work were presented remotely by the author at the virtual Vehicular Technology Conference (VTC2021-Spring) in April 2021.

The author performed the simulation work for the article [P7]. D. Sc. Mohammad Usman Sheikh and D. Sc. Hüseyin Yiğitler helped the author validate the simulation results by providing invaluable feedback. The manuscript writing for publication [P7] was done by the author and the proofreading was done by D. Sc. Hüseyin Yiğitler. Prof. Jäntti and D. Sc. Hüseyin Yiğitler helped in writing the "Multi-bounce phenomenon" section of the article. The publication [P7] was presented remotely by the author at the virtual RFID Technology and Applications (RFID-TA) in October 2021.

1.5 Methodology

The research work for this thesis was mainly performed with the help of simulations. MATLAB was the interface through which the simulations were primarily

performed. A variety of methods were utilized to perform the simulations.

Different radio propagation models and equations were utilized to perform the simulations in a variety of outdoor environments. The propagation models varied as a function of the type of simulation environment. The ray tracing technique (which was simplified to the free space path loss, FSPL model) for the line of sight (LOS) paths was utilized in the simulations performed in [P1-P5]. The Okumura-Hata path loss prediction model was utilized in [P1]. In publications [P2-P5], the radar equation was utilized to perform the simulations. The 3GPP — urban microcellular model and the ITU — device-to-device model were utilized to perform the simulations in publications [P6, P7].

2 AMBIENT BACKSCATTERING COMMUNICATIONS: AN OVERVIEW

Ambient backscattering communication (AmBC) is a wireless communication paradigm where sensors or backscatter devices (BDs) utilize ambient radio frequency (RF) signals to establish communication between the TX, BD, and RX [45]. The AmBC technology operates on the principle of the radio backscatter where a radio signal is reflected from an object toward the receiver [64]. The radio backscatter technology was first introduced in literature by Harry Stockman in 1948 [61]. The technology was utilized during the Second World War to determine the affiliation of air-crafts and classify them as friendly or hostile. In radio backscatter technology, the signal impinges on a BD which directs the signal toward the receiver. The signal is decoded at the RX and subsequently, the analysis and conclusions are derived.

Backscatter communications can be classified into three categories based on the type of transmitted signal and the location of the TX and RX with respect to the BD [14]. Mono-static backscatter communications are established by reflecting the signal towards the RX which is co-located with the TX. In traditional mono-static backscatter systems, there is a need for the transmission of a dedicated signal [14]. Radio-frequency identification (RFID) and near-field communication (NFC) are two primary examples of mono-static backscatter communication systems. However, these systems are limited by the achievable range of communication as the signal has to be reflected from a BD/sensor located in proximity to the TX/RX [22, 69].

Bi-static backscatter communications also utilize a dedicated signal in order to establish communication between the TX/RX and the BD. However, in bi-static backscatter systems, there is a separation between the TX and RX. Therefore, the BD can be placed at a location between the TX and the RX. In existing bi-static backscatter systems, the signal is transmitted by the carrier emitter which can be situated at a central location [46]. The BDs or sensors are located around the carrier emitter. After the signal from the carrier emitter impinges on the sensor it is

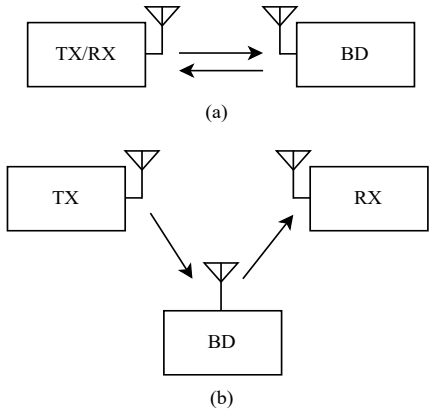

Figure 2.1 Different operating modes for ambient backscatter communications. Fig. 2.1a shows the mono-static mode of operation for AmBC systems. The bi-static mode of operation of AmBC systems is illustrated in Fig. 2.1b.

forwarded toward the RX for decoding.

The third category of backscatter systems eliminates the requirement for the generation and transmission of a dedicated signal. AmBC systems utilize ambient RF signals to establish communication between the TX and the RX [45]. Therefore, AmBC can be classified as a green technology [73]. The range of communication is dependent on the type of ambient signal utilized by the system. The AmBC systems can operate both in the mono-static and bi-static modes [15, 64, 67]. Therefore, AmBC systems provide flexibility in comparison with conventional backscatter communication systems. In mono-static AmBC systems, the TX/RX are positioned at the same location as illustrated in Fig. 2.1a. However, the TX and the RX are separate modules. The TX is the ambient source of the RF signal. The RX is a device capable of receiving the backscattered signal. Therefore, the ambient signal propagates from the TX, impinges on the BD, and then travels back toward the RX [18, 30]. Ambient mono-static backscatter communication systems are primarily utilized for the purpose of monitoring a variety of system parameters such as temperature and humidity [46].

The bi-static mode of operation of AmBC systems involves the propagation of the ambient signal from the TX to the RX after impinging on the BD [18, 67, 68]. Thus, the positioning of the TX/RX in relation to the BD allows the transmission of useful information to the end user (RX) from the BD. The illustration of ambient bi-static backscatter communication systems is shown in Fig. 2.1b.

The ambient signals may originate from a variety of sources that are generally available in the surrounding environment. The WLAN, cellular, television, and FM broadcast signals are some of the major sources of ambient signals [45, 51]. The BDs utilized in AmBC are capable of harvesting energy from the ambient signals to establish communication links between the TX and the RX [66, 73]. Thus, the utilization of ambient RF signals enables the wireless and battery-free operation of the sensors. Therefore, the sensors can be deployed in a variety of locations where regular maintenance is difficult or unfeasible [16].

The BDs utilized for AmBC are envisioned to monitor a variety of parameters such as temperature, humidity, traffic, and environmental features [16, 64]. Therefore, some BDs may be deployed in remote areas of the planet such as rural highways (to measure the level of snow), agricultural fields (to measure the level of water), or mountainous regions (to measure seismic changes). Furthermore, the BDs may be installed inside the walls of buildings to monitor a variety of parameters in indoor environments. However, it is difficult and expensive to access the BDs (for maintenance) in some of these remote areas [16]. Thus, BDs operating on the principle of AmBC technology can be installed and utilized for the long term as the need for regular maintenance is avoidable [71].

The research on AmBC has accelerated in the past two decades with the miniaturization of integrated circuits [72]. This has helped enable AmBC to become an interesting research field. The authors in [49] were able to achieve communication between two passive tags. This enabled the growth of interest in this field of research. The concept of AmBC was first studied and introduced by the authors in [45]. They utilized ambient television broadcast signals to establish communication links between the two BDs. They were able to achieve communication distances of 0.76 m and 0.46 m in outdoor and indoor environments, respectively [45]. Utilizing the ambient signals as the only source of power for the BDs, a communication rate of 1 kbps was achieved at the aforementioned distances. With the utilization of ambient WLAN signals, the throughput improved to a certain extent [38]. The authors in [6] were able to achieve a communication distance of 5 m with a throughput of 1 Mbps. However, the range of communication of AmBC was significantly limited in both outdoor and indoor environments.

3 AMBC UTILIZING LOW-FREQUENCY FM RADIO SIGNALS

In this chapter, studies were performed to determine the maximum range of backscattering communication utilizing ambient FM radio broadcast signals. The mono-static and bi-static modes of operation of AmBC were studied using ambient FM signals. The low operational frequencies between 88 and 108 MHz enable the FM radio signals to propagate further than most RF signals in a given environment [32]. Furthermore, FM radio technology is readily available worldwide. Thus, the existing network infrastructure can be utilized for the efficient deployment of AmBC systems. The simulations for the studies in this chapter were performed to investigate both mono-static and bi-static modes of operation for AmBC systems.

3.1 Propagation models and equations

The simulations were performed based on the assumption that the TX/RX are operating in the mono-static and bi-static modes. In the mono-static mode of operation, the TX and RX are co-located. Therefore, the ambient signal propagates from the TX to the BD, impinges on it, and is reflected back toward the RX (Fig. 2.1 a). In the bi-static mode, the ambient signal propagates to the BD and is transmitted forward toward the RX after impinging on the BD (Fig. 2.1 b). Simulations were performed utilizing different propagation models, the ray tracing approach, the Okumura-Hata model, and the radar equation. The results of these propagation models were later analyzed to determine the feasibility of utilizing FM signals for AmBC systems.

3.1.1 Ray-tracing

The ray-tracing technique utilizes the multi-path components of the ambient signal between the TX and the BD to evaluate the propagation in a particular environment.

The multi-path components of the ambient signal are a result of reflections from various different surfaces present in the environment. The reflections from buildings, automobiles, and other surfaces contribute to the multi-path signals between the TX and the BD. In traditional wireless communication systems, the multi-path components are aggregated at the RX. Every multi-path component can cause constructive or destructive interference based on the time and phase of the arriving signal [59].

The ray-tracing technique is characterized by individual communication links (or, individual multi-path components) which can be defined with the help of the free space path loss (FSPL) equation. The losses occurring due to the reflection of surfaces are also factored in the final computation of the path loss. The FSPL (in dB) is calculated for LOS links and can be defined by Eq. 3.1,

$$FSPL = 32.45 + 20 \cdot \log_{10}(d_{\mathrm{km}}) + 20 \cdot \log_{10}(f_{\mathrm{MHz}}), \tag{3.1}$$

where the frequency (f) is in megahertz (MHz) and the distance (d) is in kilometers (km).

3.1.2 Okumura-Hata

The Okamura-Hata model provides path loss information about signal propagation in different outdoor environments [42]. This model was developed based on the measurements in the city of Tokyo in Japan. In comparison with the FSPL, the Okumura-Hata model takes into account multiple parameters which can provide a much more accurate description of the simulation environment. The height of the base station (h_{t}, in meters) and the mobile station (h_{ms}, in meters) are factored in the simulations in addition to parameters such as frequency (f, in MHz) and distance (d, in kilometers). The environment-specific parameters such as A_{OH} and B_{OH} are based on the type of propagation environment. The parameter computed using $C - 6.55 \cdot \log_{10}(h_{\mathrm{t}}))$ represents the slope of the propagation model. This term represents the path loss exponent multiplied by 10. The area correction factor is represented by the term C_{m}. The mathematical formula of the Okumura-Hata propagation model is expressed by Eq. 3.2,

$$L = A_{OH} + B_{OH} \cdot \log_{10}(f) - 13.82 \cdot \log_{10}(h_{\mathrm{t}}) - a(h_{\mathrm{ms}}) + C_{\mathrm{m}} + (C - 6.55 \cdot \log_{10}(h_{\mathrm{t}})) \cdot \log_{10}(d), \tag{3.2}$$

where $a(h_{\mathrm{ms}})$ is selected to indicate a small or medium-sized city and is calculated using Eq. 3.3,

$$a(h_{\mathrm{ms}}) = (1.1 \cdot \log_{10}(f) - 0.7) \cdot h_{\mathrm{ms}} - (1.56 \cdot \log_{10}(f) - 0.8). \tag{3.3}$$

3.1.3 Radar equation

The radar equation basically involves the signal being reflected from the BD (target or, radar cross-section, RCS in radar terminology) toward the RX. Thus, the radar equation computes the entire communication range/link budget between the TX, BD, and RX [26]. The cross-section of the BD has a major role in the total achievable range of communication. Radar systems can generally operate in the mono-static and bi-static modes [5]. In the mono-static mode, the transmitter, and the receiver are positioned at the same location. In the bi-static mode, the TX and RX are located in separate positions. For mono-static radar systems, R in (3.4) represents the total round-trip distance between the TX/RX and the BD in kilometers. However, for bi-static systems, R is divided into two terms $R1$ and $R2$. The distance between the TX and BD is represented by $R1$ and $R2$ represents the distance between the BD and the RX. In this work, the mono-static mode of operation for radar systems is utilized and the simulations are performed accordingly.

The achievable range of communication (R) for mono-static radar systems is calculated utilizing Eq. 3.4,

$$R = \sqrt[4]{\frac{P_t G_t G_r \lambda^2 \sigma}{(4\pi)^3 P_r L}}, \tag{3.4}$$

where the terms Pt, Gt, and Gr represent the transmit power, transmitter antenna gain, and receiver antenna gain, respectively. The additional losses in the system are represented by the term L. The wavelength of the ambient signal is represented by the term λ. The term σ represents the size of the BD or the radar cross-section (RCS). In the radar equation handbook [5], σ represents a half-dipole antenna, and

Figure 3.1 Propagation environment from Google Maps. Highway 51 is a straight road as can be observed from the map. Also, there are arable lands located in the proximity of this highway.

the size of the BD is calculated utilizing Eq. 3.5,

$$\sigma = 0.88 \times \lambda^2. \tag{3.5}$$

The received power of radar systems is represented by the term Pr. In order to determine the maximum achievable range of communication, Pr is assumed to denote the receiver sensitivity of the system. The calculation of the receiver sensitivity of a system is discussed in Section 3.2.

3.2 Receiver sensitivity

The receiver sensitivity ($RX_{\text{sensitivity}}$) represents the minimum signal strength that can be received and decoded by the RX. The calculation to determine the $RX_{\text{sensitivity}}$ is performed utilizing Boltzmann's constant (k) which has a value of 1.38×10^{-23} J/K and temperature (T) of 290 K. Additionally, system-specific parameters such as the bandwidth (B), noise figure (NF), and signal-to-noise ratio (SNR) are also utilized to determine the $RX_{\text{sensitivity}}$ of the system. The $RX_{\text{sensitivity}}$ is calculated utilizing Eq. 3.4,

$$RX_{\text{sensitivity}}(\text{dBm}) = 10 \cdot \log_{10}\left(\frac{kTB}{0.001}\right) + NF + SNR. \tag{3.6}$$

The term receiver sensitivity has been used interchangeably with the terms noise floor or minimum reception level of the system in this thesis.

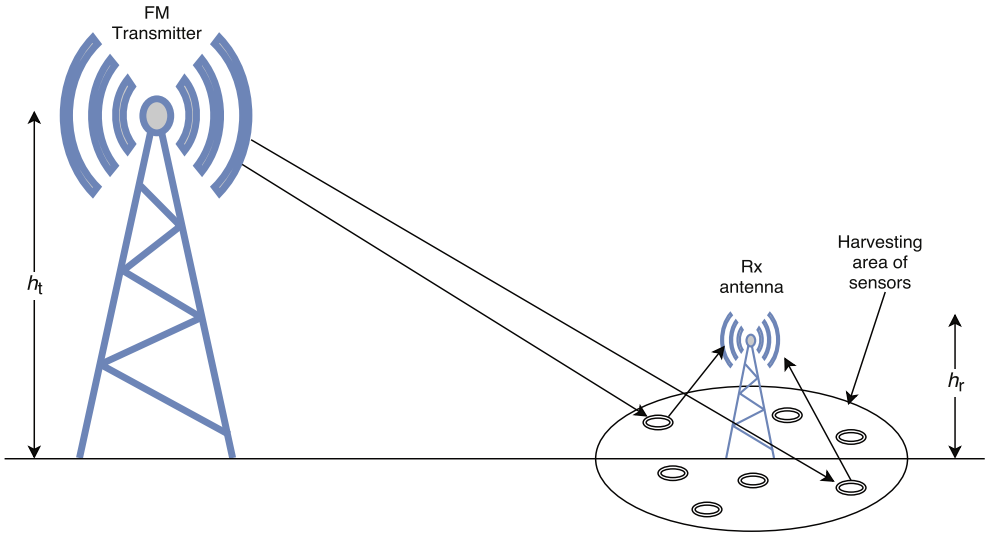

Figure 3.2 Illustration of propagation environment for bi-static AmBC utilizing ambient FM radio signals. The sensors are located around the RX antenna in its proximity.

3.3 Simulation environment

A rural open highway environment was selected for the simulations to determine the maximum achievable range of communication utilizing ambient FM radio signals. This environment was selected because it is clear of clutter, obstacles, and interference-causing signals. Furthermore, the ambient signals are able to travel to the BDs located in the direct line-of-sight (LOS) path of the TX antenna in such an environment. Fig. 3.1 shows a Google Maps view of the area considered for the simulations.

The simulation area has a flat landscape free from any significant undulations. Highway 51 is a straight road from Helsinki in the direction of Hanko in southern Finland. There are wide arable agricultural fields located beside the highway. This can also be observed from the Google Maps view as shown in Fig. 3.1. The FM radio tower is located at a height of 248 meters in the suburb of Kivenlahti [23]. Therefore, the BDs located on or around the highway have nearly clear LOS paths with the FM radio tower. Thus, the ambient signal from the FM radio is able to propagate between the TX and the RX after impinging on the BD.

Fig. 3.2 shows the illustration of the propagation environment for bi-static communication using ambient FM radio signals. The main purpose of bi-static AmBC

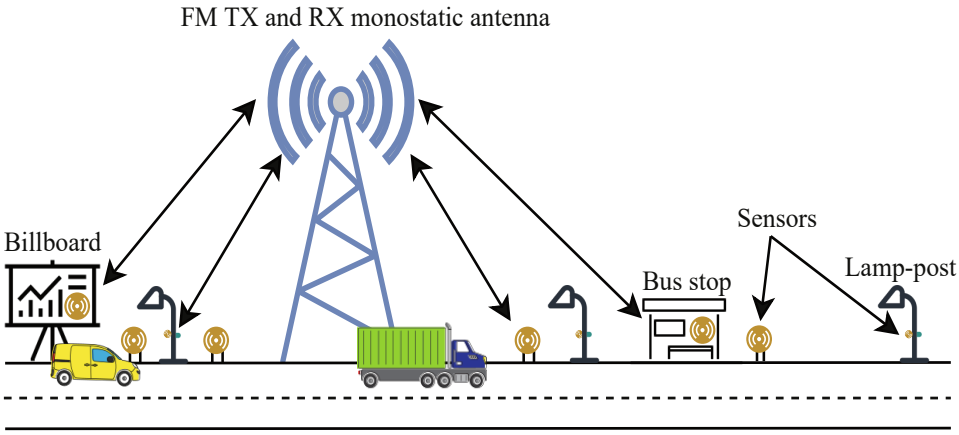

Figure 3.3 The illustration of the propagation environment for mono-static AmBC utilizing ambient FM radio signals. The sensors can be located at the street level, on billboards, or on lamp posts to monitor different parameters.

is to deliver some information to the end user having an RX module. The BDs have a clear LOS path with the ambient FM radio tower. The BDs are located around the RX and this is demarcated as the harvesting area of sensors in Fig. 3.2. Based on the use case, the BDs can be located between the TX and the RX or sometimes even beyond the RX. The height of the FM TX antenna (h_t) is 248 m. The BDs are located at the street level or at heights of around 1 m from the ground. The parameter (h_r) represents the height of the RX module. For the power budget calculations of wide-area bi-static AmBC systems, the BDs are placed at a distance of 30 km from the FM TX antenna.

The propagation environment for mono-static AmBC using ambient FM radio signals is shown in Fig. 3.3. The use-case of mono-static AmBC is to monitor certain parameters. Therefore, the BDs can be located at a variety of locations such as on the street level, on lamp posts, on bus stops, or on billboards. These different sensor locations are illustrated in Fig. 3.3. There can also be some other use cases other than the ones that are mentioned here. The ambient signals propagate from the FM TX antenna towards the BD, and after impinging, travel back towards the RX which is co-located with the TX. In the simulations, the height of the FM TX antenna is 248 m [23]. Therefore, the BDs have a clear LOS with the FM TX antenna. The RX is also assumed to be co-located with the TX antenna as a separate module.

Table 3.1 Simulation parameters.

Parameters	Unit	Value
Frequency	MHz	100
FM TX power (P_t)	kW	60
TX antenna height	m	248
Temperature (T)	K	290
Bandwidth (B)	kHz	1
Noise figure (NF)	dB	10
Signal-to-noise ratio (SNR)	dB	10
Additional loss (L)	dB	10

3.4 Simulation parameters

The FM TX antenna located in the suburb of Kivenlahti, Helsinki has a transmission power (P_t) of 60 kW or 77.78 dBm [23]. The carrier frequency (f) utilized for the simulations is 100 MHz. The value of the $RX_{\text{sensitivity}}$ of the system is calculated utilizing Eq. 3.6. The values of k and T are already discussed in Section 3.2. The value of B for the FM technology is considered to be 1 kHz for the calculation of the $RX_{\text{sensitivity}}$. The NF of 10 dB and an SNR of 10 dB are utilized in the simulations. Furthermore, there is also an additional loss (L) of 10 dB considered in the simulations due to the blockage of the Fresnel zone and other losses such as diffraction from different objects. The value of the additional loss (L) is also utilized in Eq. 3.4. The simulation parameters are summarized in Table 3.1.

There may be certain minor but negligible errors due to the utilization of the Okumura-Hata propagation model. This is because according to the specification of the model, the operating carrier frequency range varies between 150 MHz and 1500 MHz. However, the simulations are performed at the frequency of 100 MHz. Furthermore, the maximum height of the transmission antenna is specified to be 200 m. However, the FM TX antenna in the simulations is situated at a height of 248 m.

3.5 Power Budget for Wide Area Ambient Backscattering Communications

Previous research on AmBC had very limited communication ranges. Even though low-frequency television broadcast signals were utilized by the authors in [45], the achievable range of communication was very limited. Therefore, the purpose of this work was to determine the suitability of wide-area AmBC. In order to achieve wide-area communications, the FM technology was selected due to its low frequency of operation.

The power budget of a system provides a preliminary estimation of the transmitted power utilization by the different network elements [24]. The general idea of the power budget calculation is to determine the signal strength at the RX. The factors affecting the propagation of a signal in a particular environment are the gains and losses experienced by the particular signal. The gains in a particular system are a result of TX and RX antenna gains. The losses in the system can be due to feeder and cable loss. Additionally, the propagation loss between the TX and RX while the signal is traveling between them is the major contributing factor to the loss experienced in a system. The propagation loss increases proportionally with the increase in distance between the TX and RX. Overall, the strength of the received signal is computed based on the transmission power, gains, and losses utilizing Eq. 3.7,

$$P_{\mathrm{r}} = P_{\mathrm{t}} - losses + gains. \tag{3.7}$$

The calculation of the power budget is an important process in the design of a network. The propagation loss is dependent on the geography and topology of a particular environment. The simulation was performed in an open rural area shown in Fig. 3.1 as the propagation loss is the lowest in comparison with the urban and suburban environments.

The idea of this research was to determine the power budget utilizing the transmission power, the minimum reception level of the system, and the system gains and losses. In addition, the path loss due to the propagation is also factored into the power budget calculations. Based on the calculations, the available signal power remaining for the signal to propagate to the RX was determined. Additionally, the dynamic range of the system was factored into the analysis to determine the available

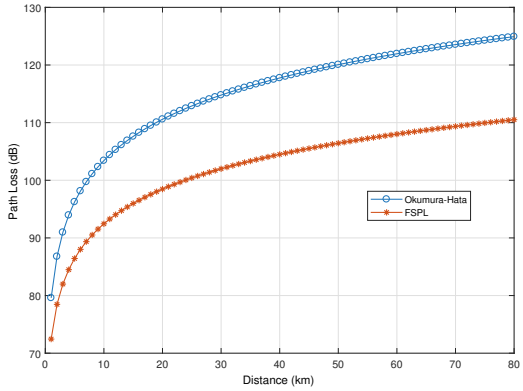

Figure 3.4 Path loss graph for the FSPL and Okumura-Hata propagation models.

path loss after the ambient signal impinges on the BD.

The propagation loss was computed between the TX antenna and the BD located at a distance of 30 km utilizing the FSPL and Okumura-Hata propagation models. For the Okumura-Hata model, the values of A_{OH} and B_{OH} were selected as 69.55 and 26.16, respectively. The propagation slope (C) was tuned so that the path loss exponent was less than 2.5 indicative of a rural area. Additionally, the area correction factor (Cm) was selected as −10 dB which is typical for an open area. The values of C and Cm were selected to be realistic of the propagation environment.

The free space path loss was calculated using Eq. 3.1 at a distance of 30 km as 102 dB. The propagation loss was also computed utilizing Eq. 3.2. The path loss at the same distance utilizing the Okumura-Hata model is 114.8 dB. The Okumura-Hata model provides a more realistic and accurate estimation of the propagation of the ambient signal between the TX and the BD in comparison with the FSPL model. The graphs for the path loss using FSPL and Okumura-Hata are shown in Fig. 3.4.

There are diffraction or scattering losses after the ambient FM signal impinges on the BD. Therefore, there is an attenuation in the signal strength. This results in the backscattered signal having a lower signal strength to propagate to the RX. These losses contribute to the losses experienced by the system and are considered to be approximately 30 dB.

The $RX_{\text{sensitivity}}$ of the system is calculated utilizing Eq. 3.6 and the value obtained for this parameter is −123.97 dBm. This represents the minimum reception level of the signal. Therefore, the RX is able to decode the signal as long as the received

Table 3.2 Power budget of bi-static AmBC systems utilizing ambient FM radio signals.

	Parameter	Unit	Value
Transmission	Transmit power	dBm	77.78
Propagation Losses	FSPL/Okumura-Hata	dB	102/115.3
Sensor Losses	Diffraction/Scattering	dB	30
R_X	Receiver sensitivity	dBm	−123.97
Available Path Loss	FSPL/Okumura-Hata	dB	69.77/56.45

signal strength is above this value.

The propagation of the backscattered signal between the BD and the RX is calculated based on these parameters. The power budget of the system is presented in Table 3.2. The calculations indicate an available path loss of approximately 55 dB to 70 dB for the backscattered signal to propagate from the BD to the RX. This value is dependent on the utilized propagation model.

The ambient signal follows two paths between the TX and the RX. This is represented in Fig. 3.5. The direct path between the TX and RX is defined by 'X'. The other path followed by the ambient signal is represented by the forward link ('Y') and the backscatter link ('Z'). The distances 'D' and 'd' represent the distance between the TX-BD and BD-RX, respectively. The aforementioned characters are utilized only for illustration purposes. The dynamic range of the system is the difference between the strongest and weakest signal impinging on the RX. The direct path signal has a much greater amplitude than the backscattered signal. Therefore, this is a key parameter to be considered in the development of the receiver module.

In this work, an assumption was made that the difference in the signal strength between the direct path signal and the backscattered signal was not more than 70 dB. This design ensures the RX is able to differentiate between the signals arriving via these two paths. For example, if the RX is located at a distance of 50 km from the TX, the received signal strength at this location is −28.65 dBm (using FSPL). Therefore, based on the aforementioned assumption, the backscattered signal can be detected by the RX if the signal strength is greater than −98.65 dBm.

In comparison with the minimum reception level of the system, the dynamic range of the system is much more of a limiting factor. It is observed that there is a 25 dB reduction in the available path loss when the dynamic range of the system is

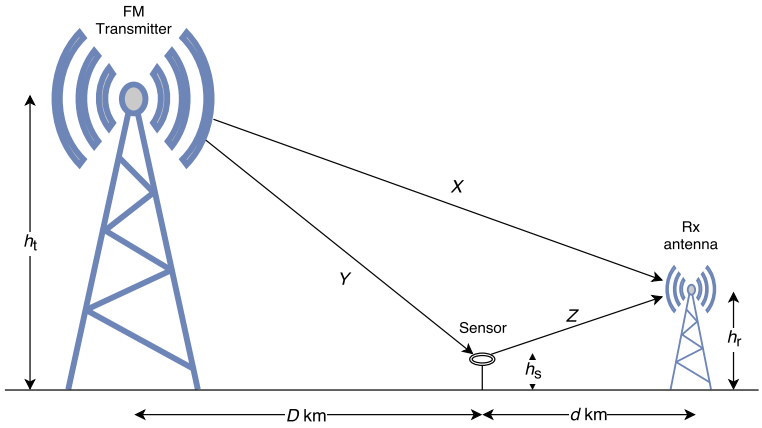

Figure 3.5 Illustration of the dynamic range for FM systems.

considered. Thus, the final available path loss utilizing the FSPL model is 44.43 dB. Therefore, communication links of '*d*' km may be established when FM radio is utilized as the ambient signal for bi-static ambient backscattering communications.

3.6 Evaluation of Maximum Range for Backscattering Communications Utilizing Ambient FM radio signals

The primary objective of mono-static backscatter communication is to monitor different parameters in the environment such as the weather, temperature, etc. The observed data is relayed back to the RX which is co-located with the TX. The signal propagates from the TX antenna toward the BD, and after impinging on the BD (where the information is added), the signal propagates back to the RX.

The mono-static mode of operation of backscattering communications is generally limited by the range of communication. The purpose of this work was to determine the maximum achievable range of communication for AmBC utilizing ambient low-frequency FM radio signals. The FM frequency band was selected as it is one of the lowest commercially accessible frequency bands which is available worldwide. The low operating frequency of FM radio technology enables wide communication ranges.

In the rural highway environment, as shown in Fig. 3.1 there is a lack of significant obstacles that help in achieving long propagation distances. Furthermore, the rural environment is also free from other signals causing significant interference with

Table 3.3 Different distances for AmBC with RT and RE propagation models.

Propagation model	RCS (σ, m^2)	Distance between TX/RX and BD (km)	Total distance (km)
Ray-tracing	-	14.5	29
Radar equation	0.001	1.43	2.87
	0.01	2.55	5.10
	0.16	5.10	10.21
	0.3	5.97	11.94
	0.7	7.38	14.76
	7.92	13.54	27.08

the system of interest. Finally, there are a lot of LOS paths available between the TX/RX and the BD. The illustration of the propagation environment is shown in Fig. 3.3. In the simulation scenario, the BDs are located in the direct LOS of the FM TX antenna. The BDs can be present on the street level, at bus stops, on lamp posts, or on billboards based on the use case. In addition, there can be other use cases different from the ones that are mentioned here.

The computation of the maximum achievable range of communication is performed using the FSPL and the radar equation and they are discussed in Section 3.1.1 and Section 3.1.3.

The transmission power of the FM TX antenna at Kivenlahti is 60 kW. The $RX_{\text{sensitivity}}$ of the system is calculated to be −123.97 dBm. This value is computed using Eq. 3.6 based on the noise figure and SNR of 10 dB each. Furthermore, an additional loss of 10 dB is considered due to the proximity of the BD with the ground which can result in a minor obstruction of the Fresnel zone. These values are summarized in Table 3.1. Subsequently, the total available path loss calculated based on the aforementioned parameters is 191.75 dB.

The total available path loss for round-trip communication between the TX/RX and the BD is 191.75 dB. Therefore, for one-way communication between the TX and BD, the available path loss is 95.87 dB. This translates to a maximum distance of 14.5 km between the TX and BD, as the corresponding path loss for that distance is 95.67 dB. Additionally, based on the principle of reciprocity, the signal experiences a similar amount of attenuation while propagating between the BD and the RX. Therefore, a total round-trip distance of 29 km is achievable between the TX/RX

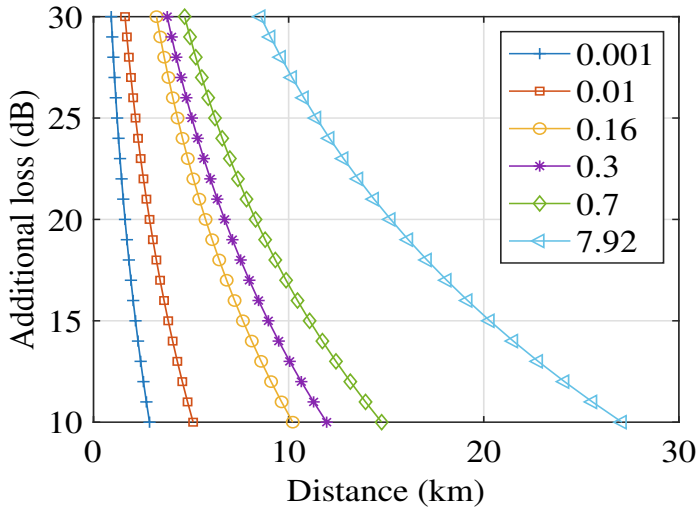

Figure 3.6 Achievable distances for different additional losses for varying RCS (σ).

and the BD. Thus, utilizing the FSPL model, it is observed that the distance between the TX/RX and the BD is 14.5 km.

The radar equation in Eq. 3.4 demonstrates the total range of communication for the mono-static mode of operation. The values of σ were varied to observe the effects of the size of the BD in the achievable range of communication. The values of the BD were selected to indicate the realistic scope of sensors utilized for IoT depending on the use case.

The worst-case scenario is when the BD is small and the ambient signal has a very small surface area to impinge on. Therefore, when a BD size of 3 cm×3 cm (or, 0.001 m^2) is utilized, a distance of 1.43 km can be established between the TX/RX and the BD. Furthermore, such a small BD may be hard to locate even at such a small distance from the TX/RX. The achievable range of communication increases to 2.5 km when the size of the BD is 10 cm×10 cm (0.01 m^2). As the size of the BD increases to 40 cm×40 cm (0.16 m^2), the achievable range of communication between the TX/RX and the BD increases to 5.1 km. A 5.97 km range in communication is achievable when the size of the BD is 54 cm×54 cm (0.3 m^2). The BD of the size of 83 cm×83 cm (0.7 m^2) enables a communication range of 7.38 km between the TX/RX and BD. Finally, when a BD representing a half-dipole antenna [5], calculated utilizing Eq. 3.5 is utilized, the achievable range of communication between the TX/RX and BD is 13.54 km. The size of the BD is 2.8 m×2.8 m (7.92 m^2). The

achievable range of communication utilizing different sizes of BDs is summarized in Table 3.3. Therefore, it can be inferred from Table 3.3 that the achievable communication distances between the TX/RX and the BD increase with the increase in the size of the BD.

In addition, a study was performed to determine how the achievable range of communication changes with respect to the additional loss experienced by the system. The achievable range of communication decreases with the increase in the additional loss in the system. This is expected as the ambient signal experiences significant attenuation which contributes to the additional loss of the system. Therefore, it can be observed for an increase of 10 dB additional loss, the round-trip achievable distance reduces by about 43 percent for every BD irrespective of the size. Fig. 3.6 shows the graph that illustrates the effect of the additional loss in the achievable range of communication.

4 MONO-STATIC AMBC UTILIZING CELLULAR NETWORK SIGNALS

In this chapter, different aspects of the mono-static AmBC system are investigated when the ambient signal originates from cellular networks. As discussed earlier, in the mono-static systems, the TX and the RX are located at roughly the same location. Therefore, the ambient signal propagates to the BD and after impinging on the BD, propagates back toward the RX. The studies were performed in the outdoor macro-cell and rural environments with the help of simulations.

4.1 Propagation models

The radar equation and FSPL were utilized to perform the simulations using ambient signals from mobile networks. The models are described in Section 3.1.3 and Section 3.1.1.

4.2 Simulation environment

The TX and RX are located at approximately the same location indicating the mono-static mode of operation for AmBC. The ambient signal propagates toward the BD and is reflected toward the RX after impinging. In the simulations, it is assumed that the BDs are located close to the ground or at most 1 meter from the ground in the LOS path of the TX/RX. Due to the proximity of the BD to the ground, additional losses are considered due to the partial blocking of the Fresnel zone. Furthermore, losses due to the presence of trees, humans, buildings, and automobiles are also considered in the simulations. The additional loss is greater in the urban environment because of the abundance of such types of interference in comparison to a suburban highway environment.

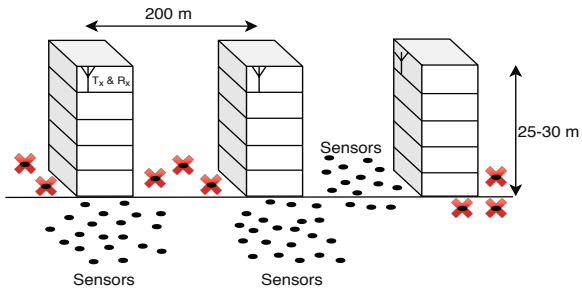

Figure 4.1 Schematic diagram of the urban macro-cellular environment. The BDs marked with red crosses are in the NLOS and cannot receive the ambient signal before it is significantly attenuated.

4.2.1 Urban macro-cell

The macro-cell environment is classified by the presence of buildings typically representative of an urban city environment. The urban environment also typically consists of wide streets with sidewalks. In the simulations, it is assumed that the BDs are located on the street level in the direct LOS path of the TX/RX antenna. In an urban macro-cellular environment, the antennas are located on or just below the rooftop level. Hence, in the simulations, the TX/RX antennas are located just below the rooftop level at a height of 30 m as shown in Fig. 4.1. This configuration is utilized to minimize the effects of the back lobe of the antenna radiation pattern. Additionally, this antenna arrangement ensures that the main lobe of the antenna is aimed toward the BDs which are placed in the LOS path of the TX/RX. Furthermore, due to this antenna deployment strategy, LOS paths exist between the TX/RX and the BD. Typically, adjacent base stations are separated by approximately 200 m to 400 m. The layout of the urban macro-cellular environment is depicted in Fig. 4.1. The BDs in the NLOS of the antenna are depicted with red crosses in Fig. 4.1.

Fig. 4.2 shows an illustration of the environment when macro cells are deployed in coherence with small cells. This type of network deployment is generally typical for 5G systems. Additionally, existing macro cell sites can be re-used by the operators for the deployment of 5G networks. Furthermore, such a network deployment is necessary for areas where there are numerous users. Therefore, the load of the macro cell can be shared by the small cell so that the network resources of the macro cell are not completely exhausted.

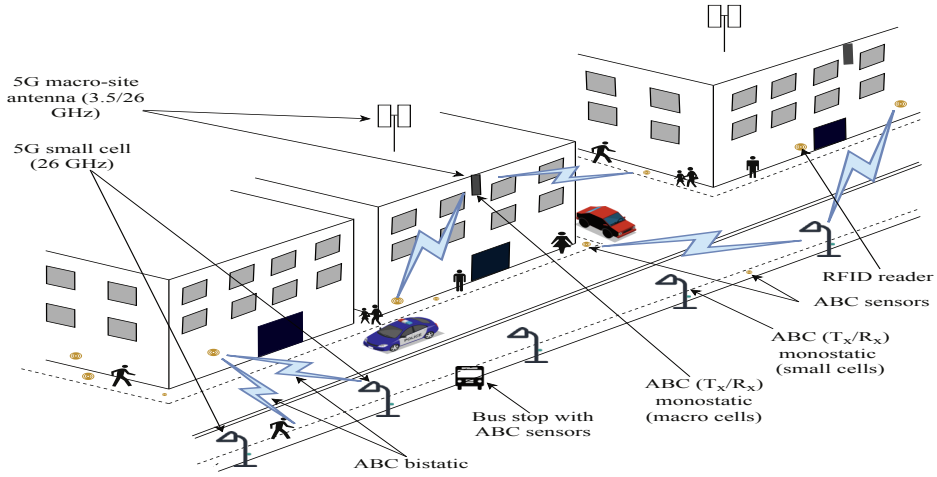

Figure 4.2 Deployment strategies of 5G and AmBC in the urban environment.

4.2.2 Small cells

The utilization of small cells generally enables network operators to provide coverage for users located at the edge of the cell. The small cell base stations are typically installed on top of lamp posts, bus stops, or inside shopping malls, etc. This deployment is performed to provide coverage for users in densely located environments such as stadiums, bus/train stations, and shopping malls. In addition, small cells provide significant improvement in coverage for users in dense urban residential areas. The aforementioned areas have a significant number of users and devices in need of using network resources. Furthermore, the applications for smart city deployments have accelerated the need for the deployment of small cells. Fig. 4.2 illustrates the deployment of small cells in an urban environment. In the simulations, it is assumed that the BDs have a direct LOS path with the small cell TX antenna.

4.2.3 Sub-urban highway

The standard height of the TX antenna in the sub-urban environment varies between 30 m to 80 m. The efficient antenna deployment strategy in the sub-urban environment involves placing the antenna at a higher elevation. This ensures a wider coverage area in addition to alleviating the hindrance caused by obstacles. As shown in Fig. 4.3, the BDs are located in the LOS path close to the TX/RX antenna. The

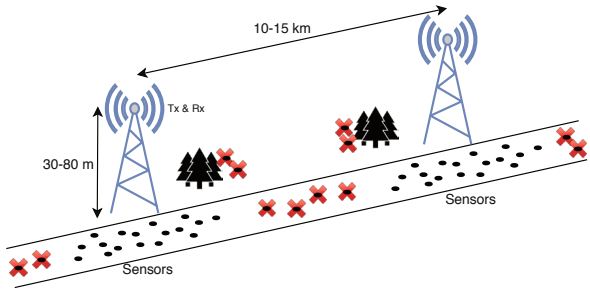

Figure 4.3 Schematic diagram of the suburban highway environment. The BDs in the NLOS of the TX/RX are marked with red crosses.

inter-site distances between adjacent cells vary between 10 km to 15 km. Therefore, there are areas within the environment without coverage for the BDs. Hence, the BDs need to be located close to the TX/RX to ensure the signal can cover the round-trip distance after impinging on the BD. The sensors that are unable to receive the signal due to being in the NLOS or being too distant are marked by red crosses in Fig. 4.3. The illustration of the propagation environment is shown in Fig. 4.3.

The sub-urban highway was selected for the simulations as this environment is free of significant interference-causing obstacles. Additionally, the BDs have a direct LOS connection with the TX and RX antenna. This setup ensures the minimum amount of path loss due to the propagation of the ambient signal. Therefore, the maximum harvesting area can be determined under specific circumstances in the rural highway environment.

4.3 Simulation parameters

The simulations are performed at the LTE and 5G carrier frequencies. The parameters were system-specific and chosen based on the frequencies at which the simulations were performed. The frequencies at which the simulations in this chapter were performed were low-frequency LTE 700 MHz, 3.5 GHz 5G, and 26 GHz millimeter-wave 5G.

In the simulations, the transmission power (P_t) of macro cells and small cells were 40 W (or, 46 dBm) and 4 W (or, 36 dBm), respectively [20]. The antenna gains for the simulations at LTE-700 were 18 dBi for the TX and 0 dBi for the RX. At the 5G frequencies, the antenna gains for both the TX and RX were 32 dBi each [3].

Table 4.1 Simulation parameters for LTE and 5G systems.

Parameter	Unit	LTE Value	5G Value
Frequency (f)	GHz	0.7	3.5, 26
Transmission power (macro cells, P_t)	dBm	46	46
Transmission power (small cells, P_t)	dBm	36	36
T_X antenna gain (G_t)	dBi	18	32
R_X antenna gain (G_r)	dBi	0	32
Cable loss (L_c)	dB	2	–
Temperature (T)	K	290	290
Bandwidth (B)	MHz	12×15	1, 20, 200
Noise figure (NF)	dB	10	8
Signal-to-noise ratio (SNR)	dB	2	4
Additional loss (L_{urban})	dB	15	10
Additional loss (L_{suburban})	dB	5	–
Reflection loss	dB	–	20

Additionally, a cable loss of 2 dB was considered for the simulations at LTE-700.

The minimum reception level of the system was calculated utilizing the typical values for Boltzmann's constant (k) and temperature (T), 1.38×10^{-23} J/K and 290 K, respectively. The system bandwidth (B) for LTE-700 was 12×15 kHz. This represents one resource block consisting of 12 sub-carriers and the spacing between them is 15 kHz [57]. Additionally, for the LTE-700 system, a NF of 10 dB and a SNR of 2 dB are utilized in the simulations.

The simulations for the 5G system were performed utilizing system bandwidths B of 1 MHz, 20 MHz, and 200 MHz, respectively. A NF of 8 dB and a SNR of 4 dB were utilized for the simulations at these carrier frequencies.

Finally, an additional loss of 15 dB in the urban environment and 5 dB in the suburban environment are utilized in the simulations performed at 700 MHz. For the 5G systems, an additional loss of 10 dB is considered. Furthermore, a reflection loss of 20 dB is also utilized in the simulations. All the values utilized in the simulations are summarized in Table 4.1.

4.4 Maximum Receiver Harvesting Area of Backscatter Signals from Ambient Low-Frequency Mobile Networks

This work intended to determine the maximum receiver harvesting area for AmBC sensors utilizing ambient signals from cellular networks. Therefore, the long-term evolution (LTE) network operating at the 700 MHz carrier frequency, LTE-700, was selected as the frequency for the simulations. The LTE-700 band is termed band 28 by 3GPP. LTE-700 is a favored carrier frequency band due to the available spectrum, good propagation characteristics, and availability in urban and suburban areas. The simulations were performed in the urban macro-cell and the suburban highway environments. A key disadvantage of using band 28 is technologies such as massive MIMO and beam-forming techniques cannot be easily supported due to the large wavelength of the signals. However, carrier aggregation can be applied to utilize band 28 in coherence with LTE-Advanced (LTE-A) or LTE-A Pro technologies by network operators [37].

The achievable range of communication of mono-static AmBC was limited based on previous research. The purpose of this work was to determine the maximum achievable range of communication utilizing commercially available cellular networks. Therefore, the lowest commercially available carrier frequency at that time, the LTE-700 frequency band was selected for the simulations. The primary reason why this carrier frequency was selected is because this network was already deployed in most countries of the world. Furthermore, the low frequency of operation of LTE-700 enabled the ambient signal to propagate further than signals from other commercially available cellular networks.

To maximize the achievable range of communication, only BDs located in the direct LOS of the TX/RX were utilized in the simulations. The attenuation experienced by the ambient signal propagating to the BDs located in the NLOS of the TX/RX is significantly greater. Therefore, the ambient signal is not strong enough to establish communication between the TX/RX and the BDs. The location of BDs in the urban macro cellular environment in the LOS and NLOS is shown in Fig. 4.1. In the suburban highway environment, the location of the BDs is shown in Fig. 4.3. The BDs located in the NLOS of the TX/RX are marked with red crosses in Fig. 4.1 and Fig. 4.3.

The $RX_{\text{sensitivity}}$ of the LTE-700 system was initially computed to be −109.42 dBm.

Thus, based on the P_t of 46 dBm, a total available path loss of 156.42 dB and 166.42 dB were available in the urban and suburban environments, respectively. The total available path loss was computed after considering the additional loss in both environments. Therefore, the aforementioned path loss was available for the ambient signal to propagate back and forth between the TX and RX after impinging on the BD. Therefore, the available path loss for one-way communication between the TX-BD (or, BD-RX) was 78.21 dB and 83.21 dB in the urban and suburban environments, respectively.

Using the FSPL equation, a distance of 275 m is achievable in the urban environment for one-way communication. The FSPL at this particular distance is 78.14 dB. Also, based on the principle of reciprocity, a similar distance can be achieved in the reverse link. Therefore, a round trip distance of 550 m can be achieved between the TX/RX and the BD. The total path loss experienced by the ambient signal is 156.28 dB, which is less than the total available path loss in the urban environment. Therefore, communication can be established with a BD located 275 m in the LOS of the TX/RX in the urban environment.

In the suburban highway environment, a one-way distance of 475 m is achievable between the TX/RX and the BD. Based on the FSPL, the signal experiences a path loss of 82.29 dB at this distance. Therefore, based on the total available path loss of 166.42 dB, a round trip distance of 950 m can be achieved in the suburban environment. At this distance, the ambient signal experiences a round-trip path loss of 164.58 dB. This value is below the total available path loss in the suburban environment. Therefore, communication can be established with a BD located 475 m away in the LOS of the TX/RX in the suburban environment.

The achievable range of communication for the radar equation is computed utilizing Eq. 3.4. The achievable distance indicates the round-trip distance between the TX/RX and the BD. The size of the BD was altered while performing the simulations to estimate the impact of the cross-section of the BD in the achievable range of communication. For the simulations, BDs of five different cross-sections were utilized.

The smallest size of the BD utilized in the simulations was $0.001\,\mathrm{m}^2$. A total round-trip communication range of 159 m and 283 m is achievable in urban and suburban environments, respectively. Therefore, a BD having a size of $0.001\,\mathrm{m}^2$ can be placed 79 m and 141 m away from the TX/RX in the urban and suburban environ-

Table 4.2 Different distances for AmBC with RT and RE propagation models.

Propagation model	RCS (σ, m^2)	Urban Total distance (m)	Sub-urban Total distance (m)
Ray Tracing	-	550	950
Radar equation	0.001	79	141
	0.01	141	251
	0.16	283	500
	0.3	331	589
	0.7	819	1456

ments, respectively. A total communication range of 283 m and 503 m is achievable in urban and suburban environments when the size of the BD is 0.01 m^2. Therefore, the BD can be located 141 m from the TX/RX in the urban environment. Also, in the suburban environment, the BD of this size can be located at a maximum distance of 251 m. When a larger BD of 0.16 m^2 surface area is utilized, a total round-trip distance of 567 m in the urban environment and 1000 m in the suburban environment was achievable based on the simulations. Therefore, utilizing 0.16 m^2 BD, the maximum one-way distance between the TX/RX and BD can be 283 m and 500 m in urban and suburban environments, respectively. The achievable range of communication is 662 m in the urban environment and 1178 m in the suburban environment utilizing a BD having the cross-section of 0.3 m^2. Therefore, the BD can be located 331 m and 589 m from the TX/RX in urban and suburban environments, respectively. Finally, a BD having the size of 0.7 m^2 represents the largest area the ambient signal can impinge on. Thus, the achievable round-trip distance in the urban and suburban environments is 819 m and 1456 m, respectively. Therefore, the maximum one-way distance between the TX/RX and BD is 409 m and 728 m in urban and suburban environments, respectively. It can be concluded that the achievable range of communication increases if the ambient LTE-700 signal has a large surface area to impinge on. The achievable distance between the TX/RX and the BD is summarized in Table 4.2.

The effect of additional loss in the achievable range of communication was also studied. Fig. 4.4 illustrates the effect of the additional loss on the achievable communication distance for each BD. It is observed that the achievable communication range decreases with the increase in the additional loss. This is due to the greater atten-

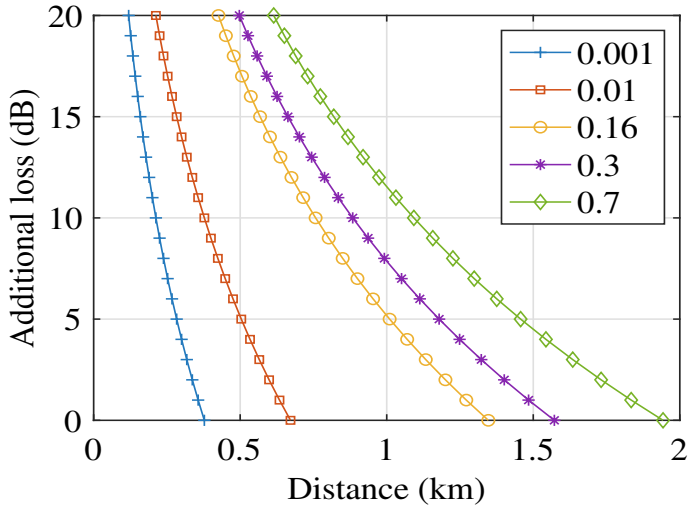

Figure 4.4 Achievable distances for different additional losses for varying RCS (σ).

uation that the ambient signal experiences while propagating between the TX/RX and the BD. It is observed that an increase in a 10 dB additional loss, reduces the achievable range of communication by approximately 43 percent.

Therefore, utilizing the FSPL equation, the BDs may be located at 550 m and 950 m in the LOS of the TX/RX in the urban and suburban environments, respectively. The achievable range of communication utilizing the radar equation varies between 159 m – 819 m and 283 m – 1456 m in the urban and suburban environment, respectively. The communication distance varies as a function of the cross-section of the BD. The achievable range of communication is higher in the suburban environment due to the low amount of interference in comparison with the urban environment. Furthermore, the additional loss has a significant impact on the achievable range of communication. Therefore, in conclusion, BDs located in the LOS of the TX/RX can be served by low-frequency ambient mobile network signals.

4.5 Assessment of 5G as an ambient signal for backscattering communications

The fifth generation of mobile communications was envisioned to provide high data rates for devices in comparison with existing technologies. In certain situations, 5G

was envisioned to provide data rates corresponding to broadband services. Additionally, high reliability and low latency communications are also some major use cases for 5G systems [21]. The requirement for high data rates, reliability, and low latency communications is driven by the advent of the huge number of connected devices with the deployment of IoT [50]. Additionally, 5G was developed with the idea of providing coverage and support for a huge number of IoT devices that are connected to each other as well as a central node. Furthermore, certain 5G use cases have the requirement for ultra-reliable low latency communications (URLLC) such as remote surgeries, remote traffic management, and autonomous vehicles [58]. These requirements can be fulfilled by the introduction of certain key technologies for RF interfaces.

Firstly, a shift toward higher carrier frequencies enables the utilization of massive multiple-input multiple-output antenna arrays at the base stations [41, 55]. Consequently, the effects of the higher propagation loss at the higher carrier frequencies can be mitigated due to the antenna arrays present at the TX. Additionally, the azimuth and elevation planes can be utilized simultaneously for the allocation of users. Furthermore, high performance in both the uplink and downlink can be achieved with beamforming [19].

Secondly, the utilization of higher frequency bands facilitates the need for increased data rates which is necessary to support the requirement for enhanced mobile broadband (eMBB) [50]. The utilization of the large bandwidth available in the millimeter wave carrier frequency (24 GHz to 100 GHz) helps to achieve the high data rate requirements of certain use cases. In practical scenarios, the sub 6 GHz carrier frequency bands are utilized in coherence with the millimeter wave frequency band to enable communications for 5G systems. The sub-6 GHz carrier frequency band would be implemented on the existing macro-cellular sites and the millimeter wave frequency would be utilized in outdoor small cells or short-range communication links in indoor environments [29]. This enables the utilization of heterogeneous networks where small cells and macro cells may operate at different carrier frequencies, even for a single operator. This type of implementation is shown in Fig. 4.2.

Finally, in heterogeneous networks, the traffic load on the macro-cells can be reduced by the utilization of the small cells. However, the requirement of the macro-cell base stations would still be necessary to carry the control plane traffic [36]. Fig. 4.2 shows an illustration of a heterogeneous network where macro cells and

small cells are simultaneously deployed. Cooperative scheduling and coordinating multipoint (CoMP) technologies may be utilized to mitigate the adjacent cell interference caused due to the utilization of heterogeneous networks [36, 60]. 3GPP has decided to utilize OFDM waveforms to support a variety of applications for the 5G air interface.

5G was envisioned to provide coverage for devices and users located primarily in the urban macro-cellular environment [21]. It was estimated that there would be a significant increase in the number of users or devices in such locations with the advent of IoT wireless communications. 5G networks were designed to support the high capacity requirements in densely populated urban areas. 5G networks can be deployed in existing macro-cellular sites. Furthermore, new small cell sites can be established to provide better connectivity for cell-edge users. The different deployment strategies of 5G sites can be observed in Fig. 4.2. Additionally, with the advent of autonomous self-driving cars, the coverage of 5G networks is also expected to be extended to highways located in suburban and rural environments. Fig. 4.3 shows an example of a suburban highway environment where AmBC sensors could be deployed.

The purpose of this study was to determine the applicability of 5G networks for AmBC in densely populated urban and rural areas. 5G networks operating at 3.5 GHz and 26 GHz millimeter wave frequencies are utilized in the simulations to determine the coverage area of AmBC BDs in urban macro-cell and small-cell environments. Additionally, the carrier frequency of 3.5 GHz is utilized to perform simulations in the suburban highway environment.

To determine the achievable range of communication between the TX/RX and the BD, it was necessary to determine the total available path loss in the respective environment. The total available path loss between the TX/RX and the BD in the urban macro cell, small cell, and suburban highway environment was computed based on the difference between the transmission power (P_t) and the minimum reception level (or, P_r) of the system. The value of P_r was calculated by utilizing Eq. 3.6. The value of P_r in the 5G system can change due to the varying system bandwidths. 5G can support system bandwidth ranging up to 400 MHz. As an example, system bandwidth values of 1 MHz, 20 MHz, and 200 MHz were utilized in the simulations. The corresponding values of P_r were calculated to be −101.97 dBm, −88.96 dBm and −78.96 dBm for 1 MHz, 20 MHz, and 200 MHz, respectively. The

Table 4.3 Receiver sensitivity at different bandwidths (in dBm).

Bandwidth (B)	1 MHz	20 MHz	200 MHz
$RX_{\text{sensitivity}}$ (P_r)	−101.97	−88.96	−78.96

Table 4.4 Ray tracing distances (monostatic) at different bandwidths (in meters).

Bandwidth (B)	1 MHz	20 MHz	200 MHz
3.5 GHz	5370 m	1200 m	375 m
26 GHz	225 m	50 m	15 m

$RX_{\text{sensitivity}}$ at different bandwidths is summarized in Table 4.3. The aforementioned values were computed utilizing an SNR of 4 dB and a NF of 8 dB. The other simulation parameters are summarized in Table 4.1.

Based on the P_r values, the total available path loss for the round-trip communication was determined to be 147.97 dB, 134.96 dB, and 124.96 dB in the urban macro-cellular environment. Similarly, in small cells, the total available path loss is 137.97 dB, 124.96 dB, and 114.96 dB, at 1 MHz, 20 MHz, and 200 MHz, respectively. The total available path loss further decreases when the additional loss and loss due to reflection (at the BD) are taken into account.

The range of communication at 3.5 GHz between the TX/RX and the BD was calculated to be 5370 m, 1200 m, and 375 m at the system bandwidths of 1 MHz, 20 MHz, and 200 MHz, respectively. These values were obtained utilizing the FSPL equation. Therefore, the BD can be placed at a distance of 2685 m, 600 m, and 187 m from the TX/RX when the carrier frequency is 3.5 GHz. The total achievable range of communication at 26 GHz between the TX/RX and the BD is 225 m, 50 m, and 15 m at the system bandwidth of 1 MHz, 20 MHz, and 200 MHz, respectively. Therefore, the BD can be located at a distance of 112 m, 20 m, and 7.5 m from the TX/RX in the small-cell environment based on the utilized system bandwidth. The total achievable range of communication using FSPL at 3.5 GHz and 26 GHz carrier frequencies utilizing different system bandwidths are summarized in Table 4.4.

The radar equation computes the total round-trip communication range achievable between the TX/RX and the BD. The total distance (R) is calculated using Eq. 3.4. The achievable range of communication is dependent on the size of the BD. The simulations are performed utilizing BDs having different cross-sections in both

Table 4.5 Distances (in meters) for AmBC with RE at 3.5 GHz frequency with different bandwidths.

RCS (σ, m^2)	1 MHz	20 MHz	200 MHz
0.0004	695 m	328 m	184 m
$half - dipole$, 0.0065	1394 m	659 m	370 m
0.01	1554 m	734 m	413 m
0.15	3059 m	1446 m	813 m
0.3	3637 m	1720 m	967 m
0.7	4495 m	2126 m	1195 m

the urban macro-cellular and small-cell environments.

The 3.5 GHz carrier frequency is utilized in the simulations performed in the macro-cellular environment. A BD having a dimension of 2 cm × 2 cm (0.0004 m^2) represents the worst-case scenario as the ambient signal has a very small surface area to impinge upon. The achievable range of communication between the TX/RX and the BD is 695 m (1 MHz), 320 m (20 MHz), and 184 m (200 MHz). It is observed that the achievable range of communication decreases with the utilization of large system bandwidth. The achievable range of communication increases to 1.39 km (1 MHz), 659 m (20 MHz), and 370 m (200 MHz) when the BD represents a half-dipole antenna (the size of which is calculated using Eq. 3.5). This is because the ambient signal has a larger surface area to impinge on. Moreover, it is observed that communication ranges of 1.5 km (1 MHz), 734 m (20 MHz), and 413 m (200 MHz) can be achieved utilizing a BD of 10 cm × 10 cm (or, 0.01 m^2). Furthermore, the achievable range of communication is 3 km (1 MHz), 1.4 km (20 MHz), and 813 m (200 MHz) when the size of the BD is 0.15 m^2. Additionally, depending on the system bandwidth, the achievable range of communication varies between 967 m and 3.63 km when the size of the BD is 0.3 m^2. Similarly, using 0.7 m^2 BD, the achievable range of communication varies between 1.19 km and 4.49 km. Therefore, it can be concluded that the achievable range of communication increases with the increase in the cross-section of the BD. The achievable communication ranges utilizing 3.5 GHz carrier frequency are summarized in Table 4.5.

It can be observed from Table 4.4 and Table 4.5 that the achievable range of communication is dependent on the system bandwidth. For example, the achievable communication range utilizing the FSPL at the 200 MHz system bandwidth is 375 m. Utilizing the radar equation, at the corresponding bandwidth, a communi-

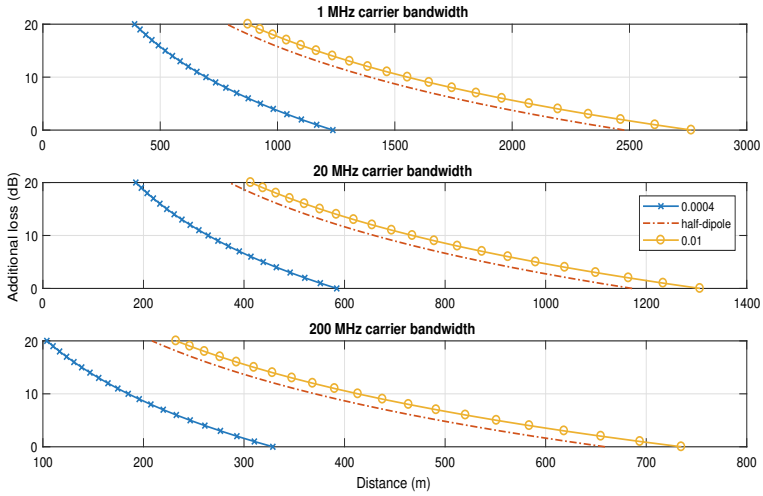

Figure 4.5 Achievable distances for different additional losses and carrier bandwidth for varying RCS (σ) at 3.5 GHz.

cation range of 370 m can be achieved with a BD of 0.0065 m^2. However, the corresponding distances achieved (for the BD having the same cross-section) at 1 MHz (5370 m and 1395 m) and 20 MHz (1200 m and 659 m) utilizing the FSPL and radar equation are contrasting. Therefore, it can be concluded that the size of the BD has a significant impact on the achievable range of communication. Thus, the FSPL equation provides an optimistic estimation of the achievable range of communication in comparison with the radar equation because the size of the BD is not taken into account.

The achievable range of communication is dependent on the type of ambient 5G signal. For instance, the 5G pilot signal is transmitted at a narrower system bandwidth than the traffic channels. The traffic channels have a system bandwidth in the region of 10 MHz — 100 MHz.

Furthermore, the additional loss has a significant impact on the achievable range of communication. The additional loss values are varied between 0 dB and 20 dB to observe the impact on the achievable communication range. Fig 4.5 shows the impact of the additional loss on BDs having cross-sections of 0.0004 m^2, 0.0065 m^2, and 0.01 m^2.

The millimeter wave (26 GHz) carrier frequency is utilized for the simulations performed in the small cell environment. At this frequency, the total achievable

Table 4.6 Distances (in meters) for AmBC with RE at 26 GHz frequency with different bandwidths.

RCS (σ, m^2)	1 MHz	20 MHz	200 MHz
$half-dipole$, 0.0001	105 m	49 m	28 m
0.0004	143 m	67 m	38 m
0.01	320 m	151 m	85 m
0.15	631 m	298 m	167 m
0.3	750 m	354 m	199 m
0.7	927 m	438 m	246 m

range of communication is minimal when a BD representing a half-dipole antenna is utilized. For this sensor size, the achievable range of communication is 105 m, 49 m, and 28 m at the system bandwidths of 1 MHz, 20 MHz, and 200 MHz, respectively. The achievable range of communication for a BD having a cross-section of 2 cm × 2 cm (0.0004 m^2) is 143 m, 67 m, and 38 m utilizing different system bandwidths. Therefore, it can be observed that the achievable range of communication increases when the ambient signal has a large surface area to impinge on. The achievable range of communication is 320 m, 151 m, and 85 m when a BD having a cross-section of 0.01 m^2 is utilized in the simulations. Furthermore, communication distances of 631 m, 298 m, and 167 m may be achieved when the cross-section of the BD is 0.15 m^2. Additionally, the achievable range of communication varies between 199 m — 750 m and 246 m — 927 m when BDs having cross-section of 0.3 m^2 and 0.7 m^2 are utilized in the simulations based on the utilized system bandwidth. Therefore, it can be concluded that the cross-section of the BD significantly affects the achievable range of communication. The values for the achievable communication range in the small cell environment utilizing 26 GHz carrier frequency are summarized in Table 4.6.

The additional loss is varied between 0 dB — 20 dB to determine the change in the achievable range of communication. Fig. 4.6 demonstrates the change in the achievable range of communication due to the variation of the additional loss at 26 GHz carrier frequency. The achievable range of communication decreases by 80 m when the additional loss increases from 10 dB to 15 dB when the cross-section of the BD is 0.01 m^2. The excess additional loss can arise due to excess interference experienced by the ambient signal. It was observed that in both the macro-cell and the small-cell environment, a 5 dB increase in the additional loss reduces the achievable

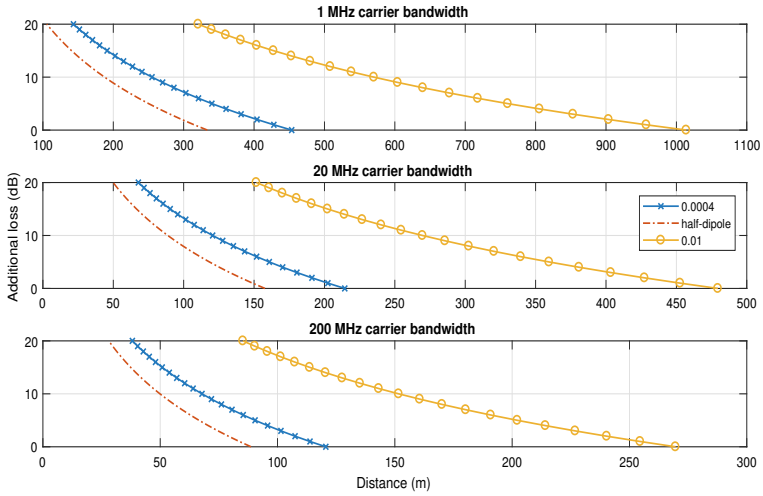

Figure 4.6 Achievable distances for different additional losses and carrier bandwidth for varying RCS (σ) at 26 GHz.

range of communication by 25 percent.

In the rural highway environment, 3.5 GHz carrier frequency is utilized to provide coverage for BDs with different use cases. The 26 GHz carrier frequency is limited by coverage and is not considered practical for deployment in the rural highway environment. Thus, the achievable range of communication is similar to the distances achieved in the urban macro-cellular environment as shown in Table 4.5. However, the additional loss in the rural highway environment is significantly lower than in the urban macro-cellular environment. Therefore, the achievable communication range in the rural highway environment is more than the communication range values shown in Table 4.5. However, based on the site distances and the practical cross-section of the BDs, communication is only possible in proximity to the TX/RX. The height of the TX antenna can range between 30 m – 80 m in the rural highway environment.

The objective of this study was to evaluate the applicability of 5G as an ambient signal for backscattering communications in outdoor environments. It was assumed that the BDs were located in the direct LOS of TX/RX. It was observed that in the urban macro-cellular environment (at 3.5 GHz) communication distances between 184 m — 4.49 km could be achieved. Similarly, communication ranges between 28 m — 927 m may be achieved in the small cell environment utilizing the carrier fre-

quency of 26 GHz. In the rural environment, the achievable range of communication was greater than in the urban macro-cellular environment. This is because the additional loss in the rural environment is less in comparison to the urban environment. It was observed that the achievable range of communication was dependent on the cross-section of the BD and the additional loss experienced by the ambient signal. The increase in the size of the BD enables a greater surface area for the ambient signal to impinge on. Thus, greater distances can be achieved with a larger BD. Furthermore, the type of ambient 5G signal (i.e. based on the bandwidth) has a significant impact on the total achievable range of communication. The increase in the system bandwidth leads to a reduction in the achievable range of communication. Therefore, it can be concluded that 5G signals can be utilized as an ambient signal for mono-static AmBC as long as the sensors are located in proximity to the 5G TX antenna.

4.6 Sensitivity analysis of ambient backscatter communications in heavily loaded cellular networks

The studies on the coverage of mono-static backscatter systems utilizing ambient signals from different mobile/cellular networks were studied in the preceding sections. In an urban environment, the cells have a 3-sector hexagonal structure. The adjacent cells can operate at different frequencies. However, similar frequencies may also be utilized by the network operator in the adjoining cell if the frequency reuse factor is 1 [56]. Fig. 4.7 shows an illustration of the layout of the cells in an urban environment. Therefore, six adjacent cells can cause interference in the serving cell. The serving and interfering cells are shown in Fig. 4.7.

In the first two articles of this chapter (Section 4.4 and Section 4.5), the maximum achievable range of communication utilizing LTE and 5G frequencies was performed assuming ideal conditions. In the studies, it was assumed that the serving cell (where the BD is located) was not subject to interference from the adjacent cell.

The ideal conditions may exist when the network load is not high, for example during the night hours (10 pm — 8 am) or the middle of the day (12 pm — 5 pm). During these particular times of the day, the traffic in the network is limited and the users/devices in the environment experience less interference. However, during hours with higher network traffic, there is a significant amount of interference from

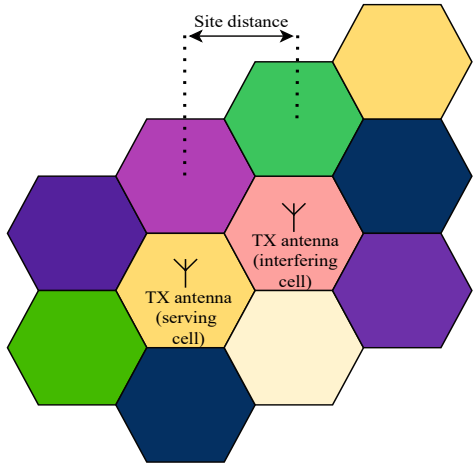

Figure 4.7 Illustration of serving and interfering cell.

adjacent cells experienced by the devices and the users in the serving cell. High network traffic is observed during morning hours (8 am — 12 pm) and evening hours (5 pm — 9 pm) when the network resources are depleted.

The purpose of this work was to determine the impact of adjacent cell interference on the BDs in the serving cell during peak hours. The effect of the interference from the adjacent cell is utilized to determine the coverage in the serving cell. The simulations were performed at LTE-700, 3.5 GHz 5G, and 26 GHz 5G millimeter wave frequencies.

In the previous studies in Section 4.4 and Section 4.5, the SNR of the system was considered to be the limiting factor in the maximum achievable range of communication. In this study, the signal-to-interference and noise ratio (SINR) was calculated based on the interference caused by the signal from the adjacent cell to the serving cell. Generally, in urban macro-cell environments, the inter-site distance ranges between (150 m – 200 m) [2]. In these simulations, the inter-site distance was considered to be 200 m. The inter-site distance between adjacent small cells was considered to be 100 m.

The power of the received signal in the serving cell is represented by the term P_{rx}. The thermal noise power of the system is represented by the term P_{n}. The signal from the TX of the adjacent cell is represented by the term P_{i}. This value indicates the strength of the interfering signal at a particular location in the cell. The SINR is calculated utilizing (4.1). Based on the strength of P_{n} or P_{i}, either the thermal

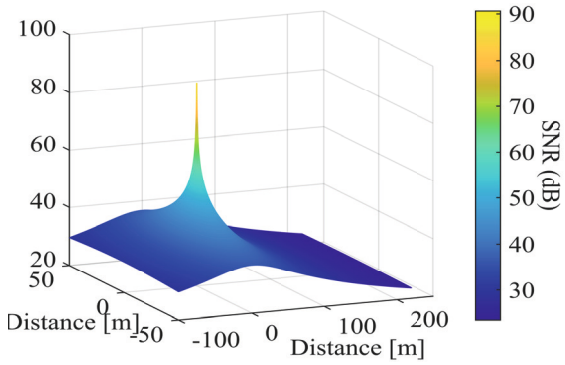

Figure 4.8 SNR for LTE-700 system. The TX/RX antenna is located at (0,0,0). The distances on the x-axis and y-axis are indicative of the coverage area of the serving cell at 700 MHz

noise or the interference-causing signal can be a greater limiting factor. Therefore, Eq. 4.1 may represent the signal-to-interference (SIR) or the SNR depending upon the parameter causing greater hindrance to the system. The SINR of the system is expressed as,

$$\text{SINR} = \frac{P_{\text{rx}}}{P_{\text{n}} + P_{\text{i}}}. \tag{4.1}$$

The BDs are designated to perform differently based on the use case and the deployment scenarios. Thus, in the simulations, the BD was located anywhere within the environment. The simulations are carried out for LTE and 5G systems based on the parameters described in Table 4.1. The noise figure and the additional loss are assumed to be 10 dB in the simulations for both systems. This is done to maintain coherence and to compare the results. In practical deployments, the values can be slightly different from the ones that are utilized in this work.

The signal-to-noise ratio graphs of 700 MHz LTE, 3.5 GHz 5G, and 26 GHz millimeter wave 5G systems are shown in Fig. 4.8, Fig. 4.9, and Fig. 4.10, respectively. The SNR is the highest at the location (0,0,0) which represents the location of the TX in all three figures. This is because the background noise does not significantly impact the signal strength in the proximity of the TX. The value of P_{rx} is calculated based on the FSPL in Eq 3.1. It can be observed from Fig. 4.8 that the SNR of the LTE system operating at a carrier frequency of 700 MHz is around 20 dB at the cell edge. For the 5G system operating at 3.5 GHz, it can be observed from Fig. 4.9 that the SNR at the cell edge is around 10 dB. The SNR at the millimeter wave frequency of 26 GHz has a rapid degradation as the cell edge is approached as ob-

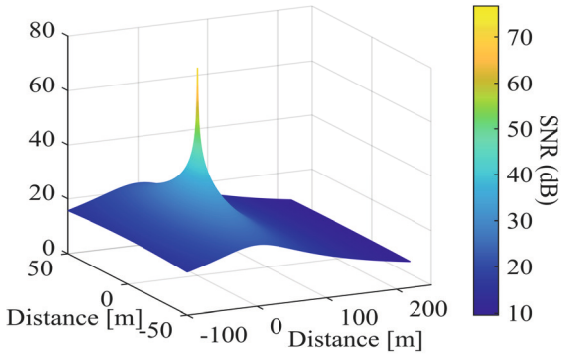

Figure 4.9 SNR for 3.5 GHz 5G system. The TX/RX antenna is located at (0,0,0). The distances on the x-axis and y-axis are indicative of the coverage area of the serving cell at 3.5 GHz

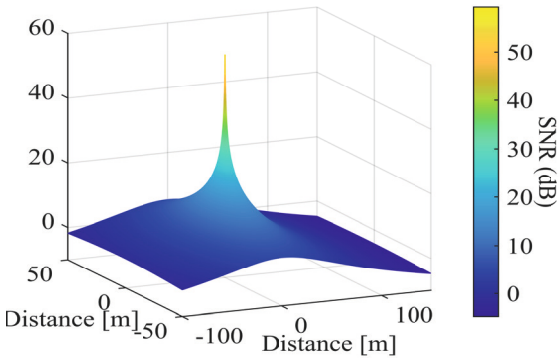

Figure 4.10 SNR for 26 GHz millimeter wave 5G system. The TX/RX antenna is located at (0,0,0). The distances on the x-axis and y-axis are indicative of the coverage area of the serving cell at 26 GHz

served from Fig. 4.10. Therefore, even during non-peak hours (when the network traffic is minimum) the coverage area of backscatter communication using ambient millimeter-wave signals is limited to the proximity of the TX.

The SIR of the system is calculated subsequently to determine the effect of the signal from the adjacent cell, P_{i}. These values were calculated based on the LOS locations where the BDs are located. Additionally, the intention was to determine if P_{i} causes a more significant hindrance to the achievable range of communication in comparison to the P_{n}. It was observed at every carrier frequency the value of the SIR at the cell edge is 0 dB. This is because the signals from the serving and adjoining cells cancel each other at the cell edge. It can be observed from Fig. 4.11, Fig. 4.12,

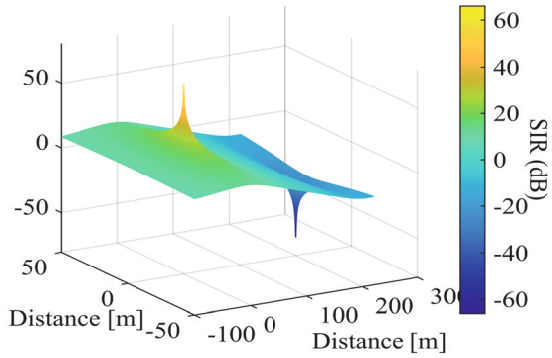

Figure 4.11 SIR for LTE-700 system. The TX/RX of the serving cell and adjacent cell are located at (0,0,0) and (200,0,0), respectively based on the inter-site distance. The distances on the x-axis and y-axis indicate the coverage area of the serving and adjacent cells.

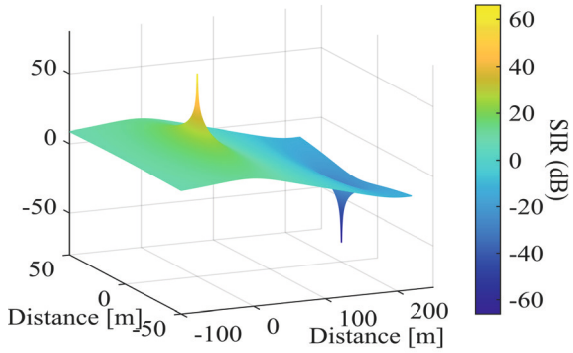

Figure 4.12 SIR for 3.5 GHz 5G system. The TX/RX of the serving cell and adjacent cell are located at (0,0,0) and (200,0,0), respectively based on the inter-site distance. The distances on the x-axis and y-axis indicate the coverage area of the serving and adjacent cells.

and Fig. 4.13 that the interfering signal is more of a limiting factor than the SNR. Thus, the coverage area shrinks due to the effect of P_{i} on the serving cell. Therefore, the SIR of the system needs to be taken into account while computing the coverage area of mono-static ambient backscatter communication systems.

Further studies were performed to observe the effects of the size of the BD in the total achievable range of communication at LTE and 5G frequencies. The achievable range of communication decreases with the decrease in the size of the BD. This is due to the small surface area of the BD that the ambient mobile network signal can impinge on. Furthermore, it was observed that the achievable range of communication decreases with the increase in the SIR, irrespective of the cross-section of the BD.

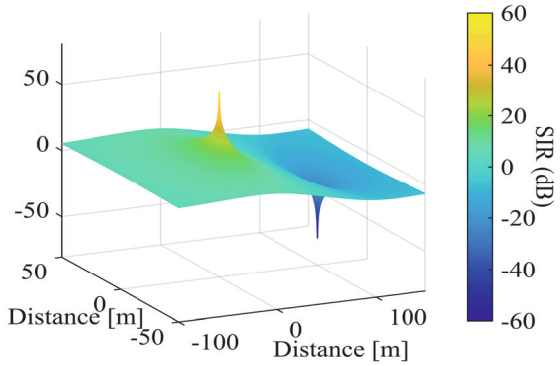

Figure 4.13 SIR for 26 GHz millimeter wave 5G system. The TX/RX of the serving cell and adjacent cell are located at (0,0,0) and (100,0,0), respectively based on the inter-site distance. The distances on the x-axis and y-axis indicate the coverage area of the serving and adjacent cells.

The total achievable round-trip communication distance at LTE-700, 3.5 GHz 5G, and 26 GHz millimeter wave 5G are shown in Fig. 4.14, Fig. 4.15, and Fig. 4.16, respectively.

It could be observed that the interfering signal from the adjacent cell significantly impacts the communication distance in comparison with the SNR. For a BD with a cross-section of 0.01 m^2, the achievable range of communication between the TX/RX and the BD is 105 m, 30 m, and 6 m at 700 MHz, 3.5 GHz, and 26 GHz, respectively. These communication distances were obtained during peak hours. However, during the non-peak hours, the achievable communication range is 185 m, 55 m, and 11 m at the same frequencies. Hence, it can be observed that the SIR causes a reduction in the achievable range of communication of about 44 percent. Furthermore, the signal degrades significantly as the cell edge is approached due to higher signal strength (interference) from the adjacent cell. Thus, it can be concluded that the range of communication is limited due to the interfering signal from the adjacent cell. Therefore, the BDs must be located in the close vicinity of the TX/RX to nullify the effect of the adjacent cell interference in mono-static AmBC systems.

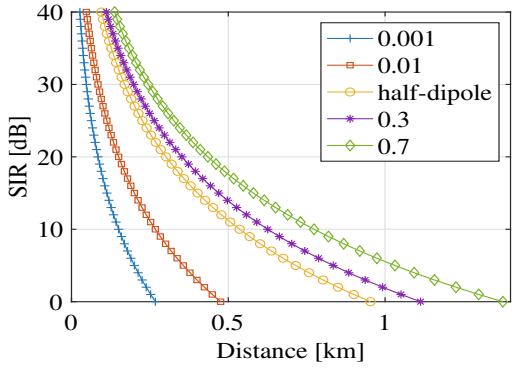

Figure 4.14 Achievable communication range for LTE-700 system utilising different σ and SIR.

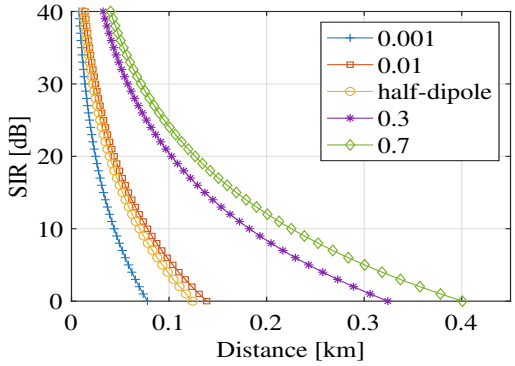

Figure 4.15 Achievable communication range for $3.5\,\mathrm{GHz}$ 5G system utilising different σ and SIR.

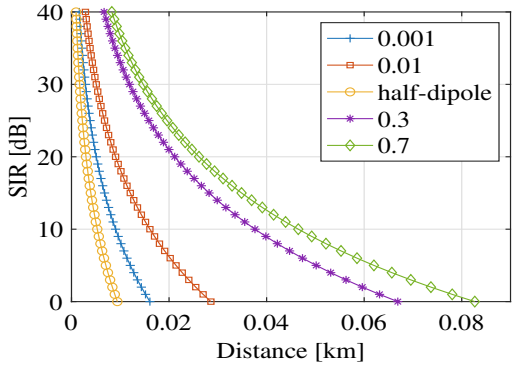

Figure 4.16 Achievable communication range for $26\,\mathrm{GHz}$ millimeter wave 5G system utilising different σ and SIR.

5 BI-STATIC AMBC UTILIZING SUB-1 GHZ SIGNALS

In this chapter, the coverage and capacity aspects of bi-static ambient backscattering communications in outdoor environments are studied. In bi-static AmBC, the TX and the RX are present in different locations. The BD is located in the space between the TX and RX. This type of communication mechanism can be utilized to transfer information from the BD to the end user (who has the RX/user equipment). The incoming signal from the TX impinges on the sensor which in turn backscatters the signal toward the receiver. The BD is also capable of utilizing the incoming ambient transmission signal as a source of energy to power itself.

5.1 Simulation environment for bi-static AmBC

The simulations were performed in the urban micro-cellular environment at different sub-1 GHz frequencies. In the bi-static mode of communication, the signal follows two paths between the TX and the RX. The first path is the more traditional communication link which exists directly between the TX and the RX. The second path is a combination of the forward link ($d1$) between the TX and the BD and the backscatter link ($d2$) between the BD and the RX (after the ambient signal impinges on the BD). Fig. 5.1 shows the two different paths the signal traverses between the TX and the RX.

The communication link between the TX and the RX (for the direct link) and the TX and BD (for the forward link) are defined in the simulations utilizing the third-generation partnership project (3GPP) urban micro-cellular model [1]. The communication link between the BD and the RX (for the backscatter link, $d2$) is defined by the International Telecommunications Union (ITU) device-to-device (D2D) model [33]. These propagation models are discussed in the following sections.

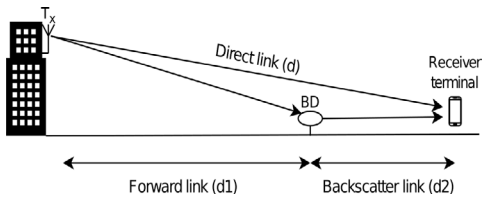

Figure 5.1 Schematic diagram for bi-static AmBC. The legacy signal follows the direct path (d). The backscattered signal follows the forward link ($d1$) and then the backscatter link ($d2$) after impinging on the backscatter device (BD).

5.1.1 3GPP — Urban microcellular model

The 3GPP proposed a model for the propagation of radio signals through the urban micro-cell environment. The model is valid for TX antennas located 10 m — 15 m on or just below the rooftop level. The propagation model takes into account the radio wave propagation in both the LOS and NLOS scenarios. Eq 5.1 and Eq 5.2 are utilized to compute the basic transmission loss in the LOS and NLOS, respectively.

$$L_{\text{LOS}}(\text{dB}) = 32.4 + 20 \cdot \log_{10}(f_{\text{GHz}}) + 21 \cdot \log_{10}(d_{\text{3D}}), \tag{5.1}$$

$$L_{\text{NLOS}}(\text{dB}) = 32.4 + 20 \cdot \log_{10}(f_{\text{GHz}}) + 31.9 \cdot \log_{10}(d_{\text{3D}}). \tag{5.2}$$

The term d_{3D} represents the distance followed by the ambient signal between the transmitter and the BD (forward link) and is expressed in meters (m). The frequency of operation (in GHz) is expressed by the term f_{GHz}. The probability of having a LOS connection is calculated using Eq 5.3,

$$P_{\text{LOS}} = \begin{cases} 1, & d_{\text{2D}} \leq 18m \\ \dfrac{18}{d_{\text{2D}}} + \left(-\dfrac{d_{\text{2D}}}{36}\right)\left(1 - \dfrac{18}{d_{\text{2D}}}\right), & 18m < d_{\text{2D}} \end{cases} \tag{5.3}$$

where d_{2D} represents the distance (in meters) between the TX and the BD. So, from Fig 5.1, it is the base of the triangle created by the BD, antenna, and the surface of the Earth. The term d_{3D} used in Eq 5.1 and Eq 5.2 represents the hypotenuse formed by the aforementioned triangle.

Finally, the total propagation loss experienced by the signal in the forward link

(L_{d1}) is calculated utilizing Eq 5.4,

$$L_{d1} = P_{LOS} \times L_{LOS} + (1 - P_{LOS}) \times L_{NLOS}. \tag{5.4}$$

5.1.2 ITU — Device-to-device model

The ITU specified a propagation model in their ITU-R P.1411-10 report for the communication between two devices located in the urban micro-cellular street canyon environment [33]. The location variability statistics for the LOS and NLOS scenarios were considered during the development of this propagation model [33].

The propagation loss in the LOS is calculated using (5.5),

$$L_{LOS}(d) = 32.45 + 20 \cdot \log_{10}(f_{MHz}) + 20 \cdot \log_{10}(d_{3D}), \tag{5.5}$$

where the frequency is represented in megahertz (MHz) and the term (d_{3D}) represents the distance in meters. Thereafter, for the required location percentage (p), the LOS location probability is computed utilizing Eq 5.6,

$$\Delta L_{LOS}(p) = 1.5624\sigma(\sqrt{-2 \cdot ln(1 - p/100)} - 1.1774). \tag{5.6}$$

The LOS location correction ($\Delta L_{LOS}(p)$) and the median value of the basic propagation LOS loss ($L_{LOS}(d)$) are summed up to determine the total loss in the LOS scenario. The total propagation loss experienced by the signal in the LOS scenario is represented by Eq 5.7.

$$L_{LOS}(d, p) = L_{LOS}(d) + \Delta L_{LOS}(p). \tag{5.7}$$

The propagation loss in the NLOS scenario is calculated utilizing Eq 5.8. The frequency and the distance (d_{3D}) are represented in megahertz (MHz) and meters, respectively. Furthermore, the term L_{urban} represents the type of environment as specified in [33]. L_{urban} has a value of 6.8 dB to represent an urban environment.

$$L_{NLOS}(d) = 9.5 + 45 \cdot \log_{10}(f_{MHz}) + 40 \cdot \log_{10}(d_{3D}) + L_{urban}. \tag{5.8}$$

The location correction in the NLOS scenario is computed using Eq 5.9,

$$\Delta L_{NLOS}(p) = \sigma \cdot N^{-1}(\frac{p}{100}), \tag{5.9}$$

where the term $N^{-1}(.)$ represents the normal cumulative distribution function.

Similar to the LOS scenario, the location correction (ΔL_{NLOS}) and the median value of the propagation loss ($L_{\mathrm{NLOS}}(d)$) are summed to determine the total propagation loss in the NLOS scenario. The total NLOS propagation loss is calculated utilizing Eq 5.10,

$$L_{\mathrm{NLOS}}(d,p) = L_{\mathrm{NLOS}}(d) + \Delta L_{\mathrm{NLOS}}(p). \tag{5.10}$$

The term d_{LOS} represents the corner distance and the calculation is performed as a function of the location percentage (p) utilizing Eq 5.11,

$$d_{\mathrm{LOS}}(p) = \begin{cases} 212 \cdot [\log_{10}(\frac{p}{100})]^2 - 64 \cdot \log_{10}(\frac{p}{100}), & p < 45 \\ 79.2 - 70 \cdot (\frac{p}{100}). & 45 \leq p \end{cases} \tag{5.11}$$

The propagation loss experienced by the signal in the backscatter link (L_{d2}) is computed on the basis of Eq 5.12. This equation is utilized to compute the final propagation loss between the BD and the RX. The propagation loss in both the LOS and NLOS region is utilized based on the relation between the corner distance (d_{LOS}) and the total distance (d) as mentioned in Eq 5.12,

$$L_{\mathrm{d2}} = \begin{cases} L_{\mathrm{LOS}}(d,p), & d < d_{\mathrm{LOS}} \\ L_{\mathrm{NLOS}}(d,p). & d > d_{\mathrm{LOS}} \end{cases} \tag{5.12}$$

5.1.3 Simulation setup and parameters

In order to calculate the signal strength at the RX, many parameters have to be considered while performing the simulations. The calculation of the basic propagation loss in the forward link (L_{d1}) and backscatter link (L_{d2}) is based on the equations provided in Section 5.1.1 and Section 5.1.2. The simulations are performed at different sub-1 GHz frequencies of 200 MHz, 500 MHz, 700 MHz, and 900 MHz. The typical transmission power (P_{tx}) in the urban micro-cellular environment is 2 W (or, 33 dBm). In the simulations, the TX antenna is located at a height of 15 m, and the gain of the TX antenna (G_{t}) is 10 dBi.

Moreover, the signal propagation also has to take into account multiple factors which cause additional losses to the propagation of the signal through the environ-

Table 5.1 Simulation parameters.

Parameters	Unit	Value
Frequency	MHz	200/500/700/900
T_x power	dBm	33
T_x antenna height	m	15
T_x antenna gain	dBi	10
BD antenna gain	dBi	0
Slow fading margin	dB	15.2
Fast fading margin	dB	16
Polarization mismatch loss	dB	3
Modulation loss	dB	6
L_{urban}	dB	6.8
Location percentage	%	50

ment. These additional losses (L_{add}) take into account the slow fading (L_{SF}) and the fast fading (L_{FF}) margin. Additionally, the modulation loss (L_{ML}) and polarization mismatch loss (L_{PM}) are also taken into account. These values were obtained from the article in [25] where a complete link budget for backscatter communications is proposed by the authors. Therefore, the additional loss (L_{add}) can be represented by Eq 5.13. The location percentage is assumed to be 50 in the simulations. All the parameters utilized in the simulations are summarized in Table 5.1.

$$L_{add} = L_{SF} + L_{FF} + L_{PM} + L_{ML} \tag{5.13}$$

The received signal strength (RX_{level}) at a particular location is computed utilising Eq 5.14,

$$RX_{level}(\text{dBm}) = P_{tx} + G_t - (L_{d1} + L_{d2} + L_{add}). \tag{5.14}$$

5.2 Direct Path Interference Suppression Requirements for Bistatic Backscatter Communication System

Conventionally, the frequency of the backscattered signal is similar to that of the signal from the legacy source. Furthermore, both signals utilize the same spectrum [28].

Therefore, one of the key research questions for bi-static AmBC is the need to distinguish between the backscattered signal and the direct path signal (i.e. the signal from the legacy source) by the receiver.

As both the direct path and backscattered signals travel to the receiver via different paths, the receiver design has to ensure that the significantly weaker backscattered signal can be differentiated by the receiver. The schematic diagram of this is shown in Fig. 5.1. This is because the signal from the legacy source has a much higher amplitude in comparison to the backscattered signal. As both these signals impinge on the receiver simultaneously, the receiver design for this kind of system is challenging. If the direct path signal from the legacy source is not suppressed in the analog domain before the automatic gain control (AGC) unit and the analog-to-digital converter (ADC), the higher bits of the digital signal are dominated by the signal from the legacy source. Therefore, the backscattered signal occupies the least significant bits of the digital signal.

For instance, if the receiver has a 12-bit resolution, the largest amplitude is quantized in approximately the 10^{th} bit when the gain of the AGC loop is adjusted. Consequently, the average signal is quantized in approximately the 6^{th} bit. Therefore, the backscatter signal is represented in the least significant bit of the ADC output if the amplitude difference between these two signals exceeds 30 dB. Thus, the signal processing techniques become ineffectual as such a low SNR operation easily reaches the SNR wall [63]. Therefore, the effect of the direct path signal from the legacy source needs to be suppressed and is a prime requirement in the design of receivers for backscatter communications. This has to be incorporated into the system design to ensure seamless connectivity.

The difference between the strongest (legacy) signal and the weakest (backscattered) signal is termed the dynamic range of the system. The receiver must be able to operate such that a range of signals can be handled by the receiver. This ensures an improvement in the data rate and/or the range of the system. Increasing the resolution of the receiver is one of the basic solutions. However, this is especially expensive for systems having a requirement for high speed.

Analog domain suppression techniques can be utilized if some differences between the signals may be exploited. For a receiver with multiple antennas, the directional difference between the antennas can be utilized to distinguish between the signals [17]. Analog filtering can be utilized where the signal can be shifted to another fre-

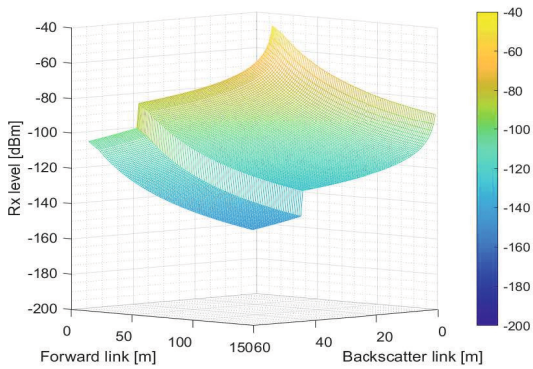

Figure 5.2 The coverage of bi-static backscatter systems at LOS and NLOS scenarios for different combinations of the forward link and backscatter link at 200 MHz.

quency band by the BD [64]. Lastly, if the system is able to operate with differently polarized signals, the polarization difference between them can be utilized to suppress the signal from the legacy source [43]. Nevertheless, irrespective of the technique utilized, the power difference between the direct path and the backscattered signal needs to be inspected in detail.

In order to determine the amount of signal that needs to be suppressed, certain steps were followed. Primarily, the objective was to determine the feasibility of the received signal strength (RX_{level}) at different locations in comparison with conventional IoT technologies such as LoRa backscatter and NB-IoT. The receiver sensitivity of LoRa backscatter and NB-IoT were documented as −149 dBm and −141 dBm, respectively [53, 62]. Therefore, these values were utilized as the threshold values in the subsequent analysis.

Fig. 5.2 shows the coverage over the LOS and NLOS regions at 200 MHz frequency. The simulations were performed for 0 m – 150 m in the forward link ($d1$) and 0 m – 60 m in the backscatter link ($d2$). Based on the receiver sensitivity of the LoRa backscatter technology, it was observed that the signal can be heard at the receiver at a distance of 210 m. Here, the forward link (150 m) and the backscatter link (60 m) have maximum values based on the set simulation criteria. However, when the receiver sensitivity of NB-IoT is considered, the range of communication for the forward link reduces to 115 m (when the backscatter link is kept constant at 60 m). Conversely, the coverage in the backscatter link shrinks to 45 m if the forward link is extended to 150 m. Furthermore, it can be observed that the signal level degrades rapidly when moving from the LOS to the NLOS region. This phenomenon is true

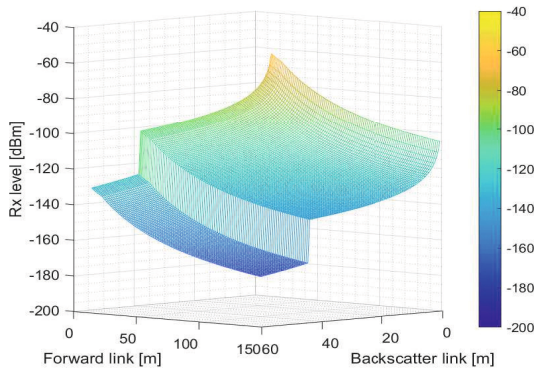

Figure 5.3 The coverage of bi-static backscatter systems at LOS and NLOS scenarios for different combinations of the forward link and backscatter link at 500 MHz.

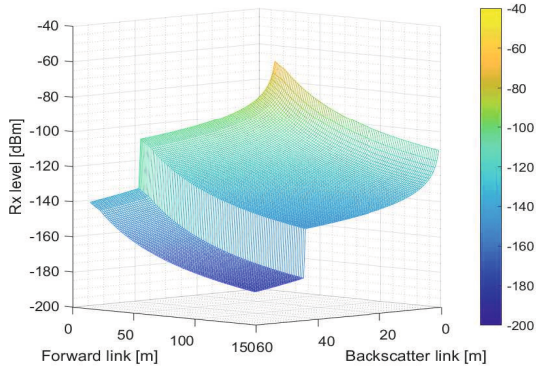

Figure 5.4 The coverage of bi-static backscatter systems at LOS and NLOS scenarios for different combinations of the forward link and backscatter link at 700 MHz.

at every carrier frequency utilized in the simulations.

In Fig. 5.3 it can be observed that although there is proper coverage in the LOS region, the coverage in the NLOS region is reduced at the carrier frequency of 500 MHz. When the RX_{level} of LoRa is considered, the maximum achievable distance in the forward link and the backscatter link is 62 m and 44 m, respectively. The distance in the forward link (42 m) is further reduced when compared with the RX_{level} of the NB-IoT technology (when the coverage distance in the backscatter link is 44 m). There can be different combinations where the forward link has a longer communication range with the reduction of the distance in the backscatter link. However, one of the key ideas of this work was to enable longer backscatter link distances.

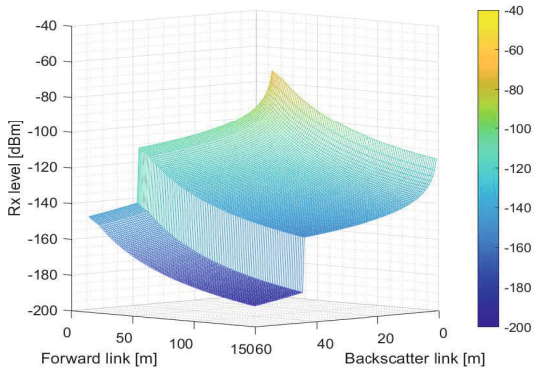

Figure 5.5 The coverage of bi-static backscatter systems at LOS and NLOS scenarios for different combinations of the forward link and backscatter link at 900 MHz.

At 700 MHz, it can be observed that the range of communication in the NLOS region is about 30 m in the forward link when the backscatter link is 60 m. This is when the RX_{level} of the LoRa backscatter system is considered. When the RX_{level} of the NB-IoT system is considered, the distance in the forward link reduces to 17 m when the backscatter link distance is still 60 m. However, it is observed that there is coverage in the complete LOS region at 700 MHz carrier frequency. Fig. 5.4 shows the RX_{level} for different combinations of the forward and backscatter links at 700 MHz.

From Fig. 5.5 it is quite evident that at 900 MHz carrier frequency, only short-range LOS communications are possible. Therefore, 900 MHz is unsuitable for long-range IoT communications even when compared to systems with very good receiver sensitivity such as LoRa and NB-IoT.

Subsequently, the dynamic range of bi-static AmBC systems is studied at different carrier frequencies. At 200 MHz, the dynamic range varies between 14 dB and 47 dB in the LOS region whereas the value is between 61.5 dB and 74 dB in the NLOS region. This can be observed from Fig. 5.6. In Fig. 5.7, the dynamic range of the bi-static backscatter system at 500 MHz is shown. It can be observed that the dynamic range in the LOS varies between approximately 20 dB and 58 dB. The dynamic range in the NLOS region varies between approximately 60 dB and 80 dB depending on the forward and backscatter link distances.

At the carrier frequency of 700 MHz, the dynamic range in the LOS region varies between 24 dB and 60 dB. The variation in the dynamic range in the NLOS region is between 68 dB and 92 dB. This can be observed from Fig. 5.8. Finally, from

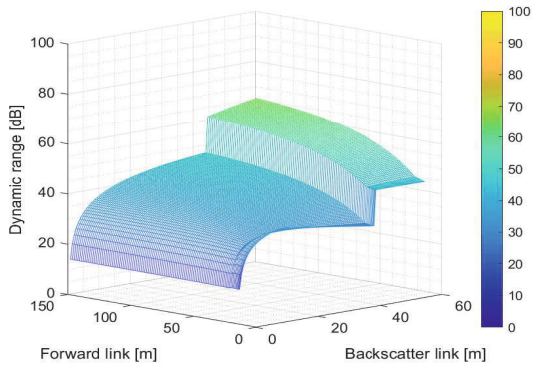

Figure 5.6 The dynamic range (in dB) of bi-static backscatter systems at 200 MHz.

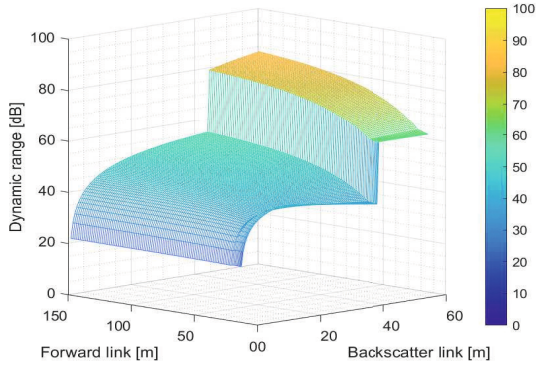

Figure 5.7 The dynamic range (in dB) of bi-static backscatter systems at 500 MHz.

Fig. 5.9, it can be observed that the dynamic range at 900 MHz in the LOS region varies between 24 dB and 60 dB. In the NLOS region, the dynamic range varies between 76 dB and 96 dB.

It was observed that the dynamic range increases with the increase in carrier frequency. Furthermore, as discussed previously, for practical AmBC systems the threshold for the dynamic range is 30 dB. This signifies that the dynamic range needs to be maintained below this particular value in order to accurately decode the signal bits. From the coverage results, it was observed that AmBC systems operating at only the 200 MHz carrier frequency can be deployed for practical purposes. Furthermore, after analyzing the results in Fig. 5.2 and Fig. 5.6 it can be concluded that at 200 MHz carrier frequency, the dynamic range is more of a limiting factor than the coverage. Therefore, interference suppression has to be performed by previously mentioned techniques or any other method in order to mitigate the effects

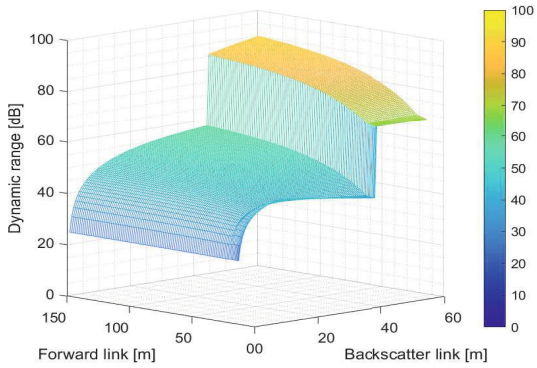

Figure 5.8 The dynamic range (in dB) of bi-static backscatter systems at 700 MHz.

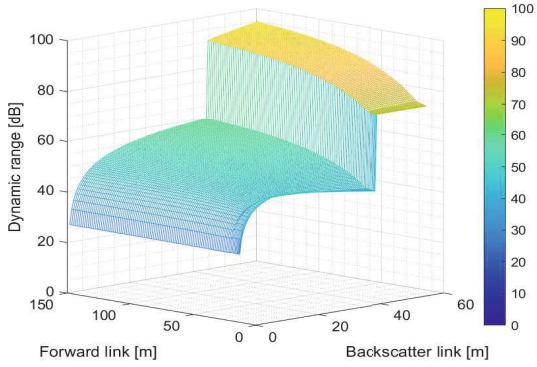

Figure 5.9 The dynamic range (in dB) of bi-static backscatter systems at 900 MHz.

of the direct path signal (from the legacy source) and properly receive and decode the backscattered signal.

5.3 Interference Analysis of Bi-static Backscatter Communication System: Two Backscatter Devices

Another important research question about bi-static AmBC systems was the effect of the introduction of a similar BD into the environment. In general, it is envisioned that there will be multiple BDs present in a practical environment. Each of these devices can perform a set of pre-defined functions independent of the other.

The ambient signal in the presence of a single BD follows two major paths toward the receiver. Firstly, the signal is backscattered (by the BD) and reaches the receiver

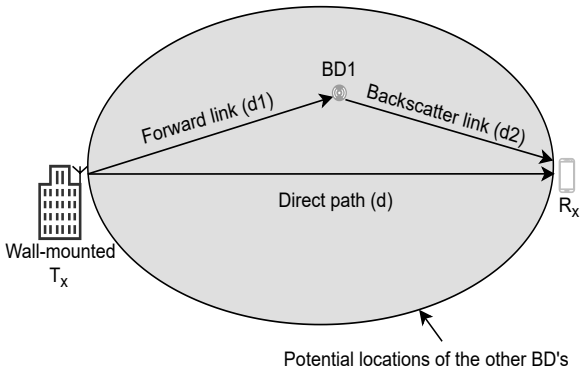

Figure 5.10 Environment for bi-static AmBC systems in the presence of BD_1. The potential location of BD_2 (in the simulations) is assumed to be anywhere in the shaded region.

which is termed the backscattered signal. The other is the direct path signal between the TX and the RX. These two signal paths are shown in Fig. 5.10. As discussed in Section 5.2 the impact of the direct signal from the TX is studied and certain interference suppression techniques are suggested so that the backscattered signal can be heard by the RX. The direct path signal is not considered in the following simulations and analysis.

However, with the introduction of a second BD (referred to as BD_2 henceforth), the ambient signal can follow multiple paths between the TX and RX. The location of the BD_2 can be anywhere in the shaded region of Fig. 5.10. The two strongest signals follow the path via the first BD (referred to as BD_1 from now on) to the RX and the path via the BD_2 to the RX. Furthermore, there may be a "ping-pong" phenomenon where the signal experiences multiple bounces between the BD_1 and the BD_2 before eventually reaching the RX. Therefore, multiple combinations for the ping-pong effect need to be analyzed to determine how the signal is affected by each bounce. The effects of self-interference (SI) and cross-interference (CI) are studied in detail in this study.

After the introduction of the BD_2 in the environment (as depicted in the shaded region of Fig. 5.10), the SI and CI were determined. The three main interference-causing paths are:

- TX $\rightarrow$ BD_2 $\rightarrow$ RX.
- TX $\rightarrow$ BD_2 $\rightarrow$ BD_1 $\rightarrow$ RX.
- TX $\rightarrow$ BD_1 $\rightarrow$ BD_2 $\rightarrow$ RX.

The interference caused due to the presence of the BD_2 is classified as SI or CI based on the signal path between the two BDs. The CI is caused by the ambient signal first impinging on the BD_2. The first two aforementioned paths contribute to the cross-interference. The third path where the ambient signal first impinges on the BD_1 and travels to the RX after impinging on the BD_2 is classified as the self-interference. The SI and CI are computed separately to determine their individual effects on the system. However, the sum of all these three interference-causing paths contributes to the total interference (P_i) experienced by the system due to the presence of BD_2. The SINR of the system is determined by utilizing Eq. 5.15,

$$\mathrm{SINR} = \frac{P_\mathrm{rx}}{P_\mathrm{n} + P_\mathrm{i}}, \tag{5.15}$$

where the terms P_rx and P_n represent the received signal strength and the thermal noise power of the system.

Furthermore, the signal can experience a ping-pong effect where the signal can bounce multiple times between the two BDs. For example, the ping-pong path can be represented by TX $\rightarrow$ BD_1 $\rightarrow$ BD_2 $\rightarrow$ BD_1 $\rightarrow$ RX. This ping-pong effect also contributes to the total interference and is therefore studied in the analysis.

The simulation parameters utilized to determine the impact of the presence of BD_2 are similar to the parameters described in Section 5.1.3. However, based on the previous research as discussed in Section 5.2, it was determined that the 200 MHz carrier frequency band was the most suitable for bi-static AmBC. The other three carrier frequency bands that were studied were limited due to both the coverage and the dynamic range. Therefore, the simulations in this study were performed at only the 200 MHz carrier frequency. The other simulation parameters utilized were similar to the parameters explained in Table 5.1.

Initially, the SNR was determined in the presence of the BD_1 in the simulation environment. It was observed that regions in the proximity of the TX and RX have a better SNR in comparison to other parts of the environment. Moreover, the likely use cases require the AmBC sensors (or, BDs) to be located close to the RX. Thus, the location of BD_1 was fixed at a distance of 10λ or 15 m. The SNR at this distance was calculated to be 18.9 dB. The SNR at different locations within the environment is shown in Fig. 5.11.

The introduction of the BD_2 causes the ambient signal to follow multiple paths between the TX and the RX. The cross-interference is caused due to the ambient

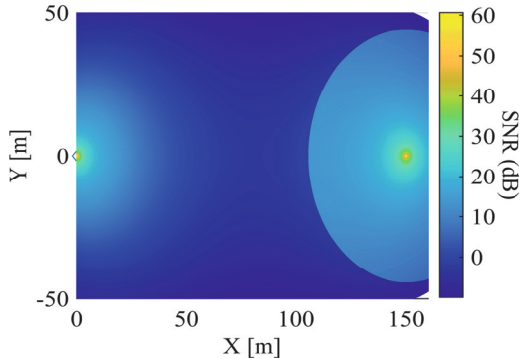

Figure 5.11 The SNR when the BD_1 is located 10λ or 15 m away from the RX.

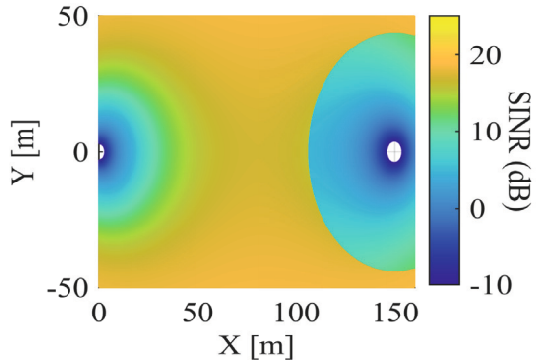

Figure 5.12 The total cross interference (CI) due to the presence of the BD_2.

signal impinging on the BD_2 first. It was observed from Fig. 5.12 that the SINR at the RX was less than -10 dB. In addition, the SINR close to the TX also had a similar value. Fig. 5.12 shows the effect of the total cross interference on the SINR at different locations within the environment. Furthermore, from the simulations, it was observed that the signal strength drops sharply when the BD_2 was located in proximity to the TX/RX. However, the signal path that contributes to the significant amount of CI is TX $\rightarrow$ BD_2 $\rightarrow$ RX. The effect of the interference can be averted by using a successive interference canceller (SIC) at the RX. The utilization of SIC provides user fairness and better system efficiency than orthogonal multiple access (OMA). Furthermore, the utilization of SIC ensures enhancement for non-orthogonally multiplexed users with dissimilar channel conditions [31].

The result obtained after SIC is performed is shown in Fig. 5.13. The CI caused by the path TX $\rightarrow$ BD_2 $\rightarrow$ BD_1 $\rightarrow$ RX, is only significant when the BD_2 is located

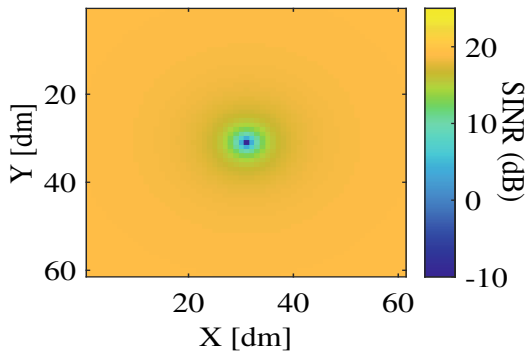

Figure 5.13 The CI after the SIC is performed at the receiver.

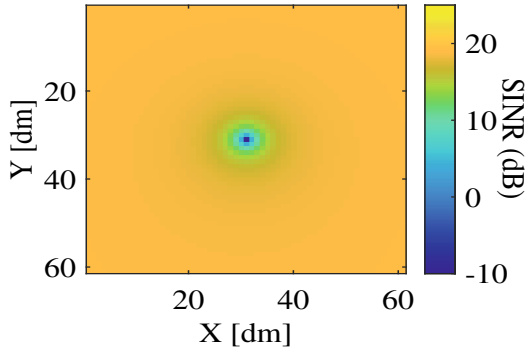

Figure 5.14 The self-interference (SI) at BD_1 in the presence of BD_2.

in proximity of the BD_1. Therefore, if the effect of the dominant component may be mitigated by the utilization of SIC, the total effect of CI can be alleviated by placing the BD_1 and BD_2 1λ meter away from each other.

The self-interference is caused due to the ambient signal impinging first on the BD_1. It was observed that the SI is noticeable when the BD_2 is located in proximity to the BD_1 or the RX. However, if the BD_2 is positioned 1λ meter away from the BD_1 or the RX the effects of the SI can be avoided. Fig. 5.14 and Fig. 5.15 illustrates the effect of the SI near the BD_1 and RX, respectively.

Furthermore, the cumulative distribution function (CDF) of the SI and CI are shown in Fig. 5.16. The SI is the most significant near the BD_1 and the RX. Therefore, the interference power levels are computed only for those locations. The interference power due to the CI is computed for the entire environment. It can be observed from Fig. 5.16 that the CI has a much higher impact than the SI. This is

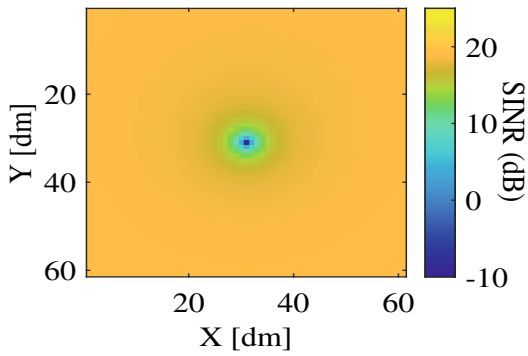

Figure 5.15 The self-interference (SI) at the RX in the presence of BD_2.

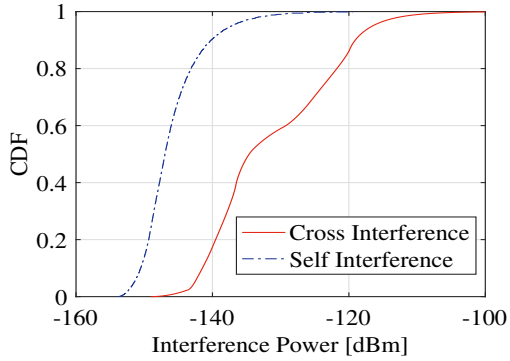

Figure 5.16 The cumulative distribution function (CDF) of the self-interference and cross-interference power levels (in dBm) for different scenarios.

due to the TX $\rightarrow$ BD_2 $\rightarrow$ RX path which causes the most significant interference to the system. Therefore, SIC at the RX is very necessary in order to mitigate the effects of CI in the bi-static AmBC system. The other effects due to the SI can be avoided by placing the BD_2 approximately 1λ meter away from the BD_1 and/or the RX.

6 CONCLUSIONS

The objective of this thesis was to evaluate the coverage, capacity, and interference aspects of AmBC in outdoor environments. The AmBC technology utilizes ambient RF signals originating from different sources to communicate between the TX, BD, and RX. AmBC systems may operate in either the mono-static or bi-static modes. In mono-static AmBC, the TX/RX are positioned at the same location. Thus, the ambient signal travels from the TX antenna, impinges on the BD, and then is reflected back toward the RX. Thus, mono-static AmBC is envisioned to provide support for BDs utilized for monitoring purposes. In bi-static AmBC systems, the ambient signal propagates from the TX antenna impinges on the BD, and then is forwarded toward the RX. Therefore, bi-static AmBC is foreseen to provide the end user with information that can be decoded at the RX module.

6.1 Summary

The studies performed in [P1, P2] were focused on determining the maximum achievable range of communication for AmBC systems. The findings of the work are summarized in Chapter 3. Ambient FM radio signals operating at 100 MHz were utilized in the simulations performed in articles [P1, P2]. FM radio technology is readily available worldwide and the low frequency of operation enables longer communication ranges in comparison to other radio technologies. In Section 3.5, the power budget for bi-static AmBC was calculated and studied to analyze the possibility of wide-area backscatter communications utilizing ambient FM radio signals. It was observed that there was a significant amount of signal strength available for the ambient FM signal to travel toward the RX after impinging on the sensor. The dynamic range of the system was also evaluated so that there was no hindrance caused by the direct path signal from the FM radio tower. In Section 3.6, the mono-static mode of operation of AmBC was studied to determine the maximum achievable

range of communication utilizing ambient FM radio signals. It was observed that the sensor having a minimum cross-section of 47 cm×47 cm needs to be utilized to establish communication. This was because the cross-section of the BD was a significant limiting factor in comparison to the wavelength of the signal. In comparison with previous research, it was observed that significantly longer communication distances could be achieved by utilizing ambient FM radio broadcast signals.

Chapter 4 is a summary of the articles [P3, P4, P5] where ambient signals from cellular base stations are utilized in the simulations. The mono-static mode of operation of AmBC is studied in Chapter 4. In Section 4.4, ambient low-frequency cellular signals from LTE-700 base stations are utilized to perform the simulations. It was observed that communication ranges of a few hundred meters could be established in the urban and suburban environments based on the additional loss experienced by the ambient signal in the respective environment. Therefore, based on the simulation results, it could be concluded that ambient low-frequency cellular signals could be utilized for AmBC systems.

In order to determine the applicability of 5G as an ambient signal for backscattering communications, signals operating at 3.5 GHz and 26 GHz were utilized for the simulations in Section 4.5. The simulations were performed in the urban macrocell and small cell deployment scenarios. Depending on the bandwidth of the 5G signal, different communication ranges could be achieved. It was also observed that the range of communication was significantly dependent on the cross-section of the BD. Furthermore, the achievable range of communication increases with the increase in the cross-section of the BD. Based on the results it could be concluded that ambient 5G signals operating at 3.5 GHz can only be utilized for short-range communications. Moreover, the communication range shrinks further when ambient 5G signals operating at the carrier frequency of 26 GHz are utilized in the simulations. Therefore, ambient 5G signals can only be utilized by mono-static AmBC systems if the backscatter devices are located in the proximity of the TX/RX.

As part of the previous studies in Section 4.4 and Section 4.5, the network was assumed to operate under ideal circumstances or, in other words, when the cell was unloaded. In Section 4.6 the effect of the interference from the adjacent cell in a heavily loaded cellular network was studied. It was observed that the adjacent cell interference was a major limiting factor during the peak hours. Additionally, it was determined that there was about a 44 percent reduction in coverage during peak

hours in comparison to non-peak hours due to the interference caused by the signal from the adjacent cell. Therefore, to mitigate the impact of the interfering signal from the adjacent cell, the backscatter devices would need to be located in the proximity of the TX/RX to provide uninterrupted connectivity for mono-static AmBC systems.

In articles [P6, P7], different aspects of bi-static AmBC systems are studied and the results are summarized in Chapter 5. In previous research, the effect of the interference caused by the direct path signal on bi-static AmBC systems from the legacy source was not examined. In Section 5.2, the coverage of bi-static AmBC systems is studied in comparison with typical IoT technologies such as NB-IoT and LoRa. Ambient sub-1 GHz signals were utilized in the simulations. It was observed that only the 200 MHz carrier frequency could be utilized for bi-static AmBC. Subsequently, the interference suppression requirement of the direct path component from the legacy source was studied. It was observed that the dynamic range of the system is a significant limiting factor in the coverage of bi-static AmBC systems.

In Section 5.3 the interference caused due to the presence of a second backscatter device in the environment is studied. The second BD causes a ping-pong effect with the first BD and this results in the attenuation of the ambient signal. The ping-pong effect is significant when the second BD is located in proximity to the first BD or the RX. The impact caused because of the ping-pong effect can be mitigated if the second BD is located one wavelength meter away from the first BD or the RX.

6.2 Discussion and Future Work

It is a well-known fact that the sensors/BDs utilized for IoT can also be deployed in indoor environments. The propagation of RF signals into the indoor environment especially from the outdoor environment is limited due to the significant amount of attenuation experienced by the signal. This is mainly due to the high penetration loss experienced by the signal due to the different kinds of building materials utilized for the construction of shopping malls, offices, and bus/stain stations. Therefore, the utilization of the ambient signals from the outdoor environment is not very useful as the strength of the signal is significantly weaker for the BDs. Therefore, studies utilizing dominant indoor ambient signals such as Wi-Fi may be conducted to study the feasibility of AmBC in such environments. The analysis must include the

high path loss experienced by the ambient signal while propagating between different cabins or rooms in an indoor environment.

The propagation of the ambient signal from the outdoor to the indoor environment may also be possible with the utilization of reflective intelligent surfaces (RIS). The research on backscattering communications has taken a significant step forward with the advancement in RIS technology. The utilization of RIS can enable the improvement in the performance of wireless systems.

The fusion of ambient backscattering communications with RIS presents several compelling advantages. Firstly, it offers the potential for low-power, even battery-free communication, given that devices do not need to generate their own RF signals. Secondly, by smartly re-configuring the wireless environment, RIS can further enhance the efficiency of backscatter communication, ensuring more reliable data transfer. Moreover, this integration can lead to more extensive coverage areas for backscatter devices, opening up new avenues for IoT deployments and other low-power applications. The amalgamation of ambient backscattering with RIS offers a transformative approach to wireless communication: making environments smarter and more energy-efficient, heralding a new era in the domain of wireless networking.

REFERENCES

[1] 3GPP. *Study on channel model for frequencies from 0.5 to 100 GHz*. Technical Report (TR) 38.901. Version 14.3.0. 3rd Generation Partnership Project (3GPP), Dec. 2017.

[2] Md Maruf Ahamed and Saleh Faruque. "5G Network Coverage Planning and Analysis of the Deployment Challenges". In: *Sensors* 21.19 (2021). ISSN: 1424-8220. DOI: 10.3390/s21196608. URL: https://www.mdpi.com/1424-8220/21/19/6608.

[3] Kyei Anim, Jung-Nam Lee, and Young-Bae Jung. "High-Gain Millimeter-Wave Patch Array Antenna for Unmanned Aerial Vehicle Application". In: *Sensors* 21.11 (2021). ISSN: 1424-8220. DOI: 10.3390/s21113914. URL: https://www.mdpi.com/1424-8220/21/11/3914.

[4] Luigi Atzori, Antonio Iera, and Giacomo Morabito. "The Internet of Things: A Survey". In: *Computer Networks* (Oct. 2010), pp. 2787–2805. DOI: 10.1016/j.comnet.2010.05.010.

[5] D.K. Barton et al. *Radar Evaluation Handbook*. Radar Library. Artech House, 1991. ISBN: 9780890064887.

[6] Dinesh Bharadia et al. "BackFi: High Throughput WiFi Backscatter". In: *SIGCOMM Comput. Commun. Rev.* 45.4 (Aug. 2015), pp. 283–296. ISSN: 0146-4833. DOI: 10.1145/2829988.2787490.

[7] Ritayan Biswas and Jukka Lempiäinen. "Assessment of 5G as an ambient signal for outdoor backscattering communications". In: *Wireless Networks 27* (Aug. 2021). DOI: 10.1007/s11276-021-02731-x.

[8] Ritayan Biswas and Jukka Lempiäinen. "Sensitivity Analysis of Ambient Backscattering Communications in Heavily Loaded Cellular Networks". In: *2023 18th Wireless On-Demand Network Systems and Services Conference (WONS)*. 2023, pp. 51–55. DOI: 10.23919/WONS57325.2023.10062021.

[9] Ritayan Biswas, Joonas Säe, and Jukka Lempiäinen. “Evaluation of Maximum Range for Backscattering Communications Utilising Ambient FM radio signals”. In: *2022 International Balkan Conference on Communications and Networking (BalkanCom)*. 2022, pp. 142–146. DOI: 10.1109/BalkanCom55633.2022.9900759.

[10] Ritayan Biswas, Joonas Säe, and Jukka Lempiäinen. “Maximum Receiver Harvesting Area of Backscatter Signals from Ambient Low-Frequency Mobile Networks”. In: *2021 IEEE Global Communications Conference (GLOBECOM)*. 2021, pp. 1–5. DOI: 10.1109/GLOBECOM46510.2021.9685741.

[11] Ritayan Biswas, Joonas Säe, and Jukka Lempiäinen. “Power Budget for Wide Area Ambient Backscattering Communications”. In: *2018 IEEE Vehicular Networking Conference (VNC)*. 2018, pp. 1–6. DOI: 10.1109/VNC.2018.8628465.

[12] Ritayan Biswas et al. “Direct Path Interference Suppression Requirements for Bistatic Backscatter Communication System”. In: *2021 IEEE 93rd Vehicular Technology Conference (VTC2021-Spring)*. 2021, pp. 1–5. DOI: 10.1109/VTC2021-Spring51267.2021.9448755.

[13] Ritayan Biswas et al. “Interference Analysis of Bi-static Backscatter Communication System: Two Backscatter Devices”. In: *2021 IEEE International Conference on RFID Technology and Applications (RFID-TA)*. 2021, pp. 85–88. DOI: 10.1109/RFID-TA53372.2021.9617234.

[14] S. H. Choi and D. I. Kim. “Backscatter radio communication for wireless powered communication networks”. In: *2015 21st Asia-Pacific Conference on Communications (APCC)*. Oct. 2015, pp. 370–374. DOI: 10.1109/APCC.2015.7412542.

[15] Donatella Darsena, Giacinto Gelli, and Francesco Verde. “Modeling and Performance Analysis of Wireless Networks With Ambient Backscatter Devices”. In: *IEEE Transactions on Communications* 65.4 (2017), pp. 1797–1814. DOI: 10.1109/TCOMM.2017.2654448.

[16] Spyridon N. Daskalakis et al. “Low Cost Ambient Backscatter for Agricultural Applications”. In: *2019 IEEE-APS Topical Conference on Antennas and Propagation in Wireless Communications (APWC)*. 2019, pp. 201–201. DOI: 10.1109/APWC.2019.8870568.

[17] R. Duan et al. “Hybrid Beamformer Design for High Dynamic Range Ambient Backscatter Receivers”. In: *2019 IEEE International Conference on Communications Workshops (ICC Workshops)*. 2019, pp. 1–6. DOI: 10.1109/ICCW.2019.8757120.

[18] Ruifeng Duan et al. “Ambient Backscatter Communications for Future Ultra-Low-Power Machine Type Communications: Challenges, Solutions, Opportunities, and Future Research Trends”. In: *IEEE Communications Magazine* 58.2 (2020), pp. 42–47. DOI: 10.1109/MCOM.001.1900464.

[19] Ericsson white paper. *Advanced antenna systems for 5G networks*. URL: https://www.ericsson.com/en/reports-and-papers/white-papers/advanced-antenna-systems-for-5g-networks.

[20] European Telecommunications Standards Institute (ETSI). *Base Station (BS) radio transmission and reception (3GPP TS 38.104 version 15.10.0 Release 15)*. July 2020.

[21] European Telecommunications Standards Institute (ETSI). *ETSI TR 138 913 V14.3.0 (2017-10), 5G; Study on scenarios and requirements for next generation access technologies (3GPP TR 38.913 version 14.3.0 Release 14)*. Jan. 2023. URL: https://www.etsi.org/deliver/etsi_tr/138900_138999/138913/14.03.00_60/tr_138913v140300p.pdf.

[22] Klaus Finkenzeller. *RFID handbook: fundamentals and applications in contactless smart cards, radio frequency identification and near-field communication*. John wiley & sons, 2010.

[23] Finnish Transport and Communications Agency. *Radio stations in Finland*. URL: https://www.traficom.fi/en/communications/tv-and-radio/radio-stations-finland.

[24] Andrea Goldsmith. *Wireless Communications*. USA: Cambridge University Press, 2005. ISBN: 0521837162.

[25] J. D. Griffin and G. D. Durgin. “Complete Link Budgets for Backscatter-Radio and RFID Systems”. In: *IEEE Antennas and Propagation Magazine* 51.2 (Apr. 2009), pp. 11–25. ISSN: 1045-9243. DOI: 10.1109/MAP.2009.5162013.

[26] H.D. Griffiths. “From a different perspective: principles, practice and potential of bistatic radar”. In: *2003 Proceedings of the International Conference on Radar (IEEE Cat. No.03EX695)*. 2003, pp. 1–7. DOI: 10.1109/RADAR.2003.1278701.

[27] Wolfgang Gruel and Joseph Stanford. “Assessing the Long-term Effects of Autonomous Vehicles: A Speculative Approach”. In: *Transportation Research Procedia* 13 (Dec. 2016), pp. 18–29. DOI: 10.1016/j.trpro.2016.05.003.

[28] H. Guo et al. “Cooperative Ambient Backscatter System: A Symbiotic Radio Paradigm for Passive IoT”. In: *IEEE Wireless Communications Letters* 8.4 (2019), pp. 1191–1194. DOI: 10.1109/LWC.2019.2911500.

[29] C. J. Hansen. “WiGiG: Multi-gigabit wireless communications in the 60 GHz band”. In: *IEEE Wireless Communications* 18.6 (2011), pp. 6–7.

[30] Chen He et al. “Monostatic MIMO Backscatter Communications”. In: *IEEE Journal on Selected Areas in Communications* 38.8 (2020), pp. 1896–1909. DOI: 10.1109/JSAC.2020.3000823.

[31] Kenichi Higuchi and Anass Benjebour. “Non-orthogonal Multiple Access (NOMA) with Successive Interference Cancellation for Future Radio Access”. In: *IEICE Transactions on Communications* E98.B.3 (2015), pp. 403–414. DOI: 10.1587/transcom.E98.B.403.

[32] P.E. Howland, D. Maksimiuk, and Gjalt Reitsma. “FM radio based bistatic radar”. In: *Radar, Sonar and Navigation, IEE Proceedings* - 152 (July 2005), pp. 107–115. DOI: 10.1049/ip-rsn:20045077.

[33] ITU-R. *Propagation data and prediction methods for the planning of short-range outdoor radio communication systems and radio local area networks in the frequency range 300 MHz to 100 GHz*. Recommendation ITU-R P.1411-10. International Telecommunication Union (ITU), Aug. 2009.

[34] Furqan Jameel, Imran Khan, and Byung Lee. “Simultaneous harvest-and-transmit ambient backscatter communications under Rayleigh fading”. In: *EURASIP Journal on Wireless Communications and Networking* 2019 (June 2019). DOI: 10.1186/s13638-019-1480-7.

[35] Sujata Joshi et al. “Developing Smart Cities: An Integrated Framework”. In: *Procedia Computer Science* 93 (Dec. 2016), pp. 902–909. DOI: 10.1016/j.procs.2016.07.258.

[36] Volker Jungnickel et al. “The role of small cells, coordinated multipoint, and massive MIMO in 5G”. In: *IEEE Communications Magazine* 52.5 (2014), pp. 44–51. DOI: 10.1109/MCOM.2014.6815892.

[37] H. Srikanth Kamath, Humdard Singh, and Aayush Khanna. “Carrier Aggregation in LTE”. In: *2020 4th International Conference on Intelligent Computing and Control Systems (ICICCS)* (2020), pp. 135–138.

[38] Bryce Kellogg et al. “Wi-fi Backscatter: Internet Connectivity for RF-powered Devices”. In: *SIGCOMM Comput. Commun. Rev.* 44.4 (Aug. 2014), pp. 607–618. ISSN: 0146-4833. DOI: 10.1145/2740070.2626319.

[39] Jaimon Kelly et al. “The Internet of Things: impact and implications for healthcare delivery (Preprint)”. In: *Journal of Medical Internet Research* 22 (May 2020). DOI: 10.2196/20135.

[40] Sachin Kumar, Prayag Tiwari, and Mikhail Zymbler. “Internet of Things is a revolutionary approach for future technology enhancement: a review”. In: *Journal of Big Data* 6 (Dec. 2019). DOI: 10.1186/s40537-019-0268-2.

[41] Erik G. Larsson et al. “Massive MIMO for next generation wireless systems”. In: *IEEE Communications Magazine* 52.2 (2014), pp. 186–195. DOI: 10.1109/MCOM.2014.6736761.

[42] J. Lempiäinen and M. Manninen. *Radio Interface System Planning for GSM/GPRS/UMTS*. Springer US, 2010. ISBN: 9781441949141. URL: https://books.google.fi/books?id=JKRZcgAACAAJ.

[43] J. Lietzén et al. “Polarization Conversion-Based Ambient Backscatter System”. In: *IEEE Access* 8 (2020), pp. 216793–216804. DOI: 10.1109/ACCESS.2020.3042018.

[44] Qiang Liu et al. “Ambient backscatter communication-based smart 5G IoT network”. In: *EURASIP Journal on Wireless Communications and Networking* 2021 (Feb. 2021). DOI: 10.1186/s13638-021-01917-3.

[45] Vincent Liu et al. “Ambient Backscatter: Wireless Communication out of Thin Air”. In: *SIGCOMM Comput. Commun. Rev.* 43.4 (Aug. 2013), pp. 39–50. ISSN: 0146-4833. DOI: 10.1145/2534169.2486015.

[46] X. Lu et al. “Ambient Backscatter Assisted Wireless Powered Communications”. In: *IEEE Wireless Communications* 25.2 (Apr. 2018), pp. 170–177. ISSN: 1536-1284. DOI: 10.1109/MWC.2017.1600398.

[47] Arumugam Manthiram. “An Outlook on Lithium Ion Battery Technology”. In: *ACS Central Science* 3 (Sept. 2017). DOI: 10.1021/acscentsci.7b00288.

[48] Yu Miao et al. “Current Li-Ion Battery Technologies in Electric Vehicles and Opportunities for Advancements”. In: *Energies* 12 (Mar. 2019), pp. 1074–1094. DOI: 10.3390/en12061074.

[49] P. V. Nikitin et al. “Passive tag-to-tag communication”. In: *2012 IEEE International Conference on RFID (RFID)*. Apr. 2012, pp. 177–184. DOI: 10.1109/RFID.2012.6193048.

[50] Afif Osseiran et al. *5G Mobile and Wireless Communications Technology*. Cambridge university press, June 2016. ISBN: 9781107130098. DOI: 10.1017/CBO9781316417744.

[51] Aaron Parks et al. “Turbocharging ambient backscatter communication”. In: *ACM SIGCOMM Computer Communication Review* 44 (Aug. 2014). DOI: 10.1145/2619239.2626312.

[52] Amir Rahmani, Suleyman Bayramov, and Behnam Kiani Kalejahi. “Internet of Things Applications: Opportunities and Threats”. In: *Wireless Personal Communications* 122 (Jan. 2022). DOI: 10.1007/s11277-021-08907-0.

[53] R. Ratasuk et al. “Overview of narrowband IoT in LTE Rel-13”. In: *2016 IEEE Conference on Standards for Communications and Networking (CSCN)*. 2016, pp. 1–7. DOI: 10.1109/CSCN.2016.7785170.

[54] Karen Rose, Scott Eldridge, and Lyman Chapin. “The internet of things: An overview”. In: *The internet society (ISOC)* 80 (2015), pp. 1–50.

[55] Fredrik Rusek et al. “Scaling Up MIMO: Opportunities and Challenges with Very Large Arrays”. In: *IEEE Signal Processing Magazine* 30.1 (2013), pp. 40–60. DOI: 10.1109/MSP.2011.2178495.

[56] Ali M. Saleh, Ngon T. Le, and Abu B. Sesay. "Inter-Cell Interference Coordination Using Fractional Frequency Reuse Scheme in Multi-Relay Multi-Cell OFDMA Systems". In: *2018 IEEE Canadian Conference on Electrical Computer Engineering (CCECE)*. 2018, pp. 1–5. DOI: 10.1109/CCECE.2018.8447574.

[57] Stefania Sesia, Issam Toufik, and Matthew Baker. *LTE, The UMTS Long Term Evolution: From Theory to Practice*. Wiley Publishing, 2009. ISBN: 0470697164.

[58] Mansoor Shafi et al. "5G: A Tutorial Overview of Standards, Trials, Challenges, Deployment, and Practice". In: *IEEE Journal on Selected Areas in Communications* 35.6 (2017), pp. 1201–1221. DOI: 10.1109/JSAC.2017.2692307.

[59] Muhammad Usman Sheikh, Ritayan Biswas, and Jukka Lempiaeinen. "Performance Evaluation of Coordinated Multipoint Transmission at 28 GHz Frequency Using 3D Ray Tracing". In: *2018 IEEE 87th Vehicular Technology Conference (VTC Spring)*. 2018, pp. 1–6. DOI: 10.1109/VTCSpring.2018.8417593.

[60] Beatriz Soret et al. "Interference coordination for dense wireless networks". In: *IEEE Communications Magazine* 53.1 (2015), pp. 102–109. DOI: 10.1109/MCOM.2015.7010522.

[61] H. Stockman. "Communication by Means of Reflected Power". In: *Proceedings of the IRE* 36.10 (Oct. 1948), pp. 1196–1204. ISSN: 0096-8390. DOI: 10.1109/JRPROC.1948.226245.

[62] Vamsi Talla et al. "LoRa Backscatter: Enabling The Vision of Ubiquitous Connectivity". In: *Proceedings of the ACM on Interactive, Mobile, Wearable and Ubiquitous Technologies* 1 (May 2017). DOI: 10.1145/3130970.

[63] R. Tandra and A. Sahai. "SNR Walls for Signal Detection". In: *IEEE Journal of Selected Topics in Signal Processing* 2.1 (2008), pp. 4–17. DOI: 10.1109/JSTSP.2007.914879.

[64] N. Van Huynh et al. "Ambient Backscatter Communications: A Contemporary Survey". In: *IEEE Communications Surveys Tutorials* 20.4 (2018), pp. 2889–2922. DOI: 10.1109/COMST.2018.2841964.

[65] S. Vishnu, S.R. Jino Ramson, and R. Jegan. "Internet of Medical Things (IoMT) - An overview". In: *2020 5th International Conference on Devices, Circuits and Systems (ICDCS)*. 2020, pp. 101–104. DOI: 10.1109/ICDCS48716.2020.243558.

[66] Georgios Vougioukas et al. "Practical Energy Harvesting for Batteryless Ambient Backscatter Sensors". In: *Electronics* 7.6 (2018). ISSN: 2079-9292. DOI: 10.3390/electronics7060095. URL: https://www.mdpi.com/2079-9292/7/6/95.

[67] Gongpu Wang et al. "Ambient Backscatter Communication Systems: Detection and Performance Analysis". In: *IEEE Transactions on Communications* 64.11 (2016), pp. 4836–4846. DOI: 10.1109/TCOMM.2016.2602341.

[68] Gongpu Wang et al. "Uplink Detection and BER Analysis for Ambient Backscatter Communication Systems". In: *2015 IEEE Global Communications Conference (GLOBECOM)*. 2015, pp. 1–6. DOI: 10.1109/GLOCOM.2015.7417704.

[69] R. Weinstein. "RFID: a technical overview and its application to the enterprise". In: *IT Professional* 7.3 (2005), pp. 27–33. DOI: 10.1109/MITP.2005.69.

[70] WiFiUS. *WiFIUS: Collaborative Research: Ambient Re-Scatter Inspired Machine Type Communication for Heterogeneous IoT Systems*. URL: https://panlab.ece.uh.edu/projects/wifius-ars4iot/.

[71] Weiqi Wu et al. "A Survey on Ambient Backscatter Communications: Principles, Systems, Applications, and Challenges". In: *Computer Networks* 216 (July 2022). DOI: 10.1016/j.comnet.2022.109235.

[72] L. Xie et al. "Managing RFID Data: Challenges, Opportunities and Solutions". In: *IEEE Communications Surveys Tutorials* 16.3 (Mar. 2014), pp. 1294–1311. ISSN: 1553-877X. DOI: 10.1109/SURV.2014.022614.00143.

[73] Wei Zhang et al. "A green paradigm for Internet of Things: Ambient backscatter communications". In: *China Communications* 16.7 (2019), pp. 109–119. DOI: 10.23919/JCC.2019.07.009.

PUBLICATIONS

PUBLICATION I

Power Budget for Wide Area Ambient Backscattering Communications

Ritayan Biswas, Joonas Säe, and Jukka Lempiäinen

DOI: 10.1109/VNC.2018.8628465

Power Budget for Wide Area Ambient Backscattering Communications

Ritayan Biswas, Joonas Säe, Jukka Lempiäinen
Laboratory of Electronics and Communications Engineering, Tampere University of Technology
Tampere, Finland
Email: {ritayan.biswas, joonas.sae, jukka.lempiainen}@tut.fi

***Abstract*—The objective of this article is to extend the range of Ambient Backscattering Communications (ABC). The ABC technology is a key enabling technology for Internet of Things (IoT) wireless communications. A rural open area towards Hanko, Finland is considered for the power budget calculations. FM radio waves are considered as the source of ambient RF waves as the FM radio waves have long communication range and the technology is readily available worldwide. The sensors are placed on a highway at an example distance of 30 km from the FM transmitter. There is a clear line of sight (LOS) connection between the FM transmitter and the sensors. The path loss is determined based on the sensor locations and the losses at the sensor occur due to diffraction and scattering. A power budget is calculated based on these aforementioned key system parameters. It is observed that there is around 44 dB of power margin available after the signal from the FM transmitter is backscattered (at the sensor) and the losses in the system are accounted for. This indicates that the receiver module is able to detect the signal as it is above the minimum reception level threshold for the system. Therefore, the radio waves are able to propagate further after the signal is backscattered at the sensor(s), utilizing the available power margin. Thus, the range of communication can be extended to a wider area.**

***Index Terms*—IoT, ABC, Power Budget, FM.**

I. Introduction

Ambient backscattering communications (ABC) is a relatively new wireless communication paradigm which enables devices to communicate by utilizing the energy from the ambient RF waves. These RF waves may be generated from a variety of sources such as television broadcasts, FM radio signals, cellular signals and wireless fidelity (WiFi) sources to name a few. The devices that enable ABC communications are small sensor-type elements which can power themselves with the ambient RF waves or be powered by an external source. By utilizing the ABC technology, battery-free devices can communicate between each other by using a technology which serves as the backbone of radio frequency identification (RFID) systems. This technology, termed as radio backscatter establishes communication by reflecting the RF waves. Radio backscatter was originally used during the second World War to determine the identity of different air-crafts. In 1948, Harry Stockman was the first researcher to publish a literature about backscatter communication [1].

Radio backscatter has been comprehensively studied during the last two decades. This was possible due to the fact that the cost of manufacturing integrated circuits (IC's) dropped drastically in the 1990s, leading to the mass development of the RFID technology and supporting devices. Research regarding the channel modelling [2], power budgets [3], coding methods [4] and multiple antennas [5] have been carried out for the RFID technology. Radio backscatter is thought of as a key enabling technology for the sensors used in the internet of things (IoT) wireless communications due to the very low power requirement and the relatively low cost of manufacturing such devices [6]. In classical backscatter systems, the reader radiates a carrier wave which is received by the sensor, relevant information is added and eventually backscattered to the reader. Therefore, systems operating with the classic radio backscatter principle suffer double the path loss. Additionally, RFID systems have very limited range (5-10 m) and the requirement of a dedicated reader has seen very restricted deployment of the technology. However, unlike the RFID technology, there is no requirement for a dedicated reader for devices utilizing the ABC technology.

The communication between two passive RFID sensors was first introduced in [7]. The tags communicate by modulating the field of the carrier signal. The backscattered signal is passed on to other tags which eventually decode the signal in order to retrieve the information [8]. According to Nikitin et al. [8], the strength of the carrier signal determines the passivity of the tag. Consequently, with ambient RF signals powering up the tags, the authors in [8] demonstrated a system where communication can take place between two passive/semi-passive tags.

The ABC concept was first introduced (in 2013) by the researchers in [9]. As part of their research, two devices can communicate between one another by utilizing energy from television broadcast signals. These signals provide the only source of power for these devices. They were able to achieve data rates of $1\,\mathrm{kbps}$ by utilizing their prototypes for ranges of $45.7\,\mathrm{cm}$ in indoor and $76.2\,\mathrm{cm}$ in outdoor environments respectively. [9] Ambient WiFi signals were used in [10] to establish

a two-way communication between the sensors and the WiFi device. This two-way communication was realized by altering the channel state information (CSI) and the received signal strength indicator (RSSI) of the WiFi channel. Therefore, such sensors were able to connect to the internet by utilizing the ambient RF waves. Thus, data rates of $0.5\,\mathrm{kbps}$ in uplink and $20\,\mathrm{kbps}$ in downlink were obtained for ranges of $1\,\mathrm{m}$ and $2.2\,\mathrm{m}$, respectively. The throughput was significantly improved in [11] where data rates of $5\,\mathrm{Mbps}$ and $1\,\mathrm{Mbps}$ are obtained for ranges of $1\,\mathrm{m}$ and $5\,\mathrm{m}$ [11].

Previous research results on ABC have obtained very small communication distances after the signal is backscattered by the sensor element. The typical values from existing research indicate that the communication ranges vary from a few centimeters to tens of meters. The aim of this article is to propose an increase in the range of ABC for wide area environments. The FM radio technology is chosen as the source for ambient RF signals as the longer wavelengths of FM radio waves enable wide area communications. Moreover, there are extensive FM radio networks available in most countries as the FM technology is standardized all over the world. In this paper, the power budget for ABC using the FM radio technology for wide area networks is presented.

II. Theory

A. Ambient Backscattering Communications

ABC sensors works on the principle of transmitting '0' and '1' bits by switching the antenna impedance states [9]. This can be achieved by transitioning between the reflecting and non reflecting states of the antenna. Consequently, the passive sensors can backscatter their own information at lower data rates to enable the receiver from distinguishing between these conventional signals and the ambient signals [9]. The authors in [9] devised a prototype to show the bit-error rate (BER) with respect to the distance for two passive devices communicating using ambient backscatter. In [12], multiple antennas are utilized at the reader (backscatter receiver) in order to receive signals from the sensors. The authors of [12] demonstrate that the increase in the number of antennas at the reader helps in achieving a lower BER.

Contrary to traditional wireless communication systems that use radiation, the ambient RF signal propagates (after backscattering) to the receiver module after scattering or diffracting from the sensor. Sensors utilizing the ABC principle have the necessary hardware to utilize or harvest the energy from the signal from a variety of ambient RF sources. The harvesting of energy from ambient RF signals help in the utilization of sensors which are free from batteries. However, ABC can also be applicable for sensors utilizing an external power source. The deployment of such sensors will enable IoT where sensors will be located at a variety of locations. In IoT, devices are expected to communicate with each other in order to exchange vital information such as real time traffic and weather updates.

The source for the ambient RF signals used for this work are the FM radio waves. The FM radio technology operates in the frequency range of $88\,\mathrm{MHz}$ to $108\,\mathrm{MHz}$ of the electromagnetic spectrum. The radio waves at the $100\,\mathrm{MHz}$ frequency band are utilized for the example power budget calculations. The available bandwidth at $100\,\mathrm{MHz}$ is $1\,\mathrm{kHz}$. The low frequency of operation of FM is the primary reason for choosing this technology as the source for the ambient RF signals. Consequently, the longer wavelengths of FM radio waves help in achieving wider communication ranges as the radio signals are able to propagate for tens of kilometers.

Despite some obvious advantages, some challenges remain in establishing ABC. First of all, extracting the power (for communication) from the ambient RF signal and their subsequent utilization at the sensor will pose a challenge for researchers. Secondly, ABC differs from traditional communications by transmitting '0' and '1'. Therefore, the channels used for the backscattered signal in ABC need to be different in comparison with regular communication technologies. Thirdly, the receiver has to discern between the ambient RF signal and the backscattered signal since the physical properties of the two signals are very similar. Furthermore, the backscattered signal from the sensor will cause interference for traditional communication systems as the two signals possess identical physical properties. Thus, studies need to be carried out in order to determine how the interference to legacy systems can be mitigated. Finally, the dynamic range of the receiver generally indicates the ratio of the strongest and weakest signals that can be decoded by the receiver module. As the received signal strength of the direct signal is greater than the backscattered signal, the dynamic range of the system needs to be studied before the receiver modules for ABC are designed.

B. Environment for ABC wide area communications

Although the communication distances achieved in the existing research are impressive, they are limited to indoor environments and have restricted range in outdoor environments. The reason is that, energy harvested from the ambient RF signals were utilized as the only power source. Fig. 1 is an illustration of the example environment that has been considered for the purpose of this article which enables communications on a wider scale utilizing ABC.

The area considered as an example for the power budget calculation is located near the Hanko region of southern Finland. A FM radio tower is located in the suburb of Kivenlahti, Espoo which serves as the ambient source of signals. The FM transmitter (T_{X} antenna) is located at a height (h_{t}) of $248\,\mathrm{m}$. FM radio waves can

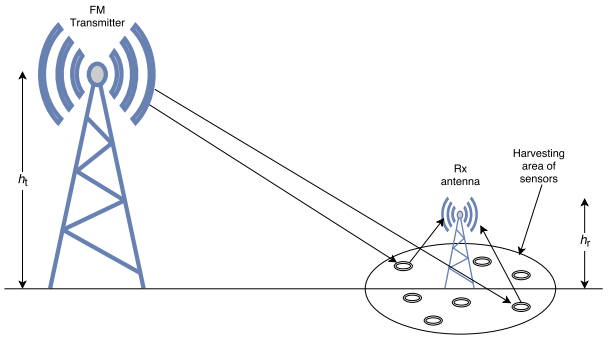

Fig. 1. Illustration of the propagation environment

Fig. 2. Propagation environment as shown in Google Maps.

propagate tens of kilometers due to their large wavelength and is therefore chosen as a source of ambient signals. The area towards Hanko is mainly a straight highway as is shown in the Google map view of the area in Fig. 2. The terrain is slightly undulating but there are no considerable losses due to this topography. There are also forests on both sides of the highway. However, there are adequate clearing of the forest on both sides of the highway. Furthermore, there are adequate arable lands located beside the highway which ensure a clear line of sight (LOS) connection between the T_{X} antenna and the sensors. The significant height of the FM radio tower helps in maintaining a LOS connection for most parts of the highway.

The area towards Hanko represents an open rural area and was selected because the propagation is excellent in this type of environment. Moreover, in order to maximize the range for the wide area communications, an environment like this is ideal. This is due to the fact that there is very little scope for interference in this type of environment. The sensors for the example power budget calculations are located on the highway 51 towards Hanko from Helsinki. The sensors are placed at some distance away from the FM radio tower at heights of approximately $1\,\mathrm{m}$ from the ground on top of dedicated poles (for sensors). In the example power budget calculations, the sensors are placed at a distance of 30 km from the T_{X} antenna. Although the FM radio technology enables the RF waves to travel nearly a hundred kilometers, the distance between the sensor and the T_{X} antenna is chosen in a cautious way so as to avoid an overestimation in the power budget calculations.

The receiver module (R_{X} antenna) is situated close to the sensor locations at a height of h_{r}. The available path loss after the signal is backscattered from the sensor helps to determine how far the signal is able to propagate. The sensors propagate the backscatterd signals towards the R_{X} antenna. The location of one or many sensors, propagating signals towards a R_{X} antenna can be termed as the harvesting area. The harvesting area is determined based on the location of the R_{X} antenna with respect to the position of the sensors. Therefore, the sensors can be placed in between the T_{X} antenna and R_{X} antenna and sometimes even beyond the R_{X} antenna as shown in Fig. 1, based on the use case.

III. Power Budget

The power budget of a system represents the manner by which the total transmit power is utilized by different components that constitute the communication system. The target of the calculation is to indicate the total gains and losses in the system in order to illustrate the total power received at the R_{X} antenna. The calculation of the power budget is a very necessary segment of any wireless communication system design. As demographic and topographic features vary for different locations, radio propagation is also different for different environments. Therefore, to predict the coverage of the system and estimate the achievable data rates, it is crucial to represent the radio channel with respect to different key system parameters.

The power budget can be calculated based on the simple formula in (1). The transmit power (P_{Tx}) and the received power (P_{Rx}) are expressed in decibel-milliwatts (dBm). The system gains and losses are expressed in the decibel (dB) scale. The system gains are calculated based on the transmit and receive antenna gains. The system losses are due to the feeder and connector losses at the transmitter and receiver. The propagation losses arise from diffraction and scattering. Additionally, the attenuation of the signal varies as a function of distance between the T_{X} and R_{X} antenna.

$$P_{\mathrm{Rx}} = P_{\mathrm{Tx}} + gains - losses. \tag{1}$$

The effective radiated power (ERP) of the FM radio tower located in Kivenlahti is $60\,\mathrm{kW}$ or $77.78\,\mathrm{dBm}$ [13]. As an example, the sensors are placed at a distance of $30\,\mathrm{km}$ from the T_{X} antenna for the power budget calculations. The free space path loss (FSPL) [14] between the transmitter and the sensor is $102\,\mathrm{dB}$ as represented by the path loss graph in Fig. 3. The curve for the FSPL is calculated based on (2).

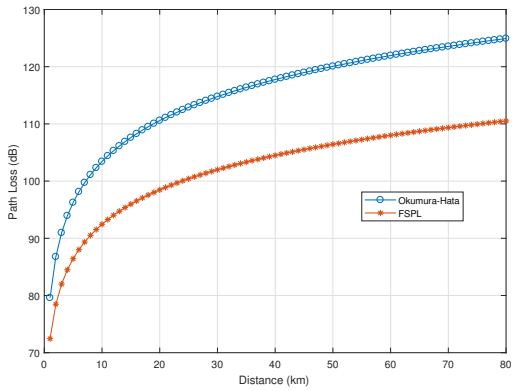

Fig. 3. Path loss

$$FSPL = 32.45 + 20 \cdot \log_{10}(d_{\text{km}}) + 20 \cdot \log_{10}(f_{\text{MHz}}). \quad (2)$$

The Okumura-Hata model [14] can be compared with the FSPL model in order to provide a more accurate or realistic estimation of the propagation between the FM transmitter and the sensor. This can be observed from the path loss graph in Fig. 3. Few parameters of the Okumura-Hata model may cause some negligible errors. For example, the range of transmit antenna heights specified for the Okumura-Hata model are in the range of $30\,\text{m}$ to $200\,\text{m}$. As the height of the transmit antenna is $248\,\text{m}$ in this work, it exceeds the upper bound of the specified range. Additionally, the lower range of the operating frequency for the Okumura-Hata model is in the range of $150\,\text{MHz}$ to $1000\,\text{MHz}$. Thus, some minor errors in the propagation may be observed as the frequency band used for the power budget calculations ($100\,\text{MHz}$) is below the lower bound of the operating frequency. The mathematical form of the model is represented in (3).

$$L = A + B \cdot \log_{10}(f_{\text{MHz}}) - 13.82 \cdot \log_{10}(h_{\text{t}}) - a(h_{\text{ms}}) + (C - 6.55 \cdot \log_{10}(h_{\text{t}})) \cdot \log_{10}(d_{\text{km}}) + C_{\text{m}}, \quad (3)$$

where $a(h_{\text{ms}})$ is calculated as,

$$a(h_{\text{ms}}) = (1.1 \cdot \log_{10}(f) - 0.7) \cdot h_{\text{r}} - (1.56 \cdot \log_{10}(f) - 0.8). \quad (4)$$

The path loss (L) from the Okumura-Hata model is calculated to be $114.8\,\text{dB}$ at a distance of $30\,\text{km}$ from the FM transmitter. The path loss curve for the Okumura-Hata model is displayed in the graph in Fig. 3. The model specific parameters, A and B are chosen to represent the low frequency of operation. The values selected for A and B are 69.55 and 26.16, respectively. The value of $a(h_{\text{ms}})$ is chosen to represent a small city. The value of C is 39.5 and is tuned to ensure the path loss exponent for the system is less than 2.5 (which represents rural area). The area correction factor (C_m) is set to $-10\,\text{dB}$ which is a very typical value for an open area. This is in coherence with the area considered in Hanko, Finland for the power budget calculations. The values selected for C and C_m are considered to be realistic or slightly even pessimistic.

TABLE I
RECEIVER SENSITIVITY PARAMETERS.

Parameter	Unit	Value
Boltzmann's Constant (k)	J/K	1.38×10^{-23}
Temperature (T)	K	290
Bandwidth (B)	kHz	1
Noise Figure (NF)	dB	10
Signal-to-Noise ratio (SNR)	dB	10

The sensitivity of the receiver is the minimum strength of the RF signal which can be decoded by the receiver module. Some different parameters play a key role in determining the sensitivity. The signal-to-noise ratio (SNR) and noise figure (NF) are some of the fundamental parameters that are utilized. Additionally, Boltzmann's constant (k), the temperature of operation (T) and the bandwidth (B) of the system are essential parameters used for calculating the minimum reception level of the system. The temperature of operation for the system is the room temperature or $290\,\text{K}$. The bandwidth of FM radio waves is $1\,\text{kHz}$. The values of the different parameters used for the calculation of the receiver sensitivity are summarized in Table I. The computation is performed based on the mathematical expression given in (5).

$$RX_{\text{sensitivity}}(\text{dBm}) = 10 \cdot \log_{10}(\frac{kTB}{0.001}) + NF + SNR. \quad (5)$$

The sensitivity of the receiver is calculated to be $-123.97\,\text{dBm}$. This value represents the minimum reception level of the system. Therefore, the signal can be decoded by the receiver module and the system can operate efficiently if the received signal strength is greater than $-123.97\,\text{dBm}$.

When the FM radio signal strikes the sensor, the signal gets split into different components which propagate to a variety of directions. This occurs due to diffraction and/or scattering. Therefore, the energy of the EM wave reduces after the signal is backscattered and subsequently propagates to the R_{X} antenna. Propagation losses due to diffraction and/or scattering at the sensor module add to the system losses and this adds up to approximately $30\,\text{dB}$. The power budget for the propagation from the transmitter to the sensor is calculated based on the aforementioned system parameters. The power budget of the system when the signal is backscattered (at the sensor) is presented in Table II.

Based on the power budget calculations there is approximately $55\,\text{dB}$ to $70\,\text{dB}$ of path loss available (Fig. 3) at the sensor location ($30\,\text{km}$) before the signal

TABLE II
POWER BUDGET.

	Parameter	Unit	Value
Transmission	Transmit power	dBm	77.78
Propagation Losses	FSPL/Okumura-Hata	dB	102/115.3
Sensor Losses	Diffraction/Scattering	dB	30
R_{X}	Receiver sensitivity	dBm	-123.97
Available Path Loss	FSPL/Okumura-Hata	dB	69.77/56.45

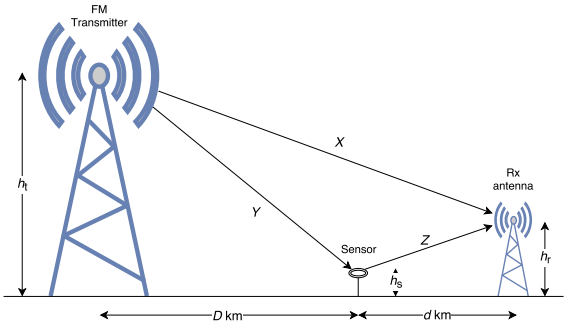

Fig. 4. Dynamic range

cannot be distinguished from the background noise. This is dependent on the minimum reception level of the system ($-123.97\,\mathrm{dBm}$). After the necessary information is added to the signal from the sensor, the backscattered signal can propagate to the R_{X} antenna. The available path loss (shown in Fig. 3) ensures that the signal is able to propagate to nearby R_{X} antennas. These R_{X} antennas are able to receive the backscattered signal from a variety of sensors located in their vicinity.

The signals follow two paths from the transmitter to the receiver module as illustrated in Fig. 4. The direct signal from the transmitter to the receiver module ('*X*') and the backscattered signal via the sensor ('*Y*') to the receiver ('*Z*'). The sensors are located at a distance of D kilometers from the T_{X} antenna with heights (h_s) from the ground. In the example power budget calculations, the value of D is $30\,\mathrm{km}$ and the value of h_s is $1\,\mathrm{m}$. The dynamic range of the system is defined as the ratio between the strongest and weakest signals measurable by the receiver module. This is a major parameter for the design of the receiver module. It is assumed to be $70\,\mathrm{dB}$ for the system used for the power budget calculations. Therefore, the difference in the received power levels of the two signals ('*X*' and '*YZ*') should not be more than $70\,\mathrm{dB}$. This enables the receiver module to distinguish between the two signals. The received signal strength of '*X*' at the R_{X} antenna, located at an example distance of $50\,\mathrm{km}$ (from the T_{X} antenna) is $-28.65\,\mathrm{dBm}$ (FSPL). '*X*' represents the strongest (direct) signal received by the R_{X} antenna. Consequently, the backscattered signal '*YZ*' can be detected by the R_{X} antenna if the received signal strength is greater than $-98.65\,\mathrm{dBm}$ (based on the FSPL model). In comparison with the minimum reception level of the system, the dynamic range of the system limits the available path loss for the transmission from the sensor to the R_{X} antenna. Therefore, the available path loss is reduced by approximately $25\,\mathrm{dB}$ after the dynamic range of the system is taken into account. Thus, the final available path loss is computed to be $44.43\,\mathrm{dB}$ for the FSPL model. So, the signal is able to propagate further to the R_{X} antenna if the power of the backscattered signal is greater than $-98.65\,\mathrm{dBm}$ (for an example distance of $50\,\mathrm{km}$). Furthermore, the communication links of d kilometers may be established between the sensor and R_{X} antenna based on the available path loss.

IV. Conclusion

ABC is considered as an enabling technology for IoT wireless communications. ABC utilizes ambient RF waves to provide power for the sensor-type devices or to simply assist in the forward propagation of the signal. The previous research on ABC have managed to accomplish communication distances of a few centimeters in indoor locations. In outdoor environments, the communication distances of tens of meters were achieved by researchers. In this article, the power budget for wide area communications using the ABC technology has been proposed. The FM radio waves at $100\,\mathrm{MHz}$ frequency, with a transmit power of $60\,\mathrm{kW}$ were utilized as the source of ambient RF waves. The sensors were placed at an example distance of $30\,\mathrm{km}$ from the transmitter on the highway which is primarily an open area. Thereafter, the power budget for the system was computed. Additionally, the dynamic range of the system limits the range of the backscatterd signal. It is observed that the reduction in the available path loss (due to the dynamic range) is approximately $25\,\mathrm{dB}$. After the signal is backscattered and additional losses (at the sensor module) are accounted for, there is around $44.43\,\mathrm{dB}$ of available path loss for the communication from the sensor to the R_{X} antenna. Therefore, the radio wave can propagate to the R_{X} antenna after diffracting or scattering from the sensor. Many such sensors located in the vicinity of the R_{X} antenna can propagate their signals to the receiver for signal detection keeping the dynamic range of the system in mind. In the future studies, the measurements will be performed in the real environment and based on the analysis of the results the propagation from the sensor to the receiver will be studied.

Acknowledgment

The authors would like to thank the Academy of Finland and European Communications Engineering (ECE) Ltd for supporting this research work.

REFERENCES

[1] H. Stockman, "Communication by means of reflected power," *Proceedings of the IRE*, vol. 36, no. 10, pp. 1196–1204, Oct 1948.

[2] J. D. Griffin and G. D. Durgin, "Gains for rf tags using multiple antennas," *IEEE Transactions on Antennas and Propagation*, vol. 56, no. 2, pp. 563–570, Feb 2008.

[3] C. Boyer and S. Roy, "Backscatter communication and rfid: Coding, energy, and mimo analysis," *IEEE Transactions on Communications*, vol. 62, no. 3, pp. 770–785, March 2014.

[4] J. D. Griffin and G. D. Durgin, "Complete link budgets for backscatter-radio and rfid systems," *IEEE Antennas and Propagation Magazine*, vol. 51, no. 2, pp. 11–25, April 2009.

[5] ——, "Multipath fading measurements at 5.8 ghz for backscatter tags with multiple antennas," *IEEE Transactions on Antennas and Propagation*, vol. 58, no. 11, pp. 3693–3700, Nov 2010.

[6] L. Xie, Y. Yin, A. V. Vasilakos, and S. Lu, "Managing rfid data: Challenges, opportunities and solutions," *IEEE Communications Surveys Tutorials*, vol. 16, no. 3, pp. 1294–1311, Third 2014.

[7] P. Maltseff, S. Winter, P. Nikitin, V. Kodukula, and E. Erosheva, "Stochastic communication protocol method and system for radio frequency identification (rfid) tags based on coalition formation, such as for tag-to-tag communication," Oct. 16 2008, uS Patent App. 12/067,554. [Online]. Available: http://www.google.ch/patents/US20080252424

[8] P. V. Nikitin, S. Ramamurthy, R. Martinez, and K. V. S. Rao, "Passive tag-to-tag communication," in *2012 IEEE International Conference on RFID (RFID)*, April 2012, pp. 177–184.

[9] V. Liu, A. Parks, V. Talla, S. Gollakota, D. Wetherall, and J. R. Smith, "Ambient backscatter: Wireless communication out of thin air," *SIGCOMM Comput. Commun. Rev.*, vol. 43, no. 4, pp. 39–50, Aug. 2013. [Online]. Available: http://doi.acm.org/10.1145/2534169.2486015

[10] B. Kellogg, A. Parks, S. Gollakota, J. R. Smith, and D. Wetherall, "Wi-fi backscatter: Internet connectivity for rf-powered devices," *SIGCOMM Comput. Commun. Rev.*, vol. 44, no. 4, pp. 607–618, Aug. 2014. [Online]. Available: http://doi.acm.org/10.1145/2740070.2626319

[11] D. Bharadia, K. R. Joshi, M. Kotaru, and S. Katti, "Backfi: High throughput wifi backscatter," *SIGCOMM Comput. Commun. Rev.*, vol. 45, no. 4, pp. 283–296, Aug. 2015. [Online]. Available: http://doi.acm.org/10.1145/2829988.2787490

[12] Z. Mat, T. Zeng, G. Wang, and F. Gao, "Signal detection for ambient backscatter system with multiple receiving antennas," in *2015 IEEE 14th Canadian Workshop on Information Theory (CWIT)*, July 2015, pp. 50–53.

[13] Finnish Communications Regulatory Authority, *Radio stations in Finland*. [Online]. Available: https://www.viestintavirasto.fi/en/spectrum/radiospectrumuse/radiostationsinfinland.html

[14] S. Saunders, "Antennas and propagation of wireless communication systems," 01 2007.

PUBLICATION
II

Evaluation of Maximum Range for Backscattering Communications Utilising Ambient FM radio signals

Ritayan Biswas, Joonas Säe, and Jukka Lempiäinen

DOI: 10.1109/BalkanCom55633.2022.9900759

Evaluation of Maximum Range for Backscattering Communications Utilising Ambient FM radio signals

Ritayan Biswas, Joonas Säe, Jukka Lempiäinen
Faculty of Information Technology and Communication Sciences (ITC), Tampere University, 33720 Tampere, Finland
Email: {ritayan.biswas, joonas.sae, jukka.lempiainen}@tuni.fi

***Abstract*—The objective of this article is to evaluate the maximum range of ambient backscattering communications (AmBC). FM radio signals operating at 100 MHz are selected as the ambient signal due to their large communication ranges. The FM radio signals operate in one of the lowest commercially available frequency bands that can be utilized for AmBC. Additionally, due to the extensive deployment of FM radio, this technology is readily available worldwide. Simulations are performed in a rural highway environment to analyse the suitability of FM radio as an ambient signal for backscattering communications. The FM transmitter and receiver antenna are located in approximately the same area representing a mono-static form of operation for backscattering communications. The sensors are located in more or less the line of sight (LOS) of the TX/RX antenna. The FM signal is reflected back from the sensor towards the receiver for detection. The ray-tracing technique and the radar equation are utilized to perform the simulations. Based on the ray-tracing simulations, a distance of 14.5 km was obtained between the TX/RX antenna and the sensor. The achievable distances utilising the radar equation depend significantly on the cross-section of the sensor and different sizes were utilised in the simulations.**

***Index Terms*—IoT, AmBC, FM, Sensor, RCS**

I. Introduction

Ambient backscattering communications (AmBC) is a wireless communication technology which utilises ambient RF signals to establish communication between devices. These ambient RF signals can originate from a variety of sources and some environments have a larger number of ambient signals than others. For example, in urban areas, ambient signals such as television broadcasts, FM radio signals, WLAN signals and cellular signals are predominantly found. However, in rural environments, there are significantly less number of ambient RF signals and those are restricted to only low frequency FM radio and television broadcast signals and intermittent cellular signals. AmBC is envisioned by researchers as a key technology for the internet of things (IoT) wireless communications. This is due to the fact that energy from the signals can be collected by the sensors utilizing the AmBC technology [1].

Sensors located in very secluded places are envisioned to be one of the key use cases of the AmBC technology. Additionally, as energy can be harvested from ambient RF signals, the AmBC technology can provide coverage to sensors located in places where maintenance is very difficult or not possible [2]. For example, sensors can be located inside walls of buildings to monitor various parameters. The installation of these sensors are integrated with the building construction, so changing batteries may prove to be difficult or even impossible once deployed. Therefore, in some cases these devices maybe permanently left inside the walls. Furthermore, the sensors may be deployed in remote locations such as in agriculture fields, highways and mountain villages to monitor environmental changes and other parameters as a result of climate change. Therefore, regular maintenance may prove to be a stumbling block as it may be very difficult and cumbersome to replace the batteries of the sensors in these locations. The AmBC technology eliminates the need for the periodic maintenance of these sensors by collecting energy from ambient RF signals [2]. This enables battery free and wireless operation of the sensors.

Radio backscatter is the fundamental backbone technology of ambient backscattering communications. The reflection of RF signals from different objects towards a receiver is the key operating principle of the radio backscatter technology. During the second world war, the radio backscatter technology was utilized to determine the identity of friendly or hostile air-crafts. The first article on radio backscatter was published by Harry Stockman in 1948 [3]. Radio frequency identification (RFID) technology works on the principle of radio backscatter. The signals are generated from a device and transmitted towards a sensor. After reflection from the sensor the signals are received and decoded by the same device [4]. RFID technology has its applications in areas such as identification and near field communication (NFC) payments. The research and development of RFID technology accelerated after the 1990s due to the reduction in cost of manufacturing sensors and readers [5].

Ambient television broadcast signals were utilised by the authors of [1] to power AmBC sensors. They were able to achieve communication distances of $0.46\,\mathrm{m}$ and $0.76\,\mathrm{m}$ in indoor and outdoor environments, respectively [1]. Data rates of $1\,\mathrm{kbps}$ were achieved for these ranges [1]. The throughput improved to a certain extent when WLAN was utilized as the ambient signal [6]. Two way communication was achieved between two tags by modifying the channel state information (CSI) and the received signal strength indicator (RSSI) of the WLAN signal [6]. Communication distances of $1\,\mathrm{m}$ and $2.2\,\mathrm{m}$ were achieved in indoor and outdoor environments with a maximum data rate of $0.5\,\mathrm{kbps}$. The throughput

significantly improved in [7], as data rates of $1\,\mathrm{Mbps}$ were achieved for $5\,\mathrm{m}$ and $5\,\mathrm{Mbps}$ for $1\,\mathrm{m}$, respectively.

The purpose of this paper is to evaluate the maximum range of AmBC. Due to the extensive worldwide availability and deployment, FM radio is selected as the preferred source of ambient RF signals. Additionally, the coverage area of FM radio signals is greater than conventional cellular systems or television broadcast signals as they operate at very low frequencies (between $88\,\mathrm{MHz}$ to $108\,\mathrm{MHz}$). FM radio signals operating at $100\,\mathrm{MHz}$ are used in the simulations. A rural highway (highway number 51) near Helsinki in southern Finland is chosen as the environment for the simulations as this area is generally free of significant obstacles and other interference. This ensures a more or less clear line of sight (LOS) path between the TX antenna and the sensors.

II. Ambient Backscattering Communications

AmBC is a wireless communication paradigm which works on the principle of energy and/or signal collection from ambient RF signals. These signals originate from a variety of sources such as television broadcasts, FM radio, cellular and WLAN signals to name a few. AmBC utilizes small devices (sensors) which have the necessary hardware to collect the energy from the ambient RF signals. The harvesting of the energy from the ambient RF signals enables wireless and battery free operation of the sensor.

Ambient backscatter is one of the three categories of backscatter systems [8]. Mono-static backscatter systems generate RF signals which are reflected back from a sensor for detection [8]. RFID is a typical example of a mono-static backscatter system. As the reader and the sensor needs to be in close proximity of each other, the range of operation is a limitation of mono-static backscatter systems. In bi-static backscatter systems, a carrier emitter generates the RF signals. The carrier emitter is located centrally (or, in different locations) and the sensors are placed within the coverage area of the carrier emitter. The signals generated by the carrier emitter are backscattered by the tags to a dedicated reader. The generation of a dedicated signal from the carrier emitter is a disadvantage of bi-static backscatter systems [9].

Ambient backscattering communications utilise ambient RF signals for its operation. Thus, a dedicated signal does not have to be generated. Furthermore, the utilization of low-frequency ambient signals overcomes the restriction of limited achievable communication range. In contrast to traditional wireless communication systems, AmBC operates by reflecting the ambient RF waves towards the receiver [2]. This operation is performed after the required information is added to the signal.

AmBC systems operate by transmitting '0' and '1' from the sensors by switching between the reflecting and non-reflecting states [1]. This functionality is achieved by modifying the electrical properties of the sensor. The receiver is able to distinguish the backscattered signals as they are transmitted at a lower data rate in comparison to traditional signals [1]. The authors in [1] also developed a prototype to demonstrate the bit-error rate (BER) in comparison with the distance between two passive AmBC sensors. The utilization of multiple antennas at the receiver helped in achieving a lower BER [10].

AmBC has certain disadvantages that needs to be addressed before this technology can be extensively deployed. Firstly, the receiver has to be able to distinguish between the traditional and the backscattered signals. Additionally, as the operating principle of AmBC is different in comparison with traditional wireless communications, separate channels for communication needs to be defined. Finally, the technology through which the energy and/or signal is harvested from ambient RF signals needs to be further developed in order to achieve seamless operation of the AmBC technology.

III. Propagation models

The maximum achievable range of AmBC is analysed with the help of simulations. The ray-tracing technique and the radar equation are used for the simulations to investigate the feasibility of the approach.

A. Ray-tracing

The ray-tracing technique is based on the detailed simulation of the entire propagation environment. The simulations are performed based on the path each individual signal travels between the transmitter and the sensor. If there are obstructions such as trees or buildings between the transmitter and the sensor then each individual signal is divided into line-of-sight (LOS) links. The free space path loss (FSPL) equation is utilized in order to calculate the path loss encountered for each LOS link of the signal. The FSPL is calculated based on eq. 1 where "d" represents the distance in kilometers and "f" represents the operating frequency in megahertz (MHz).

$$FSPL = 32.45 + 20 \cdot \log_{10}(d_{\mathrm{km}}) + 20 \cdot \log_{10}(f_{\mathrm{MHz}}). \quad (1)$$

The signal may also have a variety of multi-path components between the transmitter and the receiver. Each individual signal may experience reflection, scattering or diffraction from various objects in the environment while propagating from the transmitter to the sensor. Additional losses are factored in the simulations to account for the losses caused due to any such phenomenon. However, the environment and the location of the sensor and the receiver (with respect to the transmitter) has an important role in determining the strength of the multi-path components. In this work, the sensors are assumed to be in more or less the direct LOS of the TX/RX antenna.

B. Radar Equation

The total range of communication can also be calculated utilizing the radar equation. The operating principle of the radar equation is based on the reflection of the transmitted signal from a target (or, sensor) towards the receiver. The location of the TX and RX antenna determines the type of radar system. In mono-static radar, the TX and RX antenna are co-located. For bi-static radar systems, the TX and RX

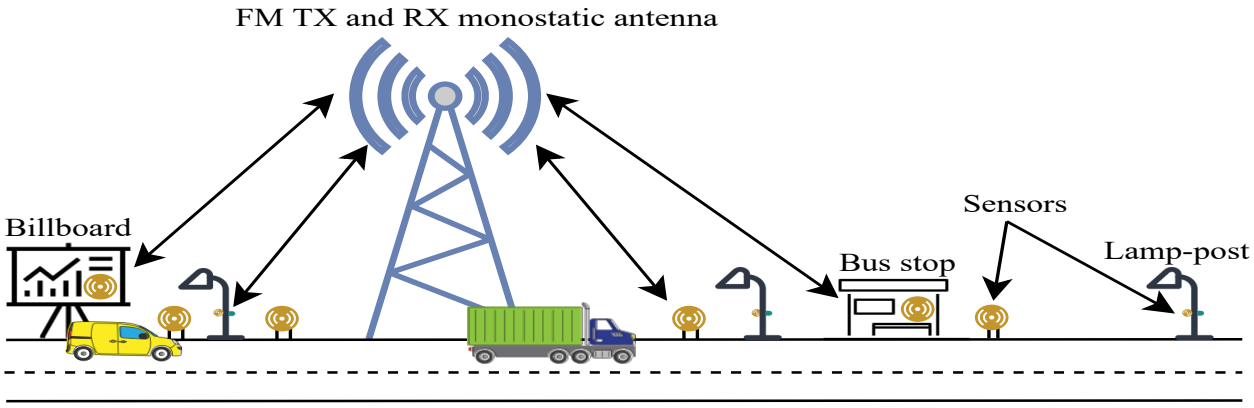

Fig. 1. Illustration of the deployment scenarios for AmBC sensors in rural highway environment.

antenna are located at different positions. The simulations in this work are performed using mono-static radar systems.

The radar equation (for mono-static systems) in represented by eq. 2. The range of the radar is represented in kilometers. In bi-static radar, the range term (R) in eq. 2 is divided into two parts to represent the distance between the transmitter and sensor (R_{t}) and the distance between the sensor and the receiver (R_{r}). For the mono-static operation of radar systems, the range terms R_{t} and R_{r} are equal and combined into R.

$$R = \sqrt[4]{\frac{P_t G_t G_r \lambda^2 \sigma}{(4\pi)^3 P_r L}}. \tag{2}$$

In eq. 2, P_{t} represents the power of the transmitted signal and P_{r} represents the power of the received signal. The units for both these terms is watts (W). The wavelength (in meters) of the signal is represented by λ. The G_{t} and G_{r} represent the antenna gains for the TX and RX antenna, respectively. The parameter L factors in the additional loss of the system. The radar cross section (RCS, σ) is expressed in square meters and is the sensor from where the ambient signal is reflected back to the RX antenna. In [11], σ is considered as a half-dipole antenna and is represented by the formula in eq. 3.

$$\sigma = 0.88 \times \lambda^2. \tag{3}$$

In the simulations, different values are considered for σ to compare how the cross-section of the sensor affects the achievable range of communication. Moreover, the cross section of the sensor in comparison to the wavelength of the signal has a significant role in determining if scattering or reflection occurs at the sensor [12]. The value of x in eq. 4 determines the phenomenon happening at the sensor.

$$x = (\frac{2\pi r}{\lambda}), \tag{4}$$

where r represents the size of the sensor and λ represents the wavelength of the signal. If the value of $x < 1$, the signal is scattered at the sensor. A clear reflection happens when the value of $x > 1$. [12]

IV. Simulation Setup

A. Simulation environment

The simulations in this work are performed beside a rural highway as shown in Fig. 1. This type of environment helps in determining the maximum achievable range of communication due to the absence of significant obstacles such as multi-storied buildings. The map of the simulation environment is obtained from Google Maps and is shown in Fig. 2. Highway 51 is mainly a straight highway and the area (beside the highway) is clear of obstacles and consist of mainly arable lands. This area is located towards the direction of Hanko in southern Helsinki, Finland. The FM TX antenna is located in the suburb of Kivenlahti and there is almost a clear LOS to highway 51. The minor obstructions are due to tree foliage located beside the highway. The typical effective isotropic radiated power (EIRP) of this FM radio TX antenna is $60\,\mathrm{kW}$ or $77.78\,\mathrm{dBm}$ [13].

The FM radio TX antenna at Kivenlahti is at a height of 248 meters. The receiver is assumed to be co-located with the FM TX antenna in approximately the same area. The ambient FM radio signals are reflected back to the receiver from the sensors. The schematic diagram of the simulation environment is illustrated in Fig. 1. The sensors are located in more or less the LOS of the TX/RX beside the highway to monitor different parameters as shown in Fig. 1. For example, the sensors can be utilized to determine the number of vehicles passing through a certain point for traffic monitoring. Additionally, some sensors installed on lamp-posts can also be utilized to determine the level of snow on highways by measuring the depth. Furthermore, sensors can be deployed on the walls of bus stops or on billboards to monitor different parameters. The deployment scenarios for AmBC sensors are shown in Fig. 1.

B. Simulation parameters

The ray-tracing technique and the radar equation are utilized to determine the maximum achievable communication range between the TX/RX antenna and the sensor after the signal impinges on it. Consequently, the noise floor

Fig. 2. Propagation environment from Google Maps.

(or, the receiver sensitivity) of the system is calculated to determine the maximum achievable range of communication. The noise floor gives an indication of the signal level that can be decoded by the receiver and is calculated based on eq. 5. The parameters represent the typical values used for the noise floor calculation for FM radio systems. The Boltzmann constant (k) is 1.38×10^{-23} J/K and the operating temperature (T) is $290\,\mathrm{K}$. The bandwidth (B) is $1\,\mathrm{kHz}$ and represents the standard bandwidth for FM radio signals.

$$RX_{\text{sensitivity}}(\text{dBm}) = 10 \cdot \log_{10}(\frac{kTB}{0.001}) + NF + SNR. \quad (5)$$

The receiver sensitivity (P_{r}) of the system is calculated to be $-123.97\,\mathrm{dBm}$ utilising eq. 5. The noise figure (NF) is $10\,\mathrm{dB}$ and the signal to noise ratio (SNR) is $10\,\mathrm{dB}$. Therefore, if the power of the backscattered signal is higher than the noise floor, the signal can be decoded by the RX antenna. The value of the receiver sensitivity is utilised as an input parameter for the received power (P_r) term in eq. 2. This helps to determine the maximum achievable communication range by using the radar equation. Moreover, based on the EIRP of the FM radio tower ($77.78\,\mathrm{dBm}$) and the receiver sensitivity ($-123.97\,\mathrm{dBm}$), the total available path loss for the system is $201.75\,\mathrm{dB}$.

In the ray-tracing approach, the path loss in the LOS links between the TX and the sensor is calculated based on eq. 1. Consequently, based on the principle of reciprocity, the path loss between the sensor and the RX has the same value. The total available path loss provides an estimation of the maximum achievable distance the signal can travel between the TX/RX and the sensor.

Furthermore, losses are experienced in the system due to the obstruction of the Fresnel zone (due to the close proximity of the sensor to the ground) and the reflection loss that is experienced at the sensor. An additional loss (L) of $10\,\mathrm{dB}$ is accounted for in the simulations. The simulation parameters are summarized in Table I.

V. Results and Analysis

The maximum achievable range of communication between the TX/RX antenna and the sensor is calculated utilizing the ray-tracing technique and radar equation.

TABLE I
SIMULATION PARAMETERS.

Parameters	Unit	Value
Frequency	MHz	100
FM TX EIRP	kW	60
TX antenna height	m	248
Temperature (T)	K	290
Bandwidth (B)	kHz	1
Noise figure (NF)	dB	10
Signal-to-noise ratio (SNR)	dB	10
Additional loss	dB	10

The ray-tracing technique provides an optimistic value for the maximum achievable communication range as the size of the sensor is not factored in the calculations. The total available path loss for round trip communication between TX-sensor-RX is $201.75\,\mathrm{dB}$. After the additional loss ($10\,\mathrm{dB}$) is factored in, the available path loss decreases to $191.75\,\mathrm{dB}$. Thus, for one-way communication between the TX-sensor (or, sensor-RX), the total available path loss is $95.87\,\mathrm{dB}$. Therefore, a maximum distance of $14.5\,\mathrm{km}$ in one direction can be achieved and the signal experiences a path loss of $95.67\,\mathrm{dB}$ at this distance. Consequently, based on the principle of reciprocity, a maximum round trip communication range of $29\,\mathrm{km}$ can be achieved. This distance represents the longest achievable range of communication where the sensor is located $14.5\,\mathrm{km}$ from the TX/RX antenna.

The range of the radar equation is calculated utilizing eq. 2 and represents the total range of communication (between the TX-sensor and sensor-RX). In the simulations, the size of the cross-section of the sensor (σ) is altered to observe the change in the achievable range. The size of the sensors utilized for IoT wireless communications varies based on the use case.

The sensor size of $0.001\,\mathrm{m}^2$ ($3\,\mathrm{cm} \times 3\,\mathrm{cm}$) represents the worst case scenario. It is observed that the total communication range achieved with such sensor sizes is about $2.8\,\mathrm{km}$. Sensors with such a small cross section may be difficult to locate and can be placed $1.4\,\mathrm{km}$ from the TX/RX antenna. A distance of $2.5\,\mathrm{km}$ is achievable between the TX/RX and the sensor having a cross section of $10\,\mathrm{cm} \times 10\,\mathrm{cm}$ ($0.01\,\mathrm{m}^2$). A distance of $5.1\,\mathrm{km}$ can be achieved when the size of the sensor is $0.16\,\mathrm{m}^2$ ($40\,\mathrm{cm} \times 40\,\mathrm{cm}$). The distance increases to $5.9\,\mathrm{km}$ when the size of the sensor is $0.3\,\mathrm{m}^2$ ($54\,\mathrm{cm} \times 54\,\mathrm{cm}$). Furthermore, when the cross section of the sensor is increased to $0.7\,\mathrm{m}^2$ ($83\,\mathrm{cm} \times 83\,\mathrm{cm}$) the achievable distance increases to $7.38\,\mathrm{km}$. A radar cross section of $7.92\,\mathrm{m}^2$ ($2.8\,\mathrm{m} \times 2.8\,\mathrm{m}$) is calculated based on the eq. 3 and represents a half dipole antenna for the intended carrier frequency [11]. The achievable distance utilizing such a sensor is $13.5\,\mathrm{km}$. The different values utilized for σ and their corresponding distances are summarised in Table II.

It is observed that with the increase in the cross section of σ the communication range increases as there is more area available for the ambient FM radio signal to reflect back from. Additionally, a study is also carried out to determine

TABLE II
DIFFERENT DISTANCES FOR AMBC WITH RT AND RE PROPAGATION MODELS.

Propagation model	RCS (σ, m^2)	Distance between TX/ RX and sensor (km)	Total distance (km)
Ray-tracing	-	14.5	29
Radar equation	0.001	1.43	2.87
	0.01	2.55	5.10
	0.16	5.10	10.21
	0.3	5.97	11.94
	0.7	7.38	14.76
	7.92	13.54	27.08

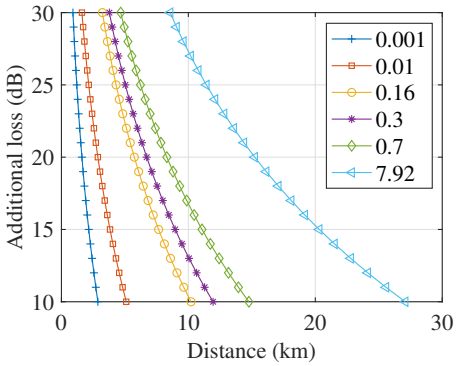

Fig. 3. Achievable distances for different additional losses for varying RCS (σ).

how the additional loss affects the range of communication. A graph illustrating the different communication ranges for different cross section of σ is shown in Fig. 3. Additional loss values of $10\,\mathrm{dB}$ to $30\,\mathrm{dB}$ are utilized to observe how the communication range is affected. It is observed that with the increase in the additional loss, the range of communication reduces for different σ sizes.

The value of x in eq. 4 determines the boundary condition for scattering or reflection to occur after the signal impinges on the sensor. The minimum required cross section of the sensor is $47\,\mathrm{cm}\times47\,\mathrm{cm}$ for the ambient signal to reflect towards the RX antenna. Sensors with a smaller cross section cannot be utilised as the ambient FM radio signal will scatter instead of reflecting. Therefore, only sensors having a cross section greater than $47\,\mathrm{cm}\times47\,\mathrm{cm}$ (or, $0.22\,\mathrm{m}^2$) can be utilised to determine the maximum achievable range of communication.

VI. CONCLUSION

The purpose of this article was to evaluate the maximum range of mono-static AmBC technology. A rural highway near Helsinki in southern Finland was chosen as the environment where the simulations were performed. The AmBC sensors were deployed beside the highway for monitoring different parameters in more or less the LOS of the FM TX antenna in Kivenlahti. The selected area is free of obstacles and therefore, the amount of interference is least in such an environment. The ambient FM radio signals (at $100\,\mathrm{MHz}$ frequency) were utilised in the simulations. Two propagation models, the ray-tracing technique and the radar equation were utilized to perform the simulations. It was observed that utilising the ray-tracing technique the sensors could be deployed $14.5\,\mathrm{km}$ from the TX/RX antenna. Utilising a mono-static radar, it was observed that the sensor could be located $5.9\,\mathrm{km}$ from the TX/RX antenna for sensor sizes of $54\,\mathrm{cm}\times54\,\mathrm{cm}$. Sensors of such cross sections can be deployed in billboards or bus-stops located beside the highway. A significant limiting factor for reflection to occur is based on the cross section of the sensor in comparison with the wavelength of the ambient signal. Consequently, for reflection of the ambient FM radio signals, the cross section of the sensor has to be a a minimum of $47\,\mathrm{cm}\times47\,\mathrm{cm}$. Therefore, the size of the sensor has an essential role in the achievable range of communication. Furthermore, it can be inferred that the achievable range utilising the radar equation is more realistic in comparison with the ray-tracing technique as the cross section of the sensor is factored in the simulations. Also, it was observed that the communication range decreases with the increase in the additional loss. In conclusion, ambient FM radio signals could offer a wide range of opportunities for monitoring purposes in rural or highway areas utilising the AmBC technology.

REFERENCES

[1] V. Liu, A. Parks, V. Talla, S. Gollakota, D. Wetherall, and J. R. Smith, "Ambient backscatter: Wireless communication out of thin air," *SIGCOMM Comput. Commun. Rev.*, vol. 43, no. 4, pp. 39–50, Aug. 2013.

[2] N. Van Huynh, D. T. Hoang, X. Lu, D. Niyato, P. Wang, and D. I. Kim, "Ambient backscatter communications: A contemporary survey," *IEEE Communications Surveys Tutorials*, vol. 20, no. 4, pp. 2889–2922, 2018.

[3] H. Stockman, "Communication by means of reflected power," *Proceedings of the IRE*, vol. 36, no. 10, pp. 1196–1204, Oct 1948.

[4] L. Xie, Y. Yin, A. V. Vasilakos, and S. Lu, "Managing rfid data: Challenges, opportunities and solutions," *IEEE Communications Surveys Tutorials*, vol. 16, no. 3, pp. 1294–1311, Third 2014.

[5] C. Boyer and S. Roy, "Backscatter communication and rfid: Coding, energy, and mimo analysis," *IEEE Transactions on Communications*, vol. 62, no. 3, pp. 770–785, March 2014.

[6] B. Kellogg, A. Parks, S. Gollakota, J. R. Smith, and D. Wetherall, "Wi-fi backscatter: Internet connectivity for rf-powered devices," *SIGCOMM Comput. Commun. Rev.*, vol. 44, no. 4, pp. 607–618, Aug. 2014.

[7] D. Bharadia, K. R. Joshi, M. Kotaru, and S. Katti, "Backfi: High throughput wifi backscatter," *SIGCOMM Comput. Commun. Rev.*, vol. 45, no. 4, pp. 283–296, Aug. 2015.

[8] S. H. Choi and D. I. Kim, "Backscatter radio communication for wireless powered communication networks," in *2015 21st Asia-Pacific Conference on Communications (APCC)*, Oct 2015, pp. 370–374.

[9] X. Lu, D. Niyato, H. Jiang, D. I. Kim, Y. Xiao, and Z. Han, "Ambient backscatter assisted wireless powered communications," *IEEE Wireless Communications*, vol. 25, no. 2, pp. 170–177, April 2018.

[10] Z. Mat, T. Zeng, G. Wang, and F. Gao, "Signal detection for ambient backscatter system with multiple receiving antennas," in *2015 IEEE 14th Canadian Workshop on Information Theory (CWIT)*, July 2015, pp. 50–53.

[11] D. Barton, C. Cook, P. Hamilton, and I. ANRO Engineering, *Radar Evaluation Handbook*, ser. Radar Library. Artech House, 1991.

[12] M. Oziel, R. Korenstein, and B. Rubinsky, "Radar based technology for non-contact monitoring of accumulation of blood in the head: A numerical study," *PLOS ONE*, vol. 12, p. e0186381, 10 2017.

[13] Finnish Transport and Communications Agency, *Radio stations in Finland*. [Online]. Available: https://www.traficom.fi/en/communications/tv-and-radio/radio-stations-finland

PUBLICATION
III

Maximum Receiver Harvesting Area of Backscatter Signals from Ambient Low-Frequency Mobile Networks

Ritayan Biswas, Joonas Säe, and Jukka Lempiäinen

DOI: 10.1109/GLOBECOM46510.2021.9685741

Maximum Receiver Harvesting Area of Backscatter Signals from Ambient Low-Frequency Mobile Networks

Ritayan Biswas, Joonas Säe, Jukka Lempiäinen
Faculty of Information Technology and Communication Sciences (ITC), Tampere University, 33720 Tampere, Finland
Email: {ritayan.biswas, joonas.sae, jukka.lempiainen}@tuni.fi

***Abstract*—The purpose of this paper is to estimate the maximum achievable range for ambient backscattering communications (AmBC) by utilizing one of the lowest available frequency bands for mobile networks. Long term evolution (LTE) networks operating at 700 MHz (LTE-700, also referred to as LTE band 28) use the frequency division duplexing (FDD) technique for communications and are utilised as the ambient signals to perform the simulations. The simulations are carried out in urban macro-cellular and suburban highway environments. For the simulations, the sensors are placed in the line-of-sight (LOS) path of the LTE-700 transmitter and receiver antenna as this ensures the maximum applicability of the AmBC technology. Two propagation models, the ray tracing approach and the radar equation are leveraged to determine the maximum range of communication when the signal is reflected by the sensor. It is observed from the analysis that distances of a few hundred meters are achievable utilising both propagation models. The size of the sensor has a pivotal role in determining the maximum range of communication while utilising the radar equation. Therefore, a thorough analysis is performed using real-world sensor sizes deployed for the internet of things (IoT) wireless communication.**

***Index Terms*—Internet of Things, Sensor, Radar cross section, AmBC, LTE, 5G.**

I. Introduction

Ambient backscattering communications (AmBC) is a wireless communication technology which utilises ambient radio frequency (RF) signals to establish communication with sensors or devices. These sensors have their applicability in the internet of things (IoT) wireless communications. These ambient signals can originate from a variety of RF sources such as television (TV) broadcasts, Wi-Fi, FM radio and cellular signals. The sensors used in AmBC are capable of harvesting energy from the ambient RF signals. This enables the battery free and wireless operation of the sensors.

AmBC systems operate on the principle of radio backscatter where a transmitted signal is reflected back from an object towards a receiver for decoding. This technique was first utilized during World War II to determine the identity of the air-crafts and classify then as friendly or hostile. The first article on backscatter communications was published by Harry Stockman in 1948 [1]. There has been a significant amount of research in the radio backscatter technology during the last two decades due to the relatively low cost and very low power requirement of manufacturing such devices [2]. Radio frequency identification (RFID) systems also utilize the concept of radio backscatter in order to perform their functionality.

The concept of AmBC was first presented by the authors of [3] in the year 2013. They were able to achieve communication distances of $45.7\,\mathrm{cm}$ in indoor environments and $76.2\,\mathrm{cm}$ in outdoor environments by utilising ambient TV broadcast signals [3]. Backscatter communication utilising ambient wireless LAN (WLAN) signals were presented by the authors in [4]. They were able to connect to the internet by connecting to the gateway network [4]. There was a significant improvement in throughput achieved in [5] in comparison with previous articles such as [3], [4]. Typically, it was observed that very short communication ranges could be achieved by AmBC systems. However, in [6], wide area communication was proposed for AmBC and it was predicted that communication distances of $30\,\mathrm{km}$ are achievable utilizing ambient FM radio signals based on power budget calculations. Furthermore, the link budget for typical backscatter communications at different frequencies were studied by the authors in [7].

In this article, ambient long term evolution (LTE) cellular signals operating at $700\,\mathrm{MHz}$ (LTE-700) frequency are utilised to estimate the maximum distance between the TX/RX antenna and the sensor in outdoor environments. To maximise the coverage, the LTE-700 carrier frequency band is utilised as this is one of the lowest operating frequencies for cellular communications. Additionally, the simulations are performed for the sensors located in the direct line-of-sight (LOS) of the TX/RX antenna in urban macro-cellular and suburban highway environments. Furthermore, the TX and the RX are placed in the same location which represents the mono-static mode of operation for AmBC systems. The simulation results demonstrate that the AmBC systems are capable of achieving distances of the order of hundreds of meters when typical real world antenna configurations are utilised.

II. Backscatter Communications

Backscatter systems can be classified into two categories based on the location of the TX and RX. In the mono-static mode of operation, the TX and RX are placed in the same location. The signal transmitted by a dedicated TX

reflects back from an object (or, sensor) towards the RX for detection [8]. The bi-static backscatter utilizes a carrier emitter to transmit a dedicated signal to the sensor which is backscattered to a RX for reading and decoding the signal [8]. This type of system can utilize a centrally located receiving device capable of decoding the signal [9]. However, a disadvantage of traditional backscatter communication systems is the requirement for a dedicated transmission.

AmBC eliminates the need of a dedicated signal by utilising the ambient RF signals present in the environment. These ambient signals can be transmitted from a variety of sources such as TV/FM broadcasts, WLAN or cellular signals to name a few. These ambient signals are utilized by the backscattering element in order to establish communication between two passive or active devices or a combination of both. The advent of IoT wireless communication necessitates the deployment of a huge number of sensors. All these sensors will have a power requirement as they are required to communicate with each other or other devices. However, it might impractical to change batteries for certain use cases and in some environments [3], [10]. Therefore, the harvesting of energy from ambient RF signals is an important feature ensured by AmBC [11].

The operating principle of the AmBC technology is based on the transmission of "1" or "0" from the sensor. For example, "1" can indicate the reflecting state and "0" can indicate the non-reflecting state [11]. In order to establish communication, the antenna impedance states are changed between the non-reflecting and reflecting states [3]. The signal transmitted from the chosen ambient RF source propagates to the sensor, where the signal is modulated and forwarded to a device capable of receiving and decoding the signal.

Although AmBC has significant advantages, there are some practical disadvantages that need to be addressed before commercial deployment is possible. Firstly, the RX/sensors must be capable in deciphering between various RF signals emitted from legacy sources. Secondly, the capability of energy harvesting at the sensor will be a challenge for hardware designers. Lastly, the mode of operation of AmBC differs from traditional wireless communications. Therefore, separate channels need to be defined for communication utilizing ambient RF signals in comparison with traditional communication systems.

III. Propagation models

To examine the signal path from the TX antenna to the sensor, each environment is analysed with the help of two propagation models. While performing the analysis, the signal is assumed to have a clear LOS between the TX antenna, RX antenna and the sensor.

A. Radar Equation

The radar equation (RE) generally computes the total range of communication. The operating principle of the radar equation is based on the reflection of the transmitted signal from the target of a given cross section back to the RX antenna. The radar can be mono-static, that is, the TX and RX is positioned at the same location. In bi-static radar, the signal travels from the TX via reflection from a target to the RX antenna which are not collocated. In this work, mono-static radar is considered for computing the range. The formula for the computation of the range using the radar equation is shown in (1).

$$R = \sqrt[4]{\frac{P_t G_t G_r \lambda^2 \sigma}{(4\pi)^3 P_r L}}. \tag{1}$$

The range from the TX antenna to the sensor is expressed by R_t, and R_r represents the range of the sensor to the RX antenna. For mono-static radar two ranges are nearly identical and can be combined into R [12]. These distances are expressed in meters. Parameters such as wavelength (λ), transmit power (P_t) and the antenna gains of the TX (G_t) and RX (G_r) has a vital role in determining the range of radar systems. L represents the propagation loss of the system. The received power (P_r) indicates the receiver sensitivity (or, noise floor) and is calculated using (2),

$$RX_{\text{sensitivity}}(\text{dBm}) = 10 \cdot \log_{10}\left(\frac{kTB}{0.001}\right) + NF + SNR. \tag{2}$$

The values for the parameters represent typical values used for the LTE power budget calculation. The temperature (T) is 290 K and Boltzmann's constant (k) is 1.38×10^{-23} J/K. For calculating the bandwidth (B), one resource block ($12 \times 15\,\text{kHz}$) is utilized. The number of sub-carriers is 12 and the spacing between them is $15\,\text{kHz}$ [13].

The cross section of the target (sensor, σ) is expressed in square meters and plays an important role in in the operation of the radar. In literature [12], the value of σ is calculated using (3),

$$\sigma = 0.88 \times \lambda^2, \tag{3}$$

when the antenna is considered to be a half dipole. The wavelength is calculated to be $0.42\,\text{m}$ for $700\,\text{MHz}$.

B. Ray Tracing

The ray tracing (RT) approach is generally based on the comprehensive simulation of the propagation environment. A proper description of the physical propagation environment is necessary in order to provide a deterministic representation of the ray path(s). The simulation is carried out by using rays to model different multi-path components of the environment in detail. The total ray paths are subdivided into LOS links. The propagation of the individual LOS link between two points is determined by the free space path loss (FSPL) utilizing (4).

$$FSPL = 32.45 + 20 \cdot \log_{10}(d_{\text{km}}) + 20 \cdot \log_{10}(f_{\text{MHz}}), \tag{4}$$

where d represents the distance (in km) between the two points and f represents the frequency (in MHz) of operation.

Generally, in an environment each ray experiences reflection, diffraction and/or scattering which can be termed as

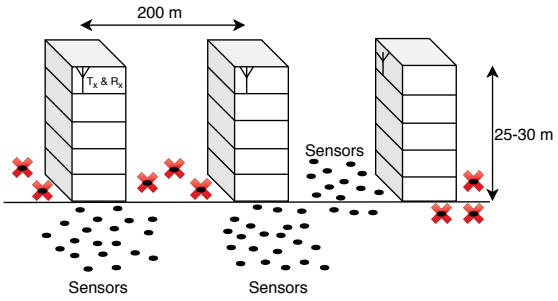

Fig. 1. Urban macro-cellular environment.

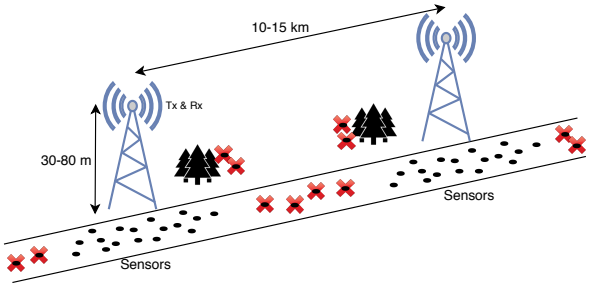

Fig. 2. Sub-urban highway environment.

the propagation loss. The total loss experienced by a certain ray is a combination of these phenomena and the loss due to the distance traveled by the signal. In order to obtain an accurate prediction of the propagation, the parameters that affect the ray tracing approach are thoroughly analysed. Building penetration losses, the permittivity of the ground and building materials, the precise locations of the TX antenna, RX antenna and the obstacles (buildings, trees) need to be accurately modelled. Losses occurring due to any of these phenomena contribute to the propagation loss. The final result is a combination of the FSPL for each individual LOS link of the ray in addition to the propagation loss. Additionally, the frequency of operation also has an important role in the simulation. The received signal power is computed based on the multi-path components that exist between the TX antenna and the RX antenna.

IV. Computation of the Receiver Harvesting Area

The receiver harvesting area is determined based on the simulation performed in two different environments, an urban macro-cellular and a suburban highway environment.

A. Environment for receiver harvesting area

The harvesting area of the receiver is determined based on the location of the sensor relative to the TX/RX. Additionally, the strength of the reflected signal also determines the area where the sensors can be deployed. This study is focused on the analysis of urban macro-cellular environment and suburban highway environment where there are direct LOS paths between the TX/RX and the sensor. It is assumed the transmitter and the receiver are placed at the same location. Therefore, the signal travels from the transmitter to the sensor and back to the receiver following the same path. Additional losses due to reflection and scattering are included while computing the total path loss. The sensors are placed at the ground level or at heights of $1\,\mathrm{m}$ from the ground in the direct LOS path of the transmitter. Thus, some additional loss is also considered for the obstruction caused by the blocking of the Fresnel zone.

1) Urban macro-cellular environment: In the urban macro-cellular environment, there are clear LOS paths present between the TX antenna and the sensor. The sensors which are located in the non line-of-sight (NLOS) with respect to the TX antenna are unable to receive and harvest the signals. These sensors are marked with red crosses in Fig. 1. Generally, in an urban macro-cellular environment the TX is located on or just below the rooftop. In this work, the location of the TX is considered to be just below the rooftop level (as depicted in Fig. 1) in order to avoid the back-lobe of the antenna radiation pattern. Also, by placing the antenna just below the rooftop level, the signal in the main beam direction is emphasised in the direct LOS with the sensor. In this work, the RX is placed at the same location of the TX at a height of $30\,\mathrm{m}$. The inter-site distance in a standard urban macro cellular environment is $200\,\mathrm{m}$. The illustration of the propagation environment for such a scenario is depicted in Fig. 1.

2) Suburban highway environment: The height of the TX antenna in a suburban highway environment is typically between $30\,\mathrm{m}$ to $80\,\mathrm{m}$. The cost efficient way is to have the TX as high as possible. This is done in order to have the maximum possible coverage and avoid the nearby obstacles such as trees. It is assumed RX antenna is located at the same height of the TX antenna. The sensors are placed near the TX ensuring a clear LOS path. The location of these sensors is depicted in Fig. 2. The sensors which are in the NLOS of the TX are represented in Fig. 2 with red crosses. The typical site distances for a highway environment is $10\,\mathrm{km}$ to $15\,\mathrm{km}$. This signifies there are parts of the highway between TX where the sensors cannot be deployed. A schematic diagram for the receiver harvesting area in a highway environment is illustrated in Fig. 2.

B. Simulation parameters

The analysis of the signal propagation in the urban macro-cellular and highway LOS environments is performed utilizing the radar equation and the ray tracing method. The sensors are located in the direct LOS of the TX/RX and an illustration of two environments are shown in Fig. 1 and Fig. 2.

The effective isotropic radiated power (EIRP) of the LTE-700 TX antenna is $62\,\mathrm{dBm}$. This is calculated based on a transmit power (P_t) of $46\,\mathrm{dBm}$ (typical for most manufacturers), a transmit antenna gain (G_t) of $18\,\mathrm{dB}$ and a cable loss of $2\,\mathrm{dB}$. The noise figure (NF) is $10\,\mathrm{dB}$ and the signal to noise ratio (SNR) is $2\,\mathrm{dB}$. These values indicate typical values utilised in the LTE power budget calculations. The value of the receiver sensitivity is calculated to be

TABLE I
SIMULATION PARAMETERS.

Parameter	Unit	Value
TX power (P_t)	dBm	46
TX antenna gain (G_t)	dBi	18
RX antenna gain (G_r)	dBi	0
Cable loss	dB	2
Temperature (T)	K	290
Bandwidth (B)	kHz	12×15
Noise figure (NF)	dB	10
Signal-to-noise ratio (SNR)	dB	2
Additional loss (urban, L_{urban})	dB	15
Additional loss (suburban, L_{suburban})	dB	5

$-109.42\,\text{dBm}$ utilising (2). Therefore, the total available path loss is $171.42\,\text{dB}$ based on the difference between the EIRP and the receiver sensitivity.

The free space path loss is calculated for the LOS link between the TX/RX and the sensor utilizing equation (4). The total path loss is a summation of the path loss between the TX and sensor and the path loss between the sensor and RX after reflection (from the sensor). In the urban environment, there is approximately $15\,\text{dB}$ additional loss (L_{urban}) considered due to the reflection off the sensor ($10\,\text{dB}$) and the minor obstruction of the first Fresnel zone ($5\,\text{dB}$). The total additional loss (L_{suburban}) in suburban environment is approximately $5\,\text{dB}$. In equation (1), the additional loss values are utilized for the L term. P_r (or, the receiver sensitivity) determines the minimum value of the signal strength that can be received at the RX. A comparison is performed for two approaches in order to determine the feasibility of these propagation models for this approach. The different parameters utilised for the simulations are summarised in the table I.

V. RESULTS AND ANALYSIS

The total available loss that an individual ray can experience in the LOS path is $156.42\,\text{dB}$ in urban and $166.42\,\text{dB}$ in suburban environments, respectively. These values are calculated after the additional loss for the respective environments are considered as stated in table I. The available path loss is basically the round-trip loss experienced by the ray when it travels from the TX to the sensor, gets reflected and travels back to the RX.

Utilizing the ray tracing method it is observed that a maximum distance of approximately $275\,\text{m}$ can be achieved between the TX and the sensor in the clear LOS link in urban environments. The FSPL at a distance of $275\,\text{m}$ from the TX is $78.14\,\text{dB}$ utilizing (4). Based on the principle of reciprocity, the path between the sensor and the RX experiences a similar path loss. Thus, the total path loss experienced by the signal is $156.28\,\text{dB}$ which is less than the maximum allowable loss for the urban environment after the additional loss is taken into account. Therefore, theoretically, a signal in the LOS path can travel $550\,\text{m}$ between the TX and the RX via reflection from the sensor. In the urban macro-cellular environment, the sensors can be placed approximately $275\,\text{m}$ away from the TX/RX antenna in the clear LOS path in order to perform various functionalities based on different use cases. The site distances in an urban environment is about $200\,\text{m}$ therefore most of the sensors are able to utilize the ambient signals. The urban macro-cellular environment represents the worst case for distance calculations due to the large amount of interference in this type of environment.

TABLE II
DIFFERENT DISTANCES FOR AMBC WITH RT AND RE PROPAGATION MODELS.

Propagation model	RCS (σ, m^2)	Urban Total distance (m)	Sub-urban Total distance (m)
Ray Tracing	-	550	950
Radar equation	0.001	159	283
	0.01	283	503
	0.16	567	1000
	0.3	662	1178
	0.7	819	1456

Similarly, a signal is able to travel $475\,\text{m}$ between the TX and the sensor in a suburban environment when a LOS link exists between them. The loss at a distance of $475\,\text{m}$ is $82.29\,\text{dB}$. Therefore, a total loss of $164.58\,\text{dB}$ is experienced by a signal travelling from the TX to the RX via reflection from the sensor. As this value is less than the total available loss, a communication link of $950\,\text{m}$ between the TX and the RX can be established after the signal is reflected from the sensor. In the highway environment, the sensors can be placed within a diameter of $0.95\,\text{km}$ centering around the TX. The site distances in highway environments are about $10\,\text{km}$ to $15\,\text{km}$ so all the sensors need to be placed in the vicinity of the TX/RX. As the interference and the additional loss is less in comparison, greater distances can be achieved by the ambient signal. Therefore, due to the lower losses experienced in highway environments these results are optimistic. Sensors located in the NLOS path of the TX/RX experience greater losses and further studies and measurements need to be performed to determine how coverage can be provided to them.

The range (R, km) is calculated utilizing the radar equation (1) using different values for the radar cross section (σ). The values considered for σ attempts to indicate the size of the sensors used in IoT wireless communications. The worst case scenario is when the value of σ is the smallest as the signal has the least surface area to reflect back from.

In the urban macro-cell environment, a total distance of $159\,\text{m}$ can be achieved when utilising a sensor of $0.001\,\text{m}^2$. The total achievable range of communication is $283\,\text{m}$ when a $0.01\,\text{m}^2$ is used. A distance of $567\,\text{m}$ is achievable when a half-dipole antenna (σ = $0.16\,\text{m}^2$) is used (based on the value calculated using (3). This distance represents the most realistic value when compared with the ray tracing technique. Longer communication distances of $662\,\text{m}$ and $819\,\text{m}$ are

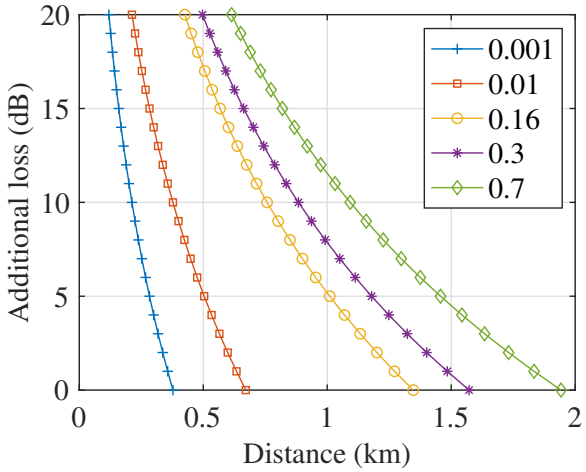

Fig. 3. Achievable distances for different system and additional losses for varying RCS (σ).

achievable when $0.3\,\mathrm{m}^2$ and $0.7\,\mathrm{m}^2$ sensors are utilised, respectively. However, such sensor sizes may be impractical in practical applications. The large sensors indicate the best case scenario as the signal has a much larger surface to reflect back from. A $15\,\mathrm{dB}$ additional loss is used for these calculations and the summary of the total distances in the urban environment for corresponding σ values are summarised in table II.

In the sub-urban environment, with an additional loss of $5\,\mathrm{dB}$, the achievable distance is $283\,\mathrm{m}$ when a $0.001\,\mathrm{m}^2$ size sensor is utilised. The total achievable distance is $503\,\mathrm{m}$ when a $0.01\,\mathrm{m}^2$ sensor is used. For a $0.16\,\mathrm{m}^2$ sensor, the total achievable range is $1000\,\mathrm{m}$. It is observed that this value is the closest to the the total distance achieved utilising the ray tracing technique in the sub-urban environment. Finally, total distances of $1178\,\mathrm{m}$ and $1456\,\mathrm{m}$ are achieved utilising $0.3\,\mathrm{m}^2$ and $0.7\,\mathrm{m}^2$ size sensors. These values are summarised for different σ values in table II.

An analysis is also carried out to determine how the additional loss affects the calculation of the range using the radar equation. Fig. 3 shows the distance the ray is able to travel between the TX and the RX for different values of additional loss. The additional loss makes a significant impact on the achievable distance. Values from $0\,\mathrm{dB}$ to $20\,\mathrm{dB}$ are used to in the graph to represent various use cases. Radar cross section (σ) values vary and are represented by the different curves in Fig. 3. It is observed that the increase in the additional loss decreases the total achievable distance.

VI. Conclusion

In this paper, an analysis was performed to determine the maximum achievable distance between the TX and the RX after reflection from the sensor utilizing ambient LTE-700 signals. This is one of the lowest available frequency band for mobile communications. Furthermore, it was assumed that the TX and RX were operating in the mono-static mode and the sensors are located in their LOS path. The ray tracing approach and the radar equation were utilized to perform simulations in the urban macro-cellular and suburban highway environments using different values for the additional loss. Due to the scarcity of interference, the suburban environment represents the best case scenario in contrast to the urban environment which has multiple sources of interference. Additionally, different values were considered for the radar cross section (which acts as the sensor) to indicate real-world IoT deployment scenarios. It was observed that by using the ray tracing approach, distances of $550\,\mathrm{m}$ and $950\,\mathrm{m}$ were achieved in urban and suburban environments, respectively. Utilising the radar equation it was observed that distances of a few hundred meters are achievable depending on the size of the sensor and the additional loss. The distances achieved by using the ray tracing approach and the radar equation demonstrate that this approach performs well for LOS links in the outdoor environment.

References

[1] H. Stockman, "Communication by means of reflected power," *Proceedings of the IRE*, vol. 36, no. 10, pp. 1196–1204, Oct 1948.

[2] L. Xie, Y. Yin, A. V. Vasilakos, and S. Lu, "Managing rfid data: Challenges, opportunities and solutions," *IEEE Communications Surveys Tutorials*, vol. 16, no. 3, pp. 1294–1311, Third 2014.

[3] V. Liu, A. Parks, V. Talla, S. Gollakota, D. Wetherall, and J. R. Smith, "Ambient backscatter: Wireless communication out of thin air," *SIGCOMM Comput. Commun. Rev.*, vol. 43, no. 4, pp. 39–50, Aug. 2013.

[4] B. Kellogg, A. Parks, S. Gollakota, J. R. Smith, and D. Wetherall, "Wi-fi backscatter: Internet connectivity for rf-powered devices," *SIGCOMM Comput. Commun. Rev.*, vol. 44, no. 4, pp. 607–618, Aug. 2014.

[5] D. Bharadia, K. R. Joshi, M. Kotaru, and S. Katti, "Backfi: High throughput wifi backscatter," *SIGCOMM Comput. Commun. Rev.*, vol. 45, no. 4, pp. 283–296, Aug. 2015.

[6] R. Biswas, J. Sae, and J. Lempiainen, "Power budget for wide area ambient backscattering communications," in *2018 IEEE Vehicular Networking Conference (VNC)*. IEEE, 12 2018.

[7] M. U. Sheikh, R. Duan, and R. Jantti, "Validation of backscatter link budget simulations with measurements at 915 mhz and 2.4 ghz," in *2019 IEEE 89th Vehicular Technology Conference (VTC2019-Spring)*, 2019.

[8] S. H. Choi and D. I. Kim, "Backscatter radio communication for wireless powered communication networks," in *2015 21st Asia-Pacific Conference on Communications (APCC)*, Oct 2015, pp. 370–374.

[9] X. Lu, D. Niyato, H. Jiang, D. I. Kim, Y. Xiao, and Z. Han, "Ambient backscatter assisted wireless powered communications," *IEEE Wireless Communications*, vol. 25, no. 2, pp. 170–177, April 2018.

[10] F. Jameel, I. Khan, and B. Lee, "Simultaneous harvest-and-transmit ambient backscatter communications under rayleigh fading," *EURASIP Journal on Wireless Communications and Networking*, vol. 2019, 12 2019.

[11] N. Van Huynh, D. T. Hoang, X. Lu, D. Niyato, P. Wang, and D. I. Kim, "Ambient backscatter communications: A contemporary survey," *IEEE Communications Surveys Tutorials*, vol. 20, no. 4, pp. 2889–2922, Fourthquarter 2018.

[12] D. Barton, C. Cook, P. Hamilton, and I. ANRO Engineering, *Radar Evaluation Handbook*, ser. Radar Library. Artech House, 1991.

[13] S. Sesia, I. Toufik, and M. Baker, *LTE, The UMTS Long Term Evolution: From Theory to Practice*. Wiley Publishing, 2009.

PUBLICATION IV

Assessment of 5G as an ambient signal for outdoor backscattering communications

Ritayan Biswas and Jukka Lempiäinen

Wireless Networks 27 (Aug. 2021)
DOI: 10.1007/s11276-021-02731-x

Wireless Networks (2021) 27:4083–4094
https://doi.org/10.1007/s11276-021-02731-x

ORIGINAL PAPER

Assessment of 5G as an ambient signal for outdoor backscattering communications

Ritayan Biswas[1] · Jukka Lempiäinen[1]

Accepted: 20 July 2021 / Published online: 4 August 2021

Abstract
The aim of this article is to evaluate the applicability of 5G technology as a possible ambient signal for backscattering communications (AmBC). This evaluation considers both urban macro-cellular, small cell as well as rural highway environments. The simulations are performed in outdoor areas including analysis about 5G implementation strategies in different scenarios. Essential aspects of 5G radio network topology such as frequency domain (3.5 GHz and 26 GHz) and antenna locations (offering line-of-sight, LOS) are highlighted and turned to applicability scenarios with AmBC. The LOS scenarios are evaluated to determine the widest applicability area of 5G for AmBC. Typical AmBC applications are studied including collection of data from several sensors to receivers. Evaluation of the applicability of 5G was based on propagation related simulations and calculations utilising the ray tracing technique and the radar equation. The results demonstrate that 5G can be used as an ambient signal for backscattering communications for short ranges for typical sensor sizes. It is also observed that the range of communication is heavily dependent on the the size of the sensor.

Keywords IoT · AmBC · 5G · Sensors

1 Introduction

The internet of things (IoT) is a wireless communication paradigm where sensors are utilised to collect information from the surrounding environment. These sensors may have the capability to measure a multitude of parameters such as temperature, humidity, location, etc. Some of the use cases of these sensors include traffic, atmosphere, health and environment monitoring. Additionally, they have the capability to communicate among themselves and with a central server. Due to the variety of use cases, these sensors will probably be deployed in huge numbers and at a variety of locations. IoT is considered a key enabling technology for future wireless technologies. IoT devices are envisioned to be connected to each other along-with the internet in order to exchange and transfer different types of data. The fifth generation (5G) of mobile communications is being developed with the provision of supporting the data needs for such a variety of devices.

Ambient backscattering communications (AmBC) is a technology where sensors are capable of harvesting (or, gathering) energy from ambient RF signals present in the atmosphere. AmBC enables battery free and wireless operation of the sensors by harvesting energy from cellular signals, television broadcasts, Wi-Fi signals and so on. Therefore, the requirement for maintenance and changing batteries are eliminated. Thus, AmBC permits the deployment of sensors in some remote as well as inaccessible locations such as inside walls (where certain ambient signals are present). The concept of AmBC was first introduced in [10] during the year 2013. Ambient television broadcast signals were utilised as part of their research and communication distances of 45.7 cm and 76.2 cm were established in indoor and outdoor environments, respectively [10]. Moreover, the channel state information (CSI) and the received signal strength indicator (RSSI) were altered to achieve communication by harvesting ambient Wi-Fi signals [8]. This enabled the sensor type devices to

✉ Ritayan Biswas
ritayan.biswas@tuni.fi

Jukka Lempiäinen
jukka.lempiainen@tuni.fi

[1] Faculty of Information Technology and Communication Sciences, Tampere University (Hervanta Campus), Korkeakoulunkatu 1, Tampere 33720, Finland

be connected to the internet. Data rates of 0.5 kbps and 20 kbps were achieved in the uplink and downlink [8]. There was a significant improvement in throughput achieved in [2] where data rates of 5 Mbps and 1 Mbps were achieved for ranges of 1 m and 5 m, respectively [2].

The AmBC technology can be used for a variety of applications. AmBC works on the principle of radio backscatter, where radio waves generated by a dedicated reader are reflected back from a sensor. Radio backscatter was introduced in literature by Harry Stockman in the year 1948 to identify friendly or hostile air-crafts during the Second World War [17]. The advancement in technology and the reduction in the cost of manufacturing integrated circuits (ICs) has stimulated the development of the radio backscatter technology [19]. This has enabled radio backscatter to become a common and mainstream technology during the past couple of decades [19]. A key application area for radio backscatter is the radio frequency identification (RFID) technology. RFID systems consist of a transmitter, receiver and tag or sensor. The signal generated from the transmitter is reflected back from the sensor. Based on the application scenario, the receiver authenticates the particular sensor. However, these RFID sensors are generally passive elements which are unable to communicate among each other. The communication between passive RFID sensors was introduced in [11] and was achieved by modulating the field of the carrier signal.

Previous studies focused on technologies such as WLAN, FM radio, television broadcasts and existing cellular signals as the possible source of ambient signals for backscattering communications. Presently, the research and development of the fifth generation (5G) of mobile communications is nearly complete (based on Release 15) and the deployment of the system has already taken place in parts of some countries. The 5G system is expected to be widely deployed commercially between 2020 and 2022. The new radio access technology for 5G termed as the 5G new radio (5G NR) was developed by 3GPP and was standardised as the air interface for the 5G systems during the end of 2017. The 5G NR utilises two frequency bands, frequency range 1 (FR1) which utilises the sub 6 GHz microwave frequency band and frequency range 2 (FR2) which utilises the millimeter wave frequency band between 24 GHz and 100 GHz.

The objective of this study is to evaluate the suitability of 5G as an ambient signal for backscattering communications in outdoor environments. The outdoor environment represents the maximum applicability area of 5G for AmBC, due to typical antenna implementations. 5G networks (which support high capacity) are generally deployed in densely populated urban environments (as shown in Fig. 1) at frequencies of 3.5 GHz and 26 GHz. IoT wireless communications are envisioned to have a lot of use cases in these environments. Therefore, AmBC sensors of different sizes are also studied in order to determine the change in the achievable range of communication due to this parameter. Furthermore, the advent of autonomous vehicles (for example) has led to the research of IoT in rural highway environments. 5G networks can provide coverage to rural highway environment (as shown in Fig. 2). Therefore, the applicability of 5G as an ambient signal for AmBC is also studied in rural highway environment.

2 System setup—5G for Ambient backscattering communications

2.1 Fifth generation (5G) mobile networks

In the near future, mobile communications are envisioned to provide data rates of the order of gigabits and also provide communications with low latency in comparison with present standards. The need for high data rates is driven by the tremendous number of devices that are thought to be connected to the internet and also with the advent of IoT [12]. It is also believed that these data rates would be comparable to fixed-line broadband services. 5G aims to provide support for IoT by enabling more capacity. In IoT wireless communications, a plethora of devices (or, things) are connected to each other as well as a central node via the internet. Additionally, 5G also aims to provide support for technologies such as augmented reality, tactile internet, machine type communications and so on [12]. Furthermore, autonomous vehicles, traffic management and remote surgeries are some of the major use cases behind achieving and establishing ultra reliable low latency communications (URLLC) which is a major requirement of 5G communications [15]. The 5G mobile communications aim to fulfil these requirements by introducing key technologies for the RF interfaces.

Firstly, utilisation of higher frequencies (in comparison with present standards) enable the use of massive multiple-input and multiple-output (MIMO) antenna arrays at the macro-cell base stations [9, 13]. Therefore, the higher path loss resulting from the use of higher frequencies can be compensated by utilising the large antenna arrays at the transmitter. Additionally, advances in the massive MIMO technology and the use of antenna arrays can help in transmission to users distributed along the azimuth and elevation plane simultaneously. Furthermore, beam-forming can help in achieving high performance in both the uplink and downlink [4]. Figure 1 shows the distribution of macro-cell towers in an urban area (for example) where massive MIMO implementation will be carried out.

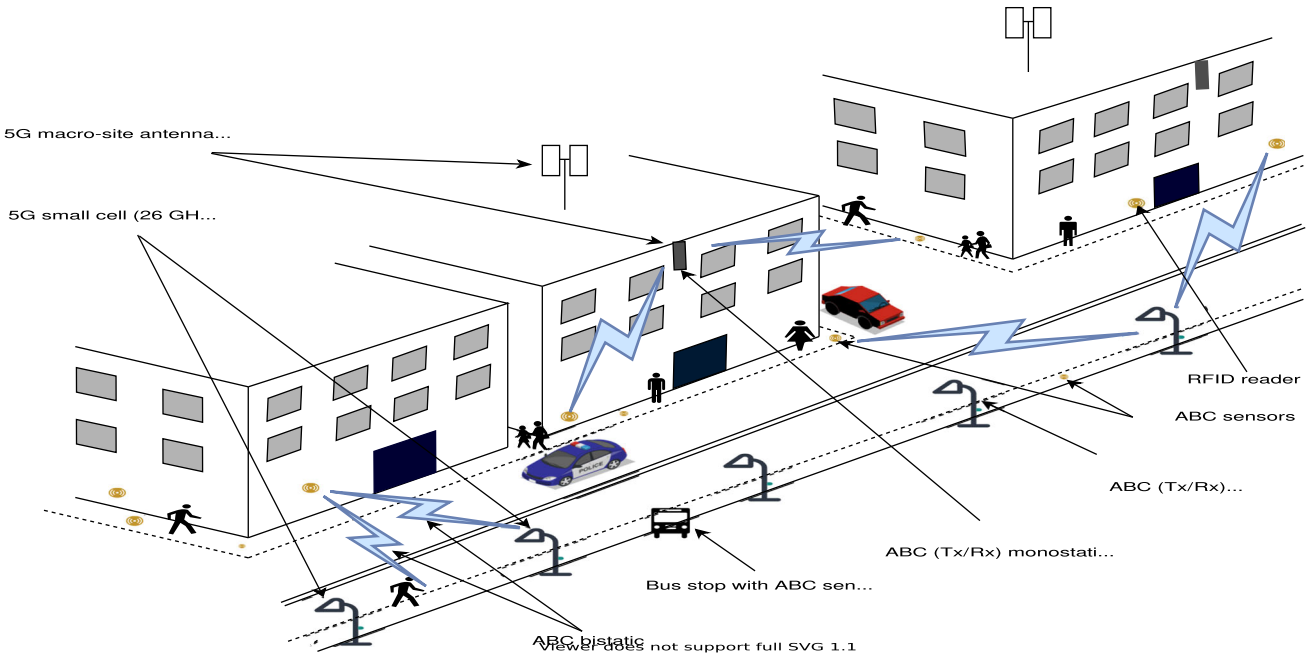

Fig. 1 Deployment strategies of 5G and AmBC in urban environment

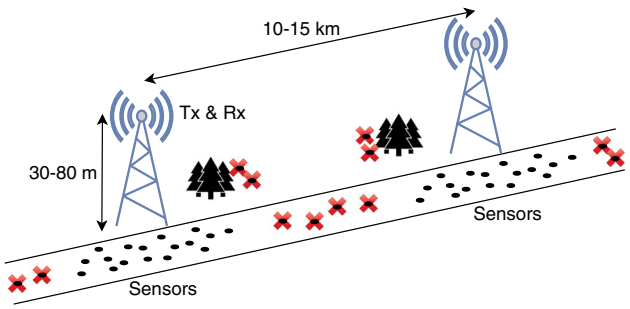

Fig. 2 Rural highway environment

Secondly, the traffic load on dense urban macro-cells can be reduced by utilising small cells in heterogeneous networks. However, to carry the control plane traffic, the requirement and utilisation of macro-cells would still be necessary even if small cells are densely deployed [7]. Figure 1 shows an example of an heterogeneous network environment where small cells are utilised in coherence with traditional macro-cellular networks. Small cells will be implemented for example on top of light-posts located beside the street. The use of heterogeneous networks may result in a higher other cell interference which can affect the capacity gains. However, the excess interference can be compensated by cooperative scheduling and coordinating multipoint (CoMP) technology [7, 16]. Additionally, the 5G air interface and the associated wave-forms need to be defined such that it is flexible enough to support a variety of applications. For 5G new radio (NR) phase 1, 3GPP has decided to utilise OFDM type wave-forms to fulfil these requirements.

Finally, a shift towards higher frequency bands is required in order to support the requirement for very high data rates and enhanced mobile broadband (eMBB) [12]. There is very large carrier bandwidth available in the millimeter wave frequency range (24 GHz–100 GHz) and the utilisation of this bandwidth can help in achieving high data rates. In 5G networks, a combination of the millimeter and the sub-6 GHz microwave frequency bands will be utilised to establish communications. The wide area coverage could be provided by utilising the sub-6 GHz frequency bands in macro-cells. For local and personal area communications, the licensed millimeter wave frequency band could be utilised [6]. The unlicensed frequency bands in the millimeter wave spectrum could be utilised for small cells and short range indoor links [6]. Macro-cells and small cells may operate at different frequencies even for the same operator as shown in Fig. 1. Generally, the 5G macro-cells are mostly implemented on existing sites and small cells are deployed on new sites such as light-posts as shown in Fig. 1.

This study is performed using ambient 5G signals transmitted at frequencies of 3.5 GHz and 26 GHz (utilised in Europe). The 3.5 GHz frequency band is generally utilised on macro sites and has already been deployed in some countries. However, there is also a possibility of utilising the millimeter wave frequency band in macro-cellular environments (as shown in Fig. 1). It is foreseen that small cells will generally operate at the 26 GHz frequency band (in Finland) though the 3.5 GHz frequency band may also be utilised in some cases. As shown in Fig. 1, the

implementation of 5G is carried out in the macro-cell and small cell environments based on the use cases and the number of users that need to be served at a particular location.

2.1.1 Urban macro-cellular

The urban macro-cellular environment has the most number of users both in terms of personal mobile users and "things" which are a key part of IoT wireless communications. Figure 1 shows a schematic diagram of the environment where the 5G urban macro-cellular T_X antenna will be deployed. Generally, the T_X antenna is located on or just below the rooftop level as shown in Fig 1. The antenna is placed below the rooftop to minimise the effect of the back lobe of the antenna radiation pattern. By modifying the base station components and configurations, existing sites can be utilised for the deployment of 5G networks which provides a profitable approach for telecom operators. The height of the T_X antenna in such an environment is typically 20 m–30 m depending on the height of the buildings. The site distance for such environments is approximately 200 m–400 m. There are various line-of-sight (LOS) paths which exist between the T_X antenna and the users because of typical antenna deployments below the rooftop. In this study, we are considering only the scenarios where a LOS path exists between the T_X antenna and the sensors to find out the maximum applicability area of 5G for AmBC.

2.1.2 Small cells

For cellular operators, small cells tend to provide coverage at the cell edge therefore extending the range of communications. Additionally, small cells are also utilised for providing enhancement in network capacity in densely populated urban areas such as city-centers, shopping malls and railway stations. As shown in Fig. 1, small cell T_X antennas may be located on light-posts which helps to provide coverage to a variety of devices. The requirement of small cells is mostly predominant in densely populated areas such as residential areas (as shown in Fig. 1), stadiums and shopping malls. Furthermore, the expansion of coverage to indoor users in dense urban areas is possible due to the use of small cells. These locations have a large number of users both in terms of personal users and devices. Therefore, the requirement for small cells has grown with smart city applications. This study is performed based on the scenarios where a clear LOS path exists between the small cell T_X antenna and the sensor.

2.1.3 Rural highway

This study is also performed in a rural highway environment because obstacles and interference causing signals are at a minimum there. The typical existing site distance in a rural highway environment is between 5 km and 15 km depending on the frequency of operation and height of the T_X antenna towers. Generally, in Finland, the height of the T_X antenna is between 30 m and 80 m. The schematic diagram of a rural highway environment is shown in Fig. 2. The cost effective method for obtaining the best possible coverage is to place the T_X antenna as high as possible. Moreover, due to the lack of obstacles in this environment clear LOS paths exist between the sensors and the T_X antenna. This study analyses the best case scenario which can be achieved in a rural highway environment.

2.2 Ambient backscattering communications (AmBC)

The AmBC technology works on the principle of energy harvesting from ambient RF signals generated from a variety of sources [10]. Enabling the battery free operation of the sensors is a major advantage of AmBC. In addition, as an external power source is not necessary these sensors can be deployed in a variety of locations where regular maintenance is not possible. The three categories which work on the principle of radio backscatter are, mono-static backscatter, bi-static backscatter and ambient backscatter.

A dedicated transmitter/receiver is necessary for the operation of mono-static backscatter systems [3]. In these systems, the transmitted signal is reflected back from the sensor towards the reader for decoding. An example of mono-static backscatter is a traditional RFID system. Automatic authentication systems and contact-less payments are two major applications of RFID systems. In bi-static backscatter, a centrally located carrier emitter transmits the ambient signals [3]. The sensors can be placed around the carrier emitter within a certain distance. The purpose of bi-static systems is different in comparison to mono-static systems as a dedicated reader is not required. Therefore, in comparison with mono-static backscatter, the range of communication for bi-static backscatter systems may be longer in some use cases. However, the transmission of a dedicated signal is still a drawback of the bi-static backscatter systems as is the case with mono-static backscatter systems.

Ambient signals present in the atmosphere are utilised to establish communication in AmBC. The source of the ambient signal can be mobile network, television broadcast, Wi-Fi signal or FM radio to name a few. The communication range of AmBC is dependent on the strength of the ambient RF signals which depends on the frequency of

the transmitted signal. For example, when FM radio signal is utilised as an ambient signal, the achievable communication range is longer than in case where the ambient signal is received from mobile networks due to the lower operating frequency of FM. The sensors utilised for AmBC need to have the necessary hardware to harvest signals from the ambient systems. The operating principle of AmBC is based on the transmission of '0' and '1' from the sensor [10]. The change of state is achieved by changing the antenna impedence states and alternating between the reflecting and the non-reflecting states of the sensor.

The AmBC technology can operate by utilising the principle of mono-static backscatter or bi-static backscatter. In this study, AmBC operates in the mono-static backscatter mode. Fig. 1 demonstrates the 5G implementations where AmBC mono-static backscatter systems are deployed. The T_X antenna of 5G macro-cell or small cell generates the signal which is subsequently reflected back towards the receiver located at approximately the same location. These communication links between the T_X/R_X antenna and the sensor are shown in Fig. 1. Moreover, AmBC can also be utilised for bi-static operation of the sensors. In this case, the ambient signals may come from the 5G T_X antenna, get reflected from a sensor and be received by an user equipment. This scenario is also illustrated in Fig. 1.

3 Simulation setup

Radio propagation simulations are needed in order to evaluate the applicability area of 5G for AmBC. 5G macro-cells and small cell configurations presented in Fig. 1 are analysed based on ray tracing simulations and radar equation calculations. Both ray tracing approach and radar equation are used in order to have a comparison and certain accuracy of the results.

3.1 Ray tracing

The first method used in order to estimate the signal propagation is the ray tracing technique. The principle of the ray tracing technique is based on the signal propagation between two points, the transmitter and the receiver antenna. A detailed and comprehensive description of the propagation environment is required to accurately predict the path the signal travels. A number of parameters such as the size, location and the height of different obstacles such as buildings, trees and light-posts need to be modelled properly to estimate the signal paths correctly. Additionally, the width of the street, building penetration losses, the rooftop and window refraction losses and other parameters need to be defined. Furthermore, diffraction and scattering losses of the signal also need to be described in detail in order to have a proper design of the simulation environment.

The ray tracing approach utilises the mirror image theory in order to find the exact path the ray travels between the T_X and the R_X antenna. Moreover, this algorithm defines the direction the signal needs to propagate. Eventually, the received signal power is calculated at the R_X antenna. If there is a signal transmitted between two points 'A' and 'B', the path loss is calculated based on (1) and the loss occurring due to diffraction or reflection is added. Subsequently, as the ray continues till the R_X antenna, the entire path is divided into smaller links.

In the ray tracing method, each individual multi-path signal component is divided into LOS point-to-point links between reflection and diffraction or between T_X and R_X. For example, a transmitted signal may reflect and diffract of three surfaces before it reaches the receiver. Therefore, there would be four LOS links for this particular scenario. The path loss for each LOS link is calculated based on (1) which represents the free space path loss (FSPL) model. Finally, the path loss for each individual LOS link is summed up to obtain the total loss that the signal experiences following that particular path. In (1), the distance (d) between two points of an LOS link is represented in kilometers and the frequency (f) is calculated in megahertz.

$$FSPL = 32.45 + 20 \cdot \log_{10}(d_{\mathrm{km}}) + 20 \cdot \log_{10}(f_{\mathrm{MHz}}). \quad (1)$$

In this study, the sensors are assumed to have a clear LOS connection from both the macro-cell and small cell T_X antennas as shown in Fig 1. Therefore, there exists only one LOS path between the T_X antenna and the sensors. In other words, the ray tracing technique gets simplified into a single FSPL link. Furthermore, an approximate reflection loss of 20 dB is considered when the signal rebounds from the sensor [14, 18].

3.2 Radar equation

Another method to calculate the range of communication for a T_X/R_X LOS scenario is the radar equation (RE). The radar equation is represented by (2) where the transmitted signal is reflected towards the R_X antenna from the sensor [1]. The range of communication for the radar equation is determined by the sum of the distance between the transmitter and the sensor and the distance between the sensor and the receiver.

$$R = \sqrt[4]{\frac{P_t G_t G_r \lambda^2 \sigma}{(4\pi)^3 P_r L_{\mathrm{add}}}}. \quad (2)$$

There are two types of radar systems, mono-static and bi-static radar. In mono-static radar, the transmitter and the

receiver are located approximately at the same location. Thus, the signal travels via the same path before and after the reflection from the sensor. Therefore, the total range of communication for a mono-static backscatter system is double the distance between the T_X/R_X antenna and the sensor. On the other hand, bi-static radar systems may have a significant separation between the transmitter and the receiver. The transmitted signal gets reflected from the sensor and travels further to reach the receiver for detection. The total range of communication for bi-static radar systems is the sum of the distance between the transmitter and the sensor and the distance between the sensor and the receiver. In this study, a mono-static radar system is considered for calculating the range of AmBC communication utilising 5G ambient signals.

In (2), the range (R) of the radar is calculated for a mono-static system. The range of a bi-static radar system is expressed by dividing the range term (R) into the distance between the transmitter and the sensor (R_t) and the distance between the receiver and the sensor (R_r). All the distances are expressed in meters. The transmit power (P_t), transmitter gain (G_t) and receiver gain (G_r) are specific for a particular system and these values are expressed in the linear scale. In this study, 32 dBi is used for G_t and G_r for all calculations. The radar equation is frequency dependent and λ represents the wavelength of the ambient 5G signal. The size of the sensor (RCS, σ) is expressed in square meters and has a vital role in determining the range of the radar equation. In literature [1], the value of σ signifies a half dipole antenna and is represented by,

$$\sigma = 0.88 \times \lambda^2. \tag{3}$$

The additional loss (L_{add}) accounts for the system and propagation losses which are different from the path loss. For example, obstacles in the the first Fresnel zone in case of LOS communications lead to an additional loss of a few decibels.

3.3 Minimum reception level and path loss

In order to evaluate the total communication distance, the path loss needs to be defined. The calculation of the path loss is done based on the difference between the transmit power (P_t) and the minimum reception level (P_r) of the system. The typical transmit power (P_t) of 40 W (or, 46 dBm) is utilised for the simulations in the urban macro-cell environment [5]. Also, a typical transmit power (P_t) of 4 W (or, 36 dBm) is used for the urban small cell simulations [5]. P_r represents the minimum reception level of the system which generally signifies the limit up to which the received signal is distinguishable from the background noise. The value of P_r is calculated based on (4). The value of the Boltzmann's constant (k) is $1.38 \times 10^{-23} J/K$ and the operating temperature (T) is 290 K.

$$RX_{\text{sensitivity}}(\text{dBm}) = 10 \cdot \log_{10}\left(\frac{kTB}{0.001}\right) + NF + SNR. \tag{4}$$

The carrier bandwidth (B) may vary in 5G as different bandwidths of 50 MHz–400 MHz are supported for example in the 26 GHz frequency band. In order to reduce the effects of the background noise, the large carrier bandwidth can also be split into smaller parts. As an example, the bandwidth values of 1 MHz, 20 MHz and 200 MHz are used for the simulations in this work. The noise figure (NF) and the signal-to-noise ratio (SNR) of the system is considered to be 8 dB and 4 dB, respectively. The values utilised for calculating the minimum reception level is summarised in Table 1.

Utilising the aforementioned values, the receiver sensitivity (P_r) equals $-$ 101.97 dBm when the carrier bandwidth is 1 MHz. When a carrier bandwidth of 20 MHz is used P_r is $-$ 88.96 dBm and for 200 MHz P_r equals -78.96 dBm. The values of P_r are summarised in Table 2. It can be observed that noise floor increases when carrier bandwidth increases.

The path loss is calculated as a difference of P_t and P_r of the system. It is observed that the path loss is 147.97 dB (1 MHz), 134.96 dB (20 MHz) and 124.96 dB (200 MHz) for macro-cells. For small cells the path loss is 137.97 dB (at 1 MHz), 124.96 dB (20 MHz) and 114.96 dB (200 MHz), respectively. The available path loss decreases once the additional loss (L_{add}) of 10 dB and the reflection loss is considered.

Table 1 Simulation parameters

Parameter	Unit	Value
Transmission power (macrocells, P_t)	dBm	46
Transmission power (smallcells, P_t)	dBm	36
T_X antenna gain (G_t)	dBi	32
R_X antenna gain (G_r)	dBi	32
Boltzmann's constant (k)	J/K	1.38×10^{-23}
Temperature (T)	K	290
Bandwidth (B)	MHz	1, 20, 200
Noise figure (NF)	dB	8
Signal-to-noise ratio (SNR)	dB	4
Additional loss (L_{add})	dB	10
Reflection loss	dB	20

Table 2 Noise floor at different bandwidths (in dBm)

Bandwidth (B)	1 MHz	20 MHz	200 MHz
Noise floor (P_r)	−101.97	−88.96	−78.96

4 Results

In typical 5G urban macro-cellular environments, the network operation is primarily performed utilising the frequency band of 3.5 GHz. Table 3 shows the distances achieved for different carrier bandwidths at 3.5 GHz utilising the ray-tracing technique for the calculations. It is observed that the signal is able to travel 5.37 km from the T_X antenna to the R_X antenna after it is reflected from the sensor (for mono-static communication). This calculation is performed utilising a carrier bandwidth of 1 MHz. A total distance of 1.2 km can be achieved when 20 MHz carrier bandwidth is used. When the carrier bandwidth of 200 MHz is utilised a total distance of 375 m is achievable. It is clearly observed that the increase in the carrier bandwidth decreases the distance. These results indicate distances that can be achieved for mono-static mode of operation.

The radar equation is also utilised in the urban macro-cellular environment to perform simulations in order to determine the achievable range between the T_X and R_X antenna, after reflection from the sensor. Table 4 gives a summary of the achievable distances at 3.5 GHz for different sensor sizes and for different carrier bandwidths. When σ is 0.0004 m^2 (which represents a sensor size of 2 cm × 2 cm), the maximum range of achievable communication is 695 m (at a carrier bandwidth of 1 MHz), 328 m (at 20 MHz) and 184 m (at 200 MHz). This value of σ represents the scenario where the signal has very small surface area to reflect back from. The sensor size of 0.0065 m^2 represents a half-dipole antenna and the maximum range of achievable communication is 1.39 km (at a carrier bandwidth of 1 MHz), 659 m (at 20 MHz) and 370 m (at 200 MHz). The range of achievable communication increases to 1.55 km (at 1 MHz), 734 m (at 20 MHz) and 413 m (at 200 MHz) when the value of σ is 0.01 m^2 (sensor size of 10 cm × 10 cm). As the sensor size is increased to 0.15 m^2 the total achievable communication range varies between 813 m (at a carrier bandwidth of 200 MHz) and 3.05 km (at 1 MHz). Correspondingly, the achievable communication range is between 967 m–3.63 km when sensor size is 0.3 m^2 and 1.19 km–4.49 km when size of the sensor is 0.7 m^2. All these distances represent the mono-static mode of operation where the T_X and R_X antenna are co-located. Furthermore, these results are based on LOS connections between T_X/R_X antenna and sensor.

Table 3 Ray tracing distances (monostatic) at different bandwidths (in meters)

Bandwidth (B)	1 MHz (m)	20 MHz (m)	200 MHz (m)
3.5 GHz	5370	1200	375
26 GHz	225	50	15

Table 4 Distances (in meters) for AmBC with RE at 3.5 GHz frequency with different bandwidths

RCS (σ, m^2)	1 MHz (m)	20 MHz (m)	200 MHz (m)
0.0004	695	328	184
Half-dipole, 0.0065	1394	659	370
0.01	1554	734	413
0.15	3059	1446	813
0.3	3637	1720	967
0.7	4495	2126	1195

Based on Tables 3 and 4 it can be observed that the achievable range of communication (in mono-static mode of operation) at 3.5 GHz frequency band varies for corresponding carrier bandwidth values for a particular sensor size. For instance, at 200 MHz carrier bandwidth the achievable distance using ray tracing technique (375 m) is similar to the achievable distance using radar equation (370 m) when a half-dipole antenna is utilised as the sensor. However, the achievable range of communication is significantly different for the ray tracing technique (1.2 km) and the radar equation (659 m at the lower carrier bandwidths. The ray tracing technique does not take into account the size of the sensor. Therefore, the corresponding values for a particular sensor size does not match at each carrier bandwidth. Additionally, the results indicate that the ray-tracing technique provides slightly optimistic values in comparison with the radar equation as the calculation is mainly based on plane wave propagation.

It can also be observed that the carrier bandwidth has a significant impact on the achievable range of communication. The increase in the carrier bandwidth decreases the achievable communication distance. For example, the achievable range of communication is three to four times higher when 1 MHz carrier bandwidth is used instead of 200 MHz. Therefore, achievable communication distance is dependent on the type of ambient 5G signal that is transmitted. A 5G pilot signal generally uses narrower carrier bandwidth in comparison with a 5G traffic channel (10 MHz–100 MHz). Furthermore, the height of the building in the macro-cellular environment plays an important role in determining how far away the sensors can

actually be deployed from the T_X antenna. For example, the distance between the T_X antenna and the sensor is $734/2 = 367$ m (at a carrier bandwidth of 20 MHz) when the sensor size is 0.01 m^2. Therefore, based on the Pythagoras's theorem, the sensors can be located 365 m away from the building (when the height of the building is 30 m) in the LOS path of the T_X antenna in order to establish communication in mono-static mode of operation.

The accuracy of the results can be analysed based on the varying additional losses (L_{add}) in the AmBC T_X/R_X communication link. Fig. 3 shows the achievable communication range for different carrier bandwidths as a function of the additional loss. In Fig. 3, the additional loss is varied between 0 dB and 20 dB. The additional loss was 10 dB for the calculation of the results in Table 4. It can be observed that when the additional loss decreases, the achievable communication range increases significantly for all the sensor sizes. Therefore, if a certain communication link experiences more loss due to an obstacle, it is still possible to establish communication, although for a shorter range. Therefore, the blocking of the first Fresnel zone due to a larger obstacle (such as a tree or building) can result in greater additional loss which results in shorter achievable distance for communication.

The 5G small cells are expected to operate mostly at 26 GHz frequency band because the required range of communication is generally short. The ray-tracing results corresponding to different carrier bandwidths at 26 GHz frequency band are summarised in Table 3. From ray tracing calculations, it is observed that the achievable range of communication is 225 m between the T_X antenna and the R_X antenna after the signal is reflected from the sensor (when carrier bandwidth of 1 MHz is utilised). The total achievable distance is 50 m and 15 m when the carrier bandwidth of 20 MHz and 200 MHz are utilised, respectively. The change in achievable communication distance is not impacted due to the height of the T_X/R_X antenna. Additionally, it can be observed from Table 3 that the range of achievable communication decreases heavily when the frequency band is changed from 3.5 GHz to 26 GHz.

The calculation of the total achievable distance is also performed using the radar equation, similar to the urban macro-cellular environment. Table 5 shows a summary of the results at 26 GHz for different carrier bandwidth and different sizes of σ. When σ represents a half-dipole antenna (0.0001 m^2), the achievable range of communication is 105 m (at a carrier bandwidth of 1 MHz), 49 m (at 20 MHz) and 28 m (at 200 MHz). When the value of σ is 0.0004 m^2 (2 cm $\times$ 2 cm), the achievable range of communication is 143 m (at a carrier bandwidth of 1 MHz), 67 m (at 20 MHz) and 38 m (at 200 MHz). When the size of σ increases to 0.01 m^2 which represents a sensor size of 10 cm $\times$ 10 cm, the achievable range of communication increases to 320 m (at 1 MHz), 151 m (at 20 MHz) and 85 m (at 200 MHz), respectively. For these three sensor sizes,

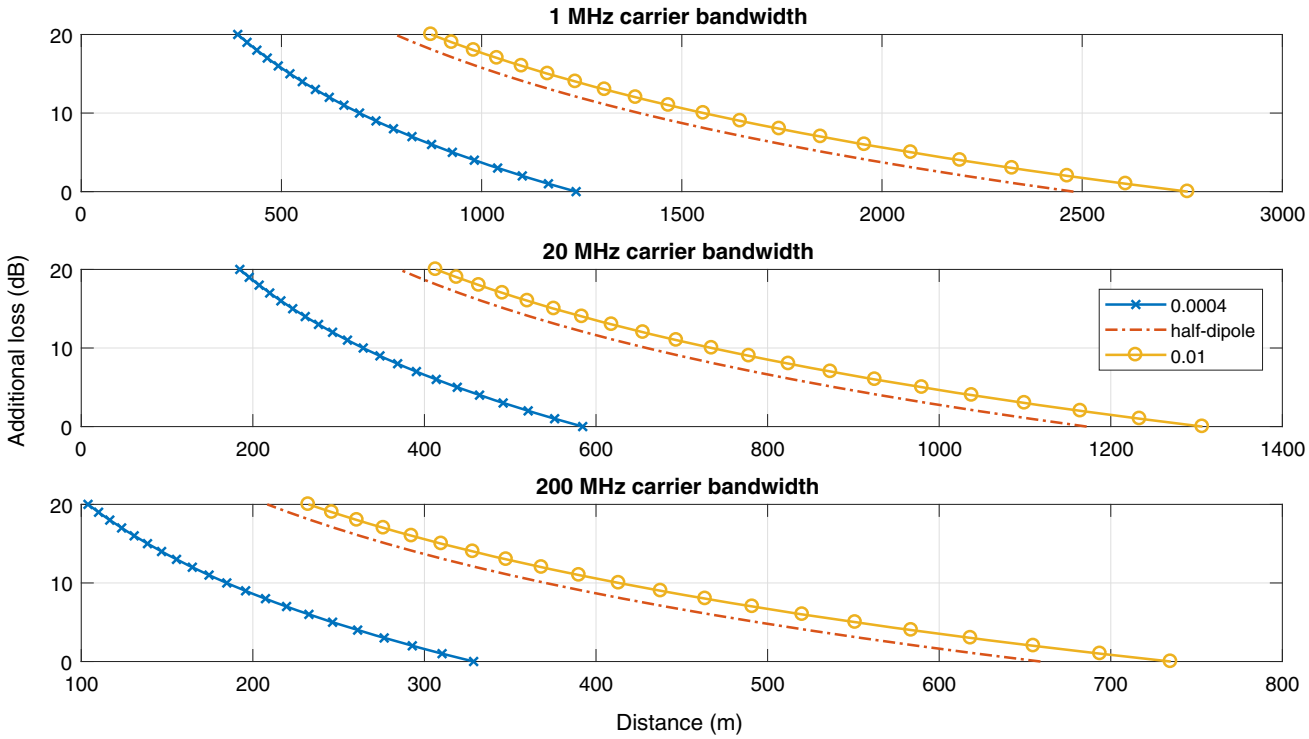

Fig. 3 Achievable distances for different additional losses and carrier bandwidth for varying RCS (σ) at 3.5 GHz

Table 5 Distances (in meters) for AmBC with RE at 26 GHz frequency with different bandwidths

RCS (σ, m^2)	1 MHz (m)	20 MHz (m)	200 MHz (m)
Half-dipole, 0.0001	105	49	28
0.0004	143	67	38
0.01	320	151	85
0.15	631	298	167
0.3	750	354	199
0.7	927	438	246

it can be observed that distances of 28 m–320 m may be possible in mono-static mode of operation depending on the carrier bandwidth utilised. The achievable range of communication is between 167 m–631 m when the size of σ is $0.15\,\mathrm{m}^2$ and when the carrier bandwidth is varied. When the size of σ is $0.3\,\mathrm{m}^2$ or $0.7\,\mathrm{m}^2$, the achievable range of communication varies between 199 m–750 m and 246 m–927 m, respectively. All these results are based on LOS connection between T_X/R_X antenna and the sensor.

Similar to 3.5 GHz frequency band, it is observed that the achievable range of communication for ray tracing and radar equation differs for a particular sensor size when different carrier bandwidths are considered in the calculations. For a half-dipole sensor, the achievable range of communication using the radar equation is 49 m at 20 MHz carrier bandwidth. This is very close to the achievable range of communication using the ray tracing technique (50 m) at the same carrier bandwidth. However, the values at 1 MHz and 200 MHz carrier bandwidth are different for the two techniques. This is due to the ray tracing calculations being independent of the size of the sensor. In this frequency band, the radar equation calculations provide more optimistic values in comparison with the ray-tracing technique.

The range of achievable communication in Table 5 is also heavily dependent on the carrier bandwidth utilised. As the carrier bandwidth is increased, the range of achievable communication decreases. The type of 5G ambient signal also has a major impact on the distance of the communication link. A 5G pilot signal (at 26 GHz) utilises a narrower carrier bandwidth in comparison to a 5G traffic channel (50 MHz–400 MHz). For example, when the size of the sensor is $0.01\,\mathrm{m}^2$, the range of achievable (mono-static) communication is 85 m at a carrier bandwidth of 200 MHz, which signifies that the sensor can be located at a maximum distance of $85/2 = 42.5$ m from the T_X antenna. However, when a carrier bandwidth of 1 MHz is utilised, the achievable mono-static communication distance is 320 m and the sensor can be located $320/2 = 160$ m from the T_X antenna. One of the 5G small cell base station deployment scenario is expected to be on top of light-posts which are approximately 10 m in height from the ground. Therefore, the sensors can be served with a signal from the small cell base station as long as they are located in the LOS path and within the proximity of the T_X/R_X antenna.

The accuracy of the results for different additional losses (0 dB–20 dB) are computed and the variation in the achievable range of communication for different sensor sizes is presented in Fig. 4. In Table 5, the calculation of the range of achievable communication was performed using an additional loss of 10 dB. For example, it is observed in Fig. 4 that the communication distance in mono-static mode is 320 m (when the sensor size is $0.01\,\mathrm{m}^2$) for an additional loss of 10 dB. However, the achievable range of communication decreases significantly (240 m for an additional loss of 15 dB) as the additional loss increases due to the presence of more obstacles between the T_X/R_X antenna and the sensor. Furthermore, from Fig. 3 it is observed that the achievable range of communication (for a similar sensor size at 3.5 GHz) is 1.55 km (for an additional loss of 10 dB) and decreases to 1.16 km (for an additional loss of 15 dB). It is observed that the mono-static distance for both the frequency bands decreases by approximately 25 percent when the additional loss increases to 15 dB from 10 dB.

In rural highway environments, mono-static communication links can be established with the sensors utilising ambient 5G signals at 3.5 GHz frequency band as long as the achievable range of communication is greater than two times the height of the base station antenna. Distances of 695 m–1.55 km can be achieved for practical sensor sizes of $0.0004\,\mathrm{m}^2$, half-dipole and $0.01\,\mathrm{m}^2$, respectively. These communication distances are achieved for sensors located in the LOS path of the T_X antenna. The distance between the sensor and the base station can be calculated using the Pythagoras' theorem. For example, the achievable range of mono-static communication is 695 m (at a carrier bandwidth of 1 MHz) if a sensor of $0.0004\,\mathrm{m}^2$ is used in the calculations. Therefore, for mono-static mode of operation, the range of achievable communication becomes half ($695/2 = 347$ m) because the signal has to travel back after reflection from the sensor. As illustrated in Fig. 5, when the base station is at a height of 80 m, it is observed that the sensors can be placed 337 m away from it. The achievable range of communication is good for a sensor of size 2 cm × 2 cm even though the signal is unable to reach near the cell edge. Although the height of the base station antenna has a major impact on the length of the communication link, it is observed that when the height of the base station antenna is reduced to 30 m from 80 m the range of achievable communication does not change significantly. Therefore, in

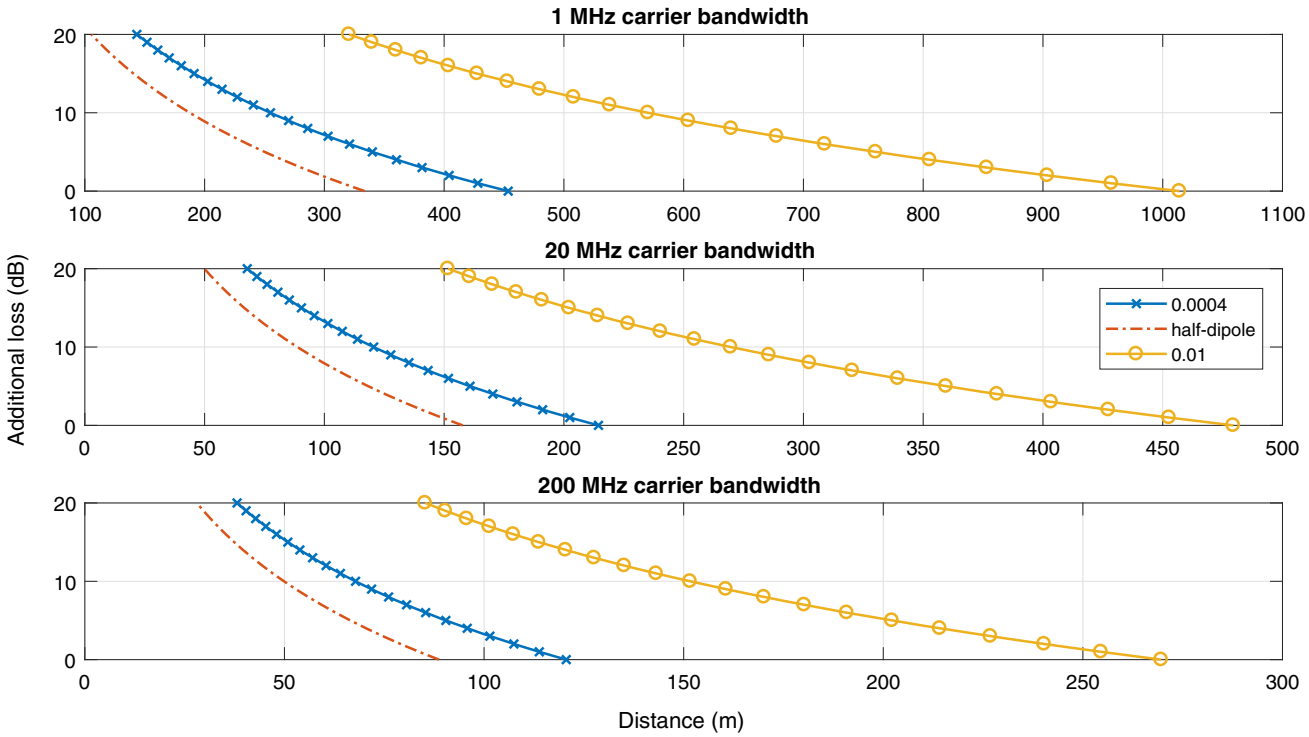

Fig. 4 Achievable distances for different additional losses and carrier bandwidth for varying RCS (σ) at 26 GHz

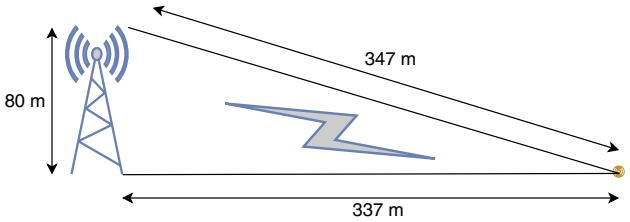

Fig. 5 Illustration of the achievable range of communication in rural highway

order to achieve communication, the sensors need to be located in close proximity of the base station. The additional loss can also be considered to be less than 10 dB as there are generally less obstacles in the rural highway environment. From Fig. 3, it can be observed that for a sensor size of 0.0004 m^2 a total distance of 926 m can be achieved (at 1 MHz carrier bandwidth) between the T_X and the R_X antenna in mono-static mode of operation (when the additional loss is 5 dB). However, in contrast to the 3.5 GHz frequency band, the 26 GHz frequency band is most probably used in a very limited way in the rural 5G environments.

5 Conclusion

The objective of this paper was to evaluate the suitability of 5G as an ambient signal for backscattering communications in the urban macro-cell, small cell and rural environments. The aim was to perform propagation simulations in outdoor environments to analyse different AmBC configurations and geographical areas which can be supported by 5G networks. The AmBC configurations at most typical 5G frequencies of 3.5 GHz and 26 GHz were analysed and it was expected that LOS communication was available between the T_X/R_X antenna and the sensor. In the urban macro-cellular outdoor environment, it was observed that the range of communication at 3.5 GHz was limited to 184 m–4.49 km from the T_X antenna in mono-static mode of operation. In the urban small cell outdoor environment, the 26 GHz frequency band was utilised for the simulations. The sensors located in the LOS path at a distance of 28 m–927 m from the T_X antenna were able to collect information and maintain communication. Additionally, it was observed for both frequency bands that the achievable range of communication significantly changed due to different carrier bandwidth and sensor size. Furthermore, it was observed that the achievable range of communication using the ray-tracing technique did not match with the range achieved utilising the radar equation for a particular sensor size. This was due to the fact the ray-tracing technique did not consider the size of the sensor and the

calculation was based on plane wave propagation. Moreover, it was also observed that the range of communication was heavily dependent on the additional loss (L_{add}) in the communication link. The communication range decreased as the additional loss in the communication link increased. In rural highway environments, sensors located at a distance of 184 m–4.49 km in the LOS of the T_X antenna were able to establish mono-static communication links. Furthermore, based on the results it was observed that the antenna height did not significantly affect the range of communication in rural environments. Therefore, it can be summarised that 5G can be utilised as an ambient signal for AmBC primarily when the sensors are located in the LOS path and in close proximity of the 5G base station T_X antenna.

Acknowledgements The authors would like to thank Tampere University and Academy of Finland for financing the work.

References

1. Barton, D., Cook, C., Hamilton, P., & ANRO Engineering, I. (1991). *Radar Evaluation handbook*. Radar Library, Artech House. https://books.google.fi/books?id=WQJTAAAAMAAJ
2. Bharadia, D., Joshi, K. R., Kotaru, M., & Katti, S. (2015). Backfi: High throughput wifi backscatter. *SIGCOMM Computer Communication Review*, *45*(4), 283–296. https://doi.org/10.1145/2829988.2787490.
3. Choi, S.H., & Kim, D. I. (2015). Backscatter radio communication for wireless powered communication networks. In *2015 21st Asia-Pacific conference on communications (APCC)* (pp. 370–374). https://doi.org/10.1109/APCC.2015.7412542
4. Ericsson white paper. (2018). *Advanced antenna systems for 5G networks*. https://www.ericsson.com/en/reports-and-papers/white-papers/advanced-antenna-systems-for-5g-networks
5. European Telecommunications Standards Institute (ETSI). (2020). *Base Station (BS) radio transmission and reception (3GPP TS 38.104 version 15.10.0 Release 15)*
6. Hansen, C. J. (2011). Wigig: Multi-gigabit wireless communications in the 60 ghz band. *IEEE Wireless Communications*, *18*(6), 6–7.
7. Jungnickel, V., Manolakis, K., Zirwas, W., Panzner, B., Braun, V., Lossow, M., et al. (2014). The role of small cells, coordinated multipoint, and massive mimo in 5g. *IEEE Communications Magazine*, *52*(5), 44–51.
8. Kellogg, B., Parks, A., Gollakota, S., Smith, J. R., & Wetherall, D. (2014). Wi-fi backscatter: Internet connectivity for rf-powered devices. *SIGCOMM Computer Communication Review*, *44*(4), 607–618. https://doi.org/10.1145/2740070.2626319.
9. Larsson, E. G., Edfors, O., Tufvesson, F., & Marzetta, T. L. (2014). Massive mimo for next generation wireless systems. *IEEE Communications Magazine*, *52*(2), 186–195.
10. Liu, V., Parks, A., Talla, V., Gollakota, S., Wetherall, D., & Smith, J. R. (2013). Ambient backscatter: Wireless communication out of thin air. *SIGCOMM Computer Communication Review*, *43*(4), 39–50. https://doi.org/10.1145/2534169.2486015.
11. Nikitin, P. V., Ramamurthy, S., Martinez, R., Rao, K. V. S. (2012). Passive tag-to-tag communication. In *2012 IEEE international conference on RFID (RFID)* (pp 177–184). https://doi.org/10.1109/RFID.2012.6193048
12. Osseiran, A., Monserrat, J., Marsch, P., Queseth, O., Tullberg, H., Fallgren, M., Kusume, K., Hoglund, A., Droste, H., Silva, I., Rost, P., Boldi, M., Sachs, J., Popovski, P., Gozalvez-Serrano, D., Fertl, P., Li, Z., Sanchez Moya, F., Fodor, G., & Lianghai, J. (2016). *5G Mobile and wireless communications technology*. Cambridge university press. https://doi.org/10.1017/CBO9781316417744.
13. Rusek, F., Persson, D., Lau, B. K., Larsson, E. G., Marzetta, T. L., Edfors, O., et al. (2012). Scaling up mimo: Opportunities and challenges with very large arrays. *IEEE Signal Processing Magazine*, *30*(1), 40–60.
14. Samimi, M. K., & Rappaport, T. S. (2014) *Characterization of the 28 ghz millimeter-wave dense urban channel for future 5g mobile cellular*. NYU Wireless TR 1
15. Shafi, M., Molisch, A. F., Smith, P. J., Haustein, T., Zhu, P., De Silva, P., et al. (2017). 5g: A tutorial overview of standards, trials, challenges, deployment, and practice. *IEEE Journal on Selected Areas in Communications*, *35*(6), 1201–1221.
16. Soret, B., Pedersen, K. I., Jørgensen, N. T. K., & Lopez, V. F. (2015). Interference Coordination for Dense Wireless Networks. *IEEE Communications Magazine*, *53*(1), 102–109. https://doi.org/10.1109/MCOM.2015.7010522
17. Stockman, H. (1948). Communication by means of reflected power. *Proceedings of the IRE*, *36*(10), 1196–1204. https://doi.org/10.1109/JRPROC.1948.226245.
18. Wilson, R. M. (2002). *Propagation losses through common building materials 2.4 ghz vs 5 ghz*. Magis Networks, Inc
19. Xie, L., Yin, Y., Vasilakos, A. V., & Lu, S. (2014). Managing rfid data: Challenges, opportunities and solutions. *IEEE Communications Surveys Tutorials*, *16*(3), 1294–1311. https://doi.org/10.1109/SURV.2014.022614.00143.

Ritayan Biswas was born in the year 1989 in Kolkata, India. He received his bachelor of technology (B.Tech) degree in Electronics and Communication Engineering from the Institute of Engineering and Management, Kolkata, India in the year 2012. He received his master of science (M.Sc.) degree in Electrical Engineering from Tampere University of Technology, Finland in 2016. Currently, he is pursuing his doctoral studies at Tampere University on future cellular communications and internet of things (IoT). His general interests include radio network planning and optimization, computer networking and future wireless technologies. He has 5 years of research experience and has authored a few conferences and journal papers and is an IEEE student member.

Jukka Lempiäinen was born in Helsinki, Finland, in 1968. He received an MSc, Lic Tech, Dr. Tech. all in Electrical Engineering, from Helsinki University of Technology, Espoo, Finland, in 1993, 1998, and 1999, respectively. He is a senior partner and the president of European Communications Engineering Ltd. He has altogether more than 10 years of experience in GSM-based mobile network planning and consulting. Currently, he is also a part-time professor of telecommunications (radio network planning) at Tampere University, Finland. He has written two international books about GSM/GPRS/UMTS cellular radio planning, several international journals, and conference papers, and he has three patents. He is a member of International Union of Radio Science (URSI) national committee, Finland.

PUBLICATION V

Sensitivity Analysis of Ambient Backscattering Communications in Heavily Loaded Cellular Networks

Ritayan Biswas and Jukka Lempiäinen

DOI: 10.23919/WONS57325.2023.10062021

Sensitivity Analysis of Ambient Backscattering Communications in Heavily Loaded Cellular Networks

Ritayan Biswas and Jukka Lempiäinen
Faculty of Information Technology and Communication Sciences (ITC), Tampere University, 33720 Tampere, Finland
Email: {ritayan.biswas, jukka.lempiainen}@tuni.fi

***Abstract*—The purpose of this article is to evaluate the impact of adjacent cell interference on monostatic ambient backscattering communication (AmBC) systems at LTE and 5G frequencies. In dense urban areas, cellular macro cell and small cell networks are utilised to provide coverage to backscatter devices (BDs) and traditional users. However, due to the close proximity of adjacent cell mobile base stations, a significant amount of interference is noticed in the serving cell during peak hours. Thus, the signal-to-interference ratio (SIR) is much more of a limiting factor than the signal-to-noise ratio (SNR) of the system. Therefore, the SIR needs to be considered in the system design of AmBC systems. AmBC systems utilise ambient signals as the only source of power, so, there is a necessity for good SIR for proper communication with the BD. Therefore, based on the simulations, the area in close proximity to the base station can be utilised for the deployment of the BDs. Furthermore, it is observed that the achievable range of communication reduces by 44 percent in a heavily loaded cell in comparison with an empty cell when the SIR increases by 10 dB.**

***Index Terms*—Sensitivity, AmBC, SIR, IoT, LTE, 5G**

I. Introduction

Ambient backscattering communications (AmBC) is a wireless communication technique where sensor-type devices utilise ambient radio frequency (RF) signals to establish communication between a transmitter (TX) and a receiver (RX) [1]. AmBC works on the principle of radio backscatter technology which was first introduced in literature by Harry Stockman [2] in 1948. The radio backscatter technology was utilised to determine the affiliation of aircrafts and distinguish them as friendly and hostile by bouncing RF signals from them. Modern technologies such as RFID and NFC utilise radio backscatter as the backbone technology for operation. However, these systems are limited by the range of communication and the requirement for the generation of a dedicated signal.

AmBC eliminates the need for the generation of dedicated signals by utilising the energy from ambient RF signals. These ambient signals are generated from a variety of sources such as cellular networks, FM radio, television broadcasts, and WLAN signals to name a few [3]. The sensors have the required hardware to gather energy from these ambient signals and establish communication [1]. Furthermore, AmBC systems are not limited in the range of communication as the frequency of the ambient signals determines the range of communication.

A number of studies have been performed to determine the range of communication of AmBC systems utilising different wireless technologies. The authors of [3] were the first to introduce the concept of AmBC in indoor environments. They were able to achieve communication ranges of tens of meters by utilising ambient television broadcast signals. Simulation-based studies were performed in outdoor macro-cell, micro-cell and rural environments to determine the feasibility of utilising ambient LTE-700 and 5G cellular network signals [4], [5]. However, these studies were performed for an ideal cell, that is, a network unaffected by the interference caused by adjacent cells. In urban environments, the inter-site distance is limited to about $150\,\mathrm{m}$ to $200\,\mathrm{m}$ [6]. The site distances are shorter to provide better coverage as the free space propagation loss increases with the increase in carrier frequency.

In this work, the effect of adjacent cell interference on the communication range of AmBC systems is studied. Simulations are performed to determine the interference caused at different locations of the serving cell. These values are utilised in further simulations to determine the range of communications for the mono-static operation of the AmBC technology. The simulations are carried out at different carrier frequencies such as low-frequency LTE-700 ($700\,\mathrm{MHz}$), mid-frequency 5G ($3.5\,\mathrm{GHz}$), and high-frequency millimeter wave 5G ($26\,\mathrm{GHz}$) bands. Eventually, a comparison is made on the achievable range of communication between the ideal cell and the cell experiencing interference.

II. Ambient Backscattering communications

AmBC is a wireless communication paradigm that utilises ambient RF signals to establish communication between a TX and RX after the signal impinges on a sensor (or, backscatter device, BD). The BDs have the capability to harness the energy from the ambient RF signals. This enables the battery-free and wireless operation of the sensors [7]. The location of the TX and RX with respect to the BD determines the type of backscattering system in use.

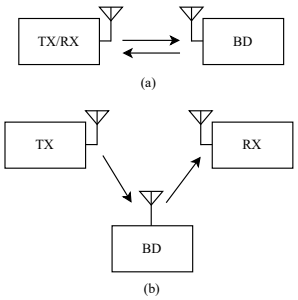

Fig. 1. (a) mono-static and, (b) bi-static backscatter.

In mono-static backscatter, the TX and RX are positioned at the same location. The ambient signal impinges on the BD and is reflected back toward the RX for decoding [8]. The illustration of a mono-static backscatter system is shown in Fig.1 (a). The phenomenon of reflection is determined by the boundary condition based on the wavelength of the incident signal [9]. This type of system is generally useful for monitoring certain parameters and no information is transferred to the end user. These parameters can range from traffic monitoring to environment monitoring such as determining the level of water or snow in certain locations. The sensors utilised for such monitoring purposes are generally located in remote areas or places where regular maintenance is not possible. Therefore, the ambient signals are the only source of power and this enables the operation of these sensors [7].

In the bi-static backscatter system, the BD is located between the TX and the RX antenna as illustrated in Fig.1 (b). The signals are forwarded towards the RX after impinging on the sensor in a bi-static backscatter system [8]. Generally, the communication range between the TX and the sensor (forward link) is much longer than the distance between the BD and the RX antenna (backscatter link) [10]. A major challenge for the bi-static backscatter communication system is the requirement for the suppression of the direct path signal from the legacy systems which transmit the ambient signal. This is due to the significantly low amplitude and power of the backscatter signal in comparison with the direct path signal. The interference suppression requirements of bi-static backscatter communication is studied in [10]. The major use case for a bi-static backscatter communication system is the transfer of information to the end user from the BD.

In this article, the study is performed to evaluate the achievable range of communication of mono-static AmBC systems when there is interference from the adjacent cell.

III. Propagation models

The simulations for the signal propagation between the TX/RX and the BD are performed utilising the radar equation and the ray-tracing technique.

A. Radar equation

The radar equation is utilised to determine the range of communication when a radio wave is backscattered towards the RX antenna after impinging on the BD (or, target in radar terminology). Equation 1 is utilised to determine the range of the radar system. This equation generally illustrates the mono-static mode of operation for the radar system as the TX and RX are positioned at the same location. This is represented by the term R (in kilometers), which is the round trip distance between the TX→BD→RX. If the TX/RX are not co-located, as in bi-static radar systems, R can be divided into two terms to demonstrate the distance between TX→BD and BD→RX [10].

$$R = \sqrt[4]{\frac{P_t G_t G_r \lambda^2 \sigma}{(4\pi)^3 P_r L}}. \tag{1}$$

The terms P_t, G_t and G_r represent the transmitted power, transmitter gain, and receiver gain, respectively. These values are in linear scale. The wavelength of the ambient signal is represented by the term λ (in meters). The size of the BD (also termed as the radar cross-section, RCS) is represented by the term σ (in square meters). The additional losses in the system due to the blockage of the Fresnel zone, and propagation losses arising due to scattering and diffraction are represented by the term L (in dB). P_r represents the received power. In the simulations, the receiver sensitivity (or, the noise floor) is utilised as the value for P_r. The $RX_{\text{sensitivity}}$ of the system is calculated utilising equation 2.

$$RX_{\text{sensitivity}}(\text{dBm}) = 10 \cdot \log_{10}\left(\frac{kTB}{0.001}\right) + NF + SNR. \tag{2}$$

The terms k, T and B represent Boltzmann's constant, temperature, and the system bandwidth respectively. The noise figure and signal-to-noise ratio of the system are represented by the terms NF and SNR. The value of the B, NF and SNR is dependent on the type of ambient cellular technology utilised. The specific values are discussed in detail in Section IV.

B. Ray tracing

The ray tracing technique is based on the comprehensive simulation of the propagation environment. The signal between the TX antenna and the BD can follow multiple paths due to reflection from different objects present in the propagation environment such as buildings, trees, automobiles, etc. In traditional wireless systems, these multi-path signals are added at the RX module based on their constructive or destructive interference. Each multi-path of the signal is segmented based on the line-of-sight (LOS) section and the path loss between these two points is computed. Subsequently, the loss due to scattering and refraction is added to determine the entire loss in that section. Finally, the propagation loss in each of these

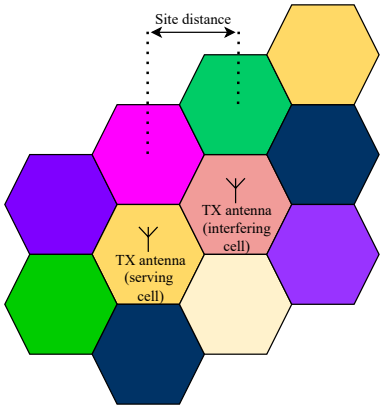

Fig. 2. Illustration of serving and interfering cell.

segments is added to determine the total path loss of a particular multi-path component of the signal.

However, in AmBC systems the ambient signal is reflected (mono-static systems) or transmitted (bi-static systems) towards a RX module. Therefore, only the strongest signal from the line-of-sight (LOS) path is considered in the simulations. The propagation path loss in the LOS path between the TX/RX and BD (in mono-static AmBC systems) is represented by the free space path loss ($FSPL$) as shown in equation 3.

$$FSPL = 32.45 + 20 \cdot \log_{10}(d_{\text{km}}) + 20 \cdot \log_{10}(f_{\text{MHz}}). \quad (3)$$

The $FSPL$ is a measure of the signal degradation between two points in the direct LOS of each other separated by a distance of d (in kilometers) and operating at a carrier frequency (f, in megahertz).

IV. Simulation Setup

A. Simulation environment

The simulations are performed in the urban macro-cell and small-cell environments at traditional LTE and 5G frequencies. The TX antennas are located on or just below the rooftop level in the macro-cell environment. This setup is mainly used to avoid the effect of the back-lobe of the antenna radiation pattern. Moreover, such type of antenna deployment enables a large amount of line-of-sight (LOS) connections between the TX/RX antenna and the BD. In small cells, the TX antennas are generally positioned to provide connectivity to cell-edge users and also to users located in dense urban areas such as stadiums, shopping malls, and bus/train stations. In this work, simulations are performed in outdoor small-cell environments. The TX/RX antenna can be located, for example, on top of light posts enabling a number of LOS connections between the TX/RX and the BD.

The network layout of the environment is represented by 3-sector hexagonal cells. Therefore, there are six adjacent cells that can cause interference with the serving cell. The amount of interference from the adjoining cell is dependent on the traffic in the network which in turn is associated with the time of day. Generally, the network is heavily loaded during peak hours and unloaded during the early morning or late night. The inter-site distance between adjacent macro-cells is generally between $150\,\text{m}$ to $200\,\text{m}$. [6] In the simulations, the inter-site distances are $200\,\text{m}$ in the urban macro-cell environment. The inter-site distance of small cells utilised in the simulations is $100\,\text{m}$. The network layout of the environment is illustrated in Fig. 2.

TABLE I
Simulation parameters.

Parameter	Unit	Value
Simulation frequencies (f)	GHz	0.7, 3.5, 26
TX power (macrocells, P_t)	dBm	46
TX power (smallcells, P_t)	dBm	36
TX/RX antenna gain (G_t/G_r)	dBi	10
BD antenna gain (G_{bd})	dBi	0
Bandwidth (B)	MHz	0.18(LTE), 1(5G)
Noise figure (NF)	dB	10
Signal-to-noise ratio (SNR)	dB	4
Additional loss (L_{add})	dB	10

The signal-to-interference and noise ratio (SINR) is calculated based on the interference caused by the signal from the adjacent cell. The signal from the TX of the serving cell is represented by the term P_{rx}. The thermal noise power and the interference power are represented by the terms P_{n} and P_{i}. The relation between P_{rx}, P_{n} and P_{i} is shown in equation 4. If either the P_{n} or P_{i} hinders the system then the thermal noise or the adjacent cell interference is the dominant limiting factor. Therefore, equation 4 can accordingly represent the SNR or SIR.

$$\text{SINR} = \frac{P_{\text{rx}}}{P_{\text{n}} + P_{\text{i}}}. \quad (4)$$

The BDs are deployed in a variety of locations based on the use case. For example, the BDs can be placed on the walls of bus stops (to enable the end-user to check for the timetables), on lamp posts, or, on the side of different buildings. The locations for the different BDs can be anywhere within the cell. The TX/RX antenna is co-located as the mono-static mode of AmBC is considered during the simulations. The BDs are deployed around the area surrounding the TX/RX of the serving cell.

B. Simulation parameters

The simulations are performed for the BDs located in the direct LOS of the TX/RX antenna operating at frequencies of $700\,\text{MHz}$, $3.5\,\text{GHz}$ and $26\,\text{GHz}$ utilising the ray tracing technique and the radar equation.

The transmit power (P_{tx}) of the macro-cell and small-cell are $46\,\text{dBm}$ and $36\,\text{dBm}$, respectively. The antenna gain for the TX and RX antenna is $10\,\text{dBi}$. The bandwidth of the LTE-700 system is 12×15 which signifies 12 resource blocks having a carrier spacing of $15\,\text{kHz}$. The simulations at 5G frequencies are performed at a system bandwidth

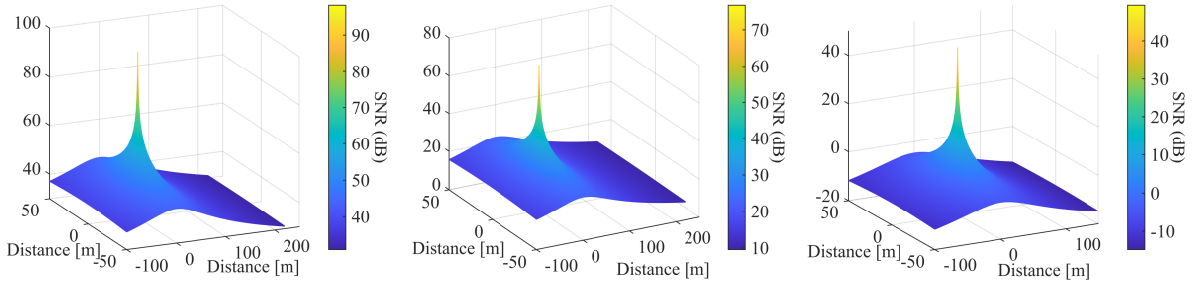

Fig. 3. The results for the representation of SNR at different locations in the serving cell. The location of the TX/RX for the serving cell is at (0,0,0). Fig. 3a illustrates the SNR at a frequency of 700 MHz. In Fig. 3b, the SNR at a carrier frequency of 3.5 GHz is shown. Fig. 3c demonstrates the variation in SNR at 26 GHz.

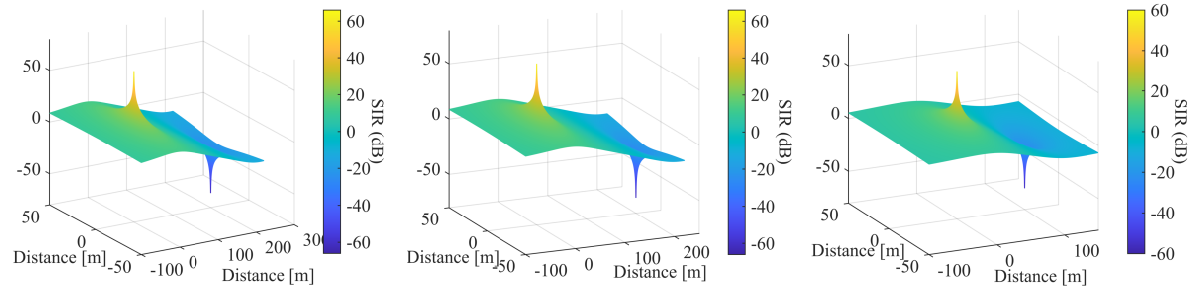

Fig. 4. The results for the representation of SIR with respect to the distance between the serving cell and adjacent cell base stations. The TX/RX of the serving cell is located at (0,0,0). The location of the adjacent cell TX/RX is at (200,0,0) in Fig. 4a and Fig. 4b. In Fig. 4c the location of the adjacent cell TX/RX is at (100,0,0). Fig. 4a illustrates the SIR at a carrier frequency of 700 MHz. In Fig. 4b, the SIR variation is demonstrated at 3.5 GHz. Fig. 4c illustrates the variation in the SIR at a carrier frequency of 26 GHz.

of 1 MHz. The noise figure utilised in the simulations is 10 dB. Furthermore, an additional loss (L_{add}) of 10 dB is utilised in the simulations for losses caused due to blockage of the Fresnel zone. The values utilised in the simulations are summarised in Table I.

V. Results and Discussion

The SNR of the system is computed as a ratio of the received signal strength (P_{rx}) at different locations in the cell and the thermal noise power (P_{n}). The calculation of P_{rx} is done using the FSPL in equation 3 for LOS paths between the TX/RX antenna and the BD. The variation of the SNR at different frequencies and locations in the cell is shown in Fig. 3. The SNR is highest at the LOS points closest to the TX antenna (located at (0,0,0) in Fig. 3) as the signal is much stronger than the background noise.

It was observed from Fig. 3a that the SNR for the LTE-700 system is a bit higher than 20 dB near the edge of the cell. The Fig. 3b and Fig. 3c SNR graphs follow a similar pattern for the 5G systems operating at 3.5 GHz and 26 GHz. At 3.5 GHz, it is observed that the SNR is about 10 dB near the cell edge. The SNR decreases rapidly at 26 GHz near the cell edge as observed in Fig. 3c.

Subsequently, the signal-to-interference ratio (SIR) of the system is computed for an adjacent cell transmitting the interfering signal (P_{i}). The LOS paths between the TX antenna and the BDs are studied in this analysis. The inter-site distances are discussed in Section IV and it varies with the type of system and the frequency of operation. The value of 0 dB SIR at the edge of the cell (at all frequencies) is logical as the two signals (serving and interfering) cancel each other. The requirement for a high SIR limits the total range of communication of the system at all carrier frequencies.

Furthermore, it can be observed from Fig. 3 and Fig 4 that the interfering signal is much more of a limiting factor than the background noise. Therefore, the SIR of each system needs to be accounted for in the simulations utilised to accurately determine the maximum achievable communication range for mono-static AmBC systems.

To compute the maximum achievable range of communication, the receiver sensitivity of the system is calculated using equation 2. These $RX_{\text{sensitivity}}$ values are utilised as the input parameter for P_{rx}, in equation 1. The achievable range of communication utilising the radar equation is also dependent on the size of the BD. Therefore, different values are utilised for the parameter σ in equation 1.

It is observed that the achievable range of communication increases with the increase in the size or surface area of the BD. The variation for the achievable range of communication (at 700 MHz, 3.5 GHz and 26 GHz carrier frequencies) utilising different size of the BD is shown in Fig. 5. The results are based on the size of the BD. The distances in Fig. 5 indicate the total round trip distance

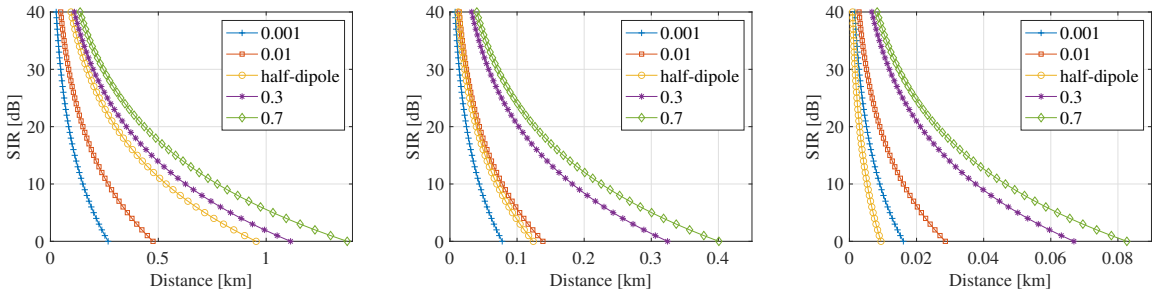

Fig. 5. The results for the total achievable range of communication (for LTE and 5G systems) with respect to the SIR requirement of the system using different sizes for the BD. Fig. 5a illustrates the total achievable range of communication at a carrier frequency of 700 MHz. In Fig. 5b, the variation in the total achievable range of communication is demonstrated at 3.5 GHz. Fig. 5c illustrates the variation in the achievable communication range at a carrier frequency of 26 GHz.

between the TX/RX and the BD. It is observed that the increase in the SIR decreases the achievable range of communication.

The achievable range of communication is restricted in comparison to the results obtained in [4] and [5] where the SNR of the system was considered as the major limiting factor. The achievable range of communication is higher when the traffic in the network is low, for example at night time. Therefore, at those hours the SIR is not the major limiting factor. In comparison, the need for having a better SIR limits the achievable range of communication due to the interfering signal from the adjoining cell.

It can be observed that utilising a BD device of $0.01\,\mathrm{m}^2$, a distance of $105\,\mathrm{m}$ (between TX/RX and BD) is achievable at $700\,\mathrm{MHz}$. Distances of $30\,\mathrm{m}$ and $6\,\mathrm{m}$ (between TX/RX and BD) are achievable at carrier frequencies of $3.5\,\mathrm{GHz}$ and $26\,\mathrm{GHz}$, respectively. These values are calculated based on a $10\,\mathrm{dB}$ increase in SIR. These are in comparison to $185\,\mathrm{m}$, $55\,\mathrm{m}$ and $11\,\mathrm{m}$ which are achievable at night when the cell is relatively empty and the interference from the adjacent cell is not a major limiting factor. Therefore, the simulations indicate a decrease of 44 percent in the achievable range of communication in a fully loaded network.

VI. Conclusion

The effect of the interference from an adjacent cell was analysed to determine the total achievable range of communication in urban macro cell and small cell environments. The signals following the LOS paths between the backscatter devices and the TX/RX antenna were studied in this paper. The simulations were performed at different cellular frequencies of $700\,\mathrm{MHz}$ (LTE-700), $3.5\,\mathrm{GHz}$ (5G) and $26\,\mathrm{GHz}$ (millimeter wave 5G). It was observed that the signal from the adjacent cell is much more of a limiting factor than the background noise. The interference from the adjacent cell causes significant signal degradation while approaching the cell edge during peak hours. Therefore, the BDs need to be located in the close vicinity of the TX/RX. In comparison, mono-static AmBC systems can achieve a higher range of communication when the network is not heavily loaded, for example, at night. However, the effect of the interference causing signals must be integrated with the system design because these BDs are envisioned to be deployed especially in dense urban areas. It was observed, that there was a 44 percent reduction in the achievable range of communication with a SIR increase of $10\,\mathrm{dB}$ Therefore, mono-static AmBC systems may be utilised where the BDs are deployed close to the base station in the LOS path of the TX/RX antenna during peak hours.

References

[1] N. Van Huynh, D. T. Hoang, X. Lu, D. Niyato, P. Wang, and D. I. Kim, "Ambient backscatter communications: A contemporary survey," *IEEE Communications Surveys Tutorials*, vol. 20, no. 4, pp. 2889–2922, Fourthquarter 2018.

[2] H. Stockman, "Communication by means of reflected power," *Proceedings of the IRE*, vol. 36, no. 10, pp. 1196–1204, Oct 1948.

[3] V. Liu, A. Parks, V. Talla, S. Gollakota, D. Wetherall, and J. R. Smith, "Ambient backscatter: Wireless communication out of thin air," *SIGCOMM Comput. Commun. Rev.*, vol. 43, no. 4, pp. 39–50, Aug. 2013.

[4] R. Biswas, J. Säe, and J. Lempiäinen, "Maximum receiver harvesting area of backscatter signals from ambient low-frequency mobile networks," in *2021 IEEE Global Communications Conference (GLOBECOM)*, 2021, pp. 1–5.

[5] R. Biswas and J. Lempiäinen, "Assessment of 5g as an ambient signal for outdoor backscattering communications," *Wirel. Netw.*, vol. 27, no. 6, p. 4083–4094, aug 2021. [Online]. Available: https://doi.org/10.1007/s11276-021-02731-x

[6] M. M. Ahamed and S. Faruque, "5g network coverage planning and analysis of the deployment challenges," *Sensors*, vol. 21, no. 19, 2021. [Online]. Available: https://www.mdpi.com/1424-8220/21/19/6608

[7] G. Wang, F. Gao, R. Fan, and C. Tellambura, "Ambient backscatter communication systems: Detection and performance analysis," *IEEE Transactions on Communications*, vol. 64, no. 11, pp. 4836–4846, 2016.

[8] R. Duan, X. Wang, H. Yigitler, M. U. Sheikh, R. Jantti, and Z. Han, "Ambient backscatter communications for future ultra-low-power machine type communications: Challenges, solutions, opportunities, and future research trends," *IEEE Communications Magazine*, vol. 58, no. 2, pp. 42–47, 2020.

[9] M. Oziel, R. Korenstein, and B. Rubinsky, "Radar based technology for non-contact monitoring of accumulation of blood in the head: A numerical study," *PLOS ONE*, vol. 12, p. e0186381, 10 2017.

[10] R. Biswas, M. U. Sheikh, H. Yiğitler, J. Lempiäinen, and R. Jäntti, "Direct path interference suppression requirements for bistatic backscatter communication system," in *2021 IEEE 93rd Vehicular Technology Conference (VTC2021-Spring)*, 2021, pp. 1–5.

PUBLICATION VI

Direct Path Interference Suppression Requirements for Bistatic Backscatter Communication System

Ritayan Biswas, Muhammad Usman Sheikh, Hüseyin Yiğitler, Jukka Lempiäinen, and Riku Jäntti

DOI: 10.1109/VTC2021-Spring51267.2021.9448755

Direct Path Interference Suppression Requirements for Bistatic Backscatter Communication System

Ritayan Biswas*, Muhammad Usman Sheikh†, Hüseyin Yiğitler†, Jukka Lempiäinen*, and Riku Jäntti†
*Laboratory of Electronics and Communications Engineering, Tampere University, 33720 Tampere, Finland
Email: {ritayan.biswas, jukka.lempiainen}@tuni.fi
†Department of Communications and Networking, Aalto University, 02150 Espoo, Finland.
Email: {muhammad.sheikh, yusein.ali, riku.jantti}@aalto.fi

***Abstract*—The ambient backscatter communication (AmBC) system utilizes the existing ambient RF signals present in the atmosphere for backscattering the signal. One of the challenges for AmBC system is the interference at the receiver module caused by the direct path signal from the ambient source. The purpose of this paper is to study the coverage aspects of the bi-static backscatter communication system in a typical urban environment at sub-1GHz frequencies using simulations in MATLAB. For the simulation, 3rd generation partnership project (3GPP) urban microcellular and international telecommunication union (ITU) device-to-device (D2D) propagation models are used. Moreover, the dynamic range i.e., the difference in the received power level of the direct path and the backscatter path is investigated. For correctly decoding the backscatter signal at the reader, the target value set for the dynamic range is less than 30 dB. This paper studies the importance of direct path interference suppression for the successful deployment of a bi-static backscatter communication system.**

***Index Terms*—IoT, Backscatter communications, AmBC, Dynamic range, Interference suppression**

I. Introduction

The Internet of things (IoT) is a wireless communication paradigm where sensors are utilised to collect and process the information from the environment [1], and for sending the data for post processing. IoT is considered as a key enabling technology for the future wireless technologies i.e., for fifth generation (5G) and beyond. IoT has various applications in our daily lives e.g., the IoT sensors can be used to measure the temperature, humidity, air pollution, car traffic density, health related parameters, agriculture, for counting the objects, and for detecting different events [1].

Low power wide area networks (LPWAN) such as long range (LoRa) radio, Sigfox and narrow band IoT (NB-IoT) have been proposed as key enabling technologies for the practical deployment of IoT in real life cases [2]. These technologies are designed to provide wide coverage for a large number of sensors simultaneously. Additionally, these technologies incur low costs and consume low energy. Due to the variety of use cases, IoT sensors are expected to be deployed in huge numbers and at a variety of locations, especially in the urban environment. Although, there are certain advantages of the aforementioned LPWAN technologies, the major drawback associated with these technologies is the energy consumption, and the need for a dedicated transmission signal [3].

Backscatter communication (BC) is a technology where an IoT sensor i.e., in this case called a backscatter device (BD) receives the incoming RF signal from the transmitter (Tx) antenna, modulates and forwards it to the receiver also known as reader [3]. In case of the ambient BC (AmBC), the radio signal generated by a non-dedicated transmitter is reflected back from a BD to the reader. In AmBC, the BDs can operate in a passive or semi-passive mode. In semi-passive mode, the BDs are capable of harvesting the energy from the cellular networks, television broadcasts and from WiFi signals to name a few. Therefore, AmBC is a step towards battery free and the wireless operation of the sensors [3].

The authors in [4] were the first to introduce the concept of AmBC by utilising the ambient television broadcast signal in the year 2013. They were able to achieve an AmBC link for a short range. The link budgets for different modes of backscatter systems were presented in references [5], [6]. Although the maturing of the technology has helped in achieving improvements over traditional backscatter systems. The performance of the BC system is limited by the short communication ranges and low data rates. This is due to the direct path interference and weak backscatter signal, since these two signals are summed at the receiver. Therefore, the limitations of BC must be investigated to identify the bottlenecks and check the feasibility of the technology for application specific scenarios. In this work, considering a legacy cellular system, first the power difference between the direct path and backscatter signal is computed, then the required amount of direct path signal suppression requirement is found, prior to the analog-to-digital conversion of the composite signal. Although this work is not limited on a specific type of direct path signal suppression method, a realistic assumption about the receiver hardware is made, where the signal power difference is lower than a threshold so that digital processing can be successfully applied.

II. Backscatter communication

A. Asymbiotic Backscatter Communications

The two major variants of the asymbiotic backscatter technology are the mono-static and bi-static backscatter. In the mono-static backscatter, the Tx antenna and the receiver module are essentially the same device. Thus, the signal propagates from the Tx antenna and reflects back at the receiver module

from the sensor. Radio frequency identification (RFID) is an example of mono-static backscatter technology. The Tx antenna and the receiver module are located away from each other while operating in the bi-static backscatter mode of operation. The signal from the Tx antenna is forwarded to the receiver terminal after reflection from the sensor. A major drawback of an asymbiotic backscatter system is the need to generate a dedicated signal.

B. Symbiotic (Ambient) Backscatter Communications

Ambient backscatter communication is a symbiotic wireless communication technique where the signals from ambient RF sources are conveyed forward by BDs, without needing active RF components. Generally, the frequency of operation of the backscatter signal is the same as that of the incoming signal source and utilises the same spectrum [7]. However, it is stated in [3] that frequency of the backscatter signal can be shifted to the adjacent non-overlapping frequency band for robust decoding. AmBC promises to provide high spectral and energy efficiency [7]. There are numerous sources of ambient RF signals such as television broadcasts, WLAN signals and cellular signals. Furthermore, as no external power source is utilised, AmBC is a green technology having a very low environmental footprint.

The schematic diagram of the bi-static backscatter system is illustrated in Fig. 1. AmBC has several advantages over the traditional BC system. The backscatter signal has much lower amplitude compared with the legacy system's signal i.e., the direct path. The receiver decodes the backscatter signal that impinges at the receiver antenna together with the legacy systems' direct path signal. The receiver design for these systems is challenging. In particular, if the direct path is not suppressed in the analog domain before the automatic gain control (AGC) unit and the analog-to-digital converter (ADC) the numerical values of the digital signal are dominated by the legacy system signal, and the backscatter signal is pushed toward the least significant bits. For example, if the receiver effectively has 12-bits of resolution (here, one may include the number of AGC gain steps into the resolution), the AGC loop would adjust its gain so that the largest amplitude is quantized into the approximately 10^{th} bit, and the average signal approximately into the 6^{th} bit. As a consequence, when the amplitude difference between these two signals exceeds $30\,\mathrm{dB}$, the backscatter signal would be only be represented in the least significant bit of the ADC output. Such a low SNR operation easily reaches the SNR wall of the signal detection [8], which makes digital signal processing techniques ineffective. Therefore, studying direct path interference requirements for backscattering receivers is a fundamental problem and must be addressed for each deployment.

The dynamic range of the system is defined by the difference in the signal strength of the strongest (legacy) and the weakest (backscatter) signal. In order to improve the range and/or data rate of the backscatter system, the receiver must be able to handle the large difference between these two signals. The easiest solution is to increase the receiver resolution, which is costly for high-speed systems. The other solutions include analog domain suppression techniques, which requires to exploit certain differences between these two signals. In case of shifting the signal to another band by the BD [3], analog filtering can be used. Whereas, for a receiver with multiple antennas, directional difference can be used [9]. Finally, if two systems are able to work on differently polarized signals, their polarization differences can be used for suppressing the legacy system signal [10]. Regardless of the adopted technique, the power difference of these signals should be investigated for deployment before selecting the suppression technique.

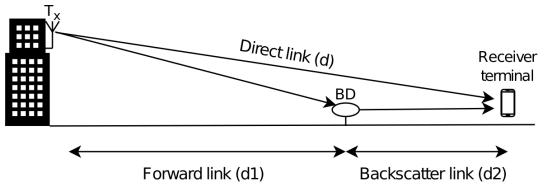

Fig. 1. Schematic diagram of the propagation environment.

III. Propagation models

A. 3GPP - Urban microcellular model

The 3GPP has developed a propagation model operating at different frequencies in an urban microcellular environment [11]. This model is valid for the scenarios where the Tx antennas are mounted below the rooftops ($10\,\mathrm{m}$ to $15\,\mathrm{m}$) of surrounding buildings. The basic path loss in line of sight (LOS) and non-LOS (NLOS) condition is computed by using eq. 1 and eq. 2, respectively.

$$L_{\mathrm{LOS}}(\mathrm{dB}) = 32.4 + 20 \cdot \log_{10}(f_{\mathrm{GHz}}) + 21 \cdot \log_{10}(d_{\mathrm{3D}}), \quad (1)$$

$$L_{\mathrm{NLOS}}(\mathrm{dB}) = 32.4 + 20 \cdot \log_{10}(f_{\mathrm{GHz}}) + 31.9 \cdot \log_{10}(d_{\mathrm{3D}}). \quad (2)$$

where the term d_{3D} is expressed in meters and represents the direct path followed by the signal (to the BD). The frequency of the signal is expressed in GHz, and subsequently, the LOS probability is calculated using eq. 3,

$$P_{\mathrm{LOS}} = \begin{cases} 1, & d_{\mathrm{2D}} \leq 18m \\ \dfrac{18}{d_{\mathrm{2D}}} + \left(-\dfrac{d_{\mathrm{2D}}}{36}\right)\left(1 - \dfrac{18}{d_{\mathrm{2D}}}\right), & 18m < d_{\mathrm{2D}} \end{cases} \quad (3)$$

where the term d_{2D} represents the distance between the T_{x} antenna and the BD in meters. Therefore, d_{2D} is the base of the triangle formed by the antenna, the ground and the sensor. The term d_{3D} represents the hypotenuse of this triangle. The total loss in the forward link (L_{d1}) is computed using eq. 4,

$$L_{\mathrm{d1}} = P_{\mathrm{LOS}} \times L_{\mathrm{LOS}} + (1 - P_{\mathrm{LOS}}) \times L_{\mathrm{NLOS}}, \quad (4)$$

B. ITU - Device to device (D2D) model

International telecommunication union (ITU) specifies a model for communication between two devices located in an urban microcellular street canyon environment [12]. The model calculates the basic transmission loss while taking into account the location variability statistics for the LOS and

the NLOS regions [12]. The calculation of the LOS basic transmission loss is performed by using eq. 5,

$$L_{\text{LOS}}(d) = 32.45 + 20 \cdot \log_{10}(f_{\text{MHz}}) + 20 \cdot \log_{10}(d_{\text{3D}}), \quad (5)$$

where f_{MHz} is the frequency expressed in MHz and the distance (d_{3D}) is expressed in meters. Subsequently, the LOS location correction is computed for the required location percentage (p) by using eq. 6,

$$\Delta L_{\text{LOS}}(p) = 1.5624\sigma(\sqrt{-2 \cdot ln(1-p/100)} - 1.1774). \quad (6)$$

Subsequently, the LOS location correction ($\Delta L_{\text{LOS}}(p)$) is added to the median value of the LOS basic transmission loss ($L_{\text{LOS}}(d)$) using eq. 7,

$$L_{\text{LOS}}(d,p) = L_{\text{LOS}}(d) + \Delta L_{\text{LOS}}(p). \quad (7)$$

The NLOS basic transmission loss is computed using eq. 8, where the frequency is expressed in MHz and the distance in meters. The value of L_{urban} is $6.8\,\text{dB}$ and is indicative of the type of urban environment [12]. The NLOS location correction is computed for the required location percentage using eq. 9,

$$L_{\text{NLOS}}(d) = 9.5 + 45 \cdot \log_{10}(f_{\text{MHz}}) + 40 \cdot \log_{10}(d_{\text{3D}}) + L_{\text{urban}}, \quad (8)$$

$$\Delta L_{\text{NLOS}}(p) = \sigma \cdot N^{-1}(\frac{p}{100}), \quad (9)$$

where $N^{-1}(.)$ is the inverse normal cumulative distribution function. Subsequently, the NLOS location correction (ΔL_{NLOS}) is added to the median value of the NLOS basic transmission loss $L_{\text{NLOS}}(d)$ to obtain the total NLOS loss using eq. 10,

$$L_{\text{NLOS}}(d,p) = L_{\text{NLOS}}(d) + \Delta L_{\text{NLOS}}(p). \quad (10)$$

Furthermore, the corner distance, d_{LOS} is calculated as a function of the location percentage p and is calculated using eq. 11,

$$d_{\text{LOS}}(p) = \begin{cases} 212 \cdot [\log_{10}(\frac{p}{100})]^2 - 64 \cdot \log_{10}(\frac{p}{100}), & p < 45 \\ 79.2 - 70 \cdot (\frac{p}{100}), & 45 \leq p \end{cases} \quad (11)$$

Finally, the total loss in the backscatter link (L_{d2}) is computed utilising the criteria stated in eq. 12, taking into account the loss in the LOS and NLOS regions,

$$L_{\text{d2}} = \begin{cases} L_{\text{LOS}}(d,p), & d < d_{\text{LOS}} \\ L_{\text{NLOS}}(d,p), & d > d_{\text{LOS}} \end{cases} \quad (12)$$

IV. Simulation setup and parameters

A schematic diagram of the propagation environment is shown in Fig. 1. The propagation for bi-static AmBC is a combination of two links. The first link ($d1$, forward link) is the connection between the T_{x} antenna and the sensor. The second link ($d1$, backscatter link) is the connection between the sensor and the receiver equipment. In this work, the definition of the forward link is provided by 3GPP and the backscatter link for communication between two devices is defined by the ITU. The simulations are performed in an environment depicting an urban street canyon. The transmit power ($P_{T_{\text{x}}}$) of the T_{x} antenna in such an environment is $2\,\text{W}$ i.e., $33\,\text{dBm}$. Typical cellular frequencies operating at less than $1\,\text{GHz}$ are utilised for the simulations. The received power level is calculated using eq. 13.

TABLE I
Simulation parameters.

Parameters	Unit	Value
Frequency	MHz	200/500/700/900
T_{x} power	dBm	33
T_{x} antenna height	m	15
T_{x} antenna gain	dBi	10
BD antenna gain	dBi	0
Slow fading margin	dB	15.2
Fast fading margin	dB	16
Polarization mismatch loss	dB	3
Modulation loss	dB	6
L_{urban}	dB	6.8
Location percentage	%	50

$$RX_{\text{level}}(\text{dBm}) = P_{\text{tx}} + G_{\text{t}} - (L_{\text{d1}} + L_{\text{d2}} + L_{\text{add}}), \quad (13)$$

where L_{d1} and L_{d2} is the basic transmission loss in the forward and the backscatter link, respectively. G_{t} represents the gain of the T_{x} antenna. The additional losses (L_{add}) in the communication link is contributed by the slow fading (L_{SF}), fast fading (L_{FF}), polarization mismatch (L_{PM}) and modulation loss (L_{ML}) and is calculated using eq. 14,

$$L_{\text{add}} = L_{\text{SF}} + L_{\text{FF}} + L_{\text{PM}} + L_{\text{ML}} \quad (14)$$

The reference values of the aforementioned losses and margins are obtained from [6] where a complete link budget is provided for backscatter systems. The values of these parameters are summarised in Table I, and are used for the simulation work of this paper.

V. Results and Analysis

Fig. 2(a-d) shows the received signal level at the receiver i.e., reader, for different combinations of the forward and the backscatter link distances at four different sub-GHz frequencies. The target is to determine the feasibility of the received power with respect to the receivers' sensitivity of typical IoT technologies such as the LoRa backscatter and NB-IoT. It is reported at references [13], [14] that the LoRa backscatter and NB-IoT have a receiver sensitivity of $-149\,\text{dBm}$ and $-141\,\text{dBm}$, respectively. Therefore, in the rest of our analysis these threshold values are used as a reference for coverage.

It can be seen in Fig. 2(a), that considering LoRa backscatter technology at $200\,\text{MHz}$ there is good coverage at considered distances in the forward and backscatter link. It was found that considering the LoRa receiver sensitivity level the reader should be able to hear the signal at $150\,\text{m}$ for the forward link and $60\,\text{m}$ for the backscatter link. Whereas, for NB-IoT, the coverage area is reduced to $115\,\text{m}$ and $60\,\text{m}$ for the forward and backscatter link, respectively. In other words the coverage

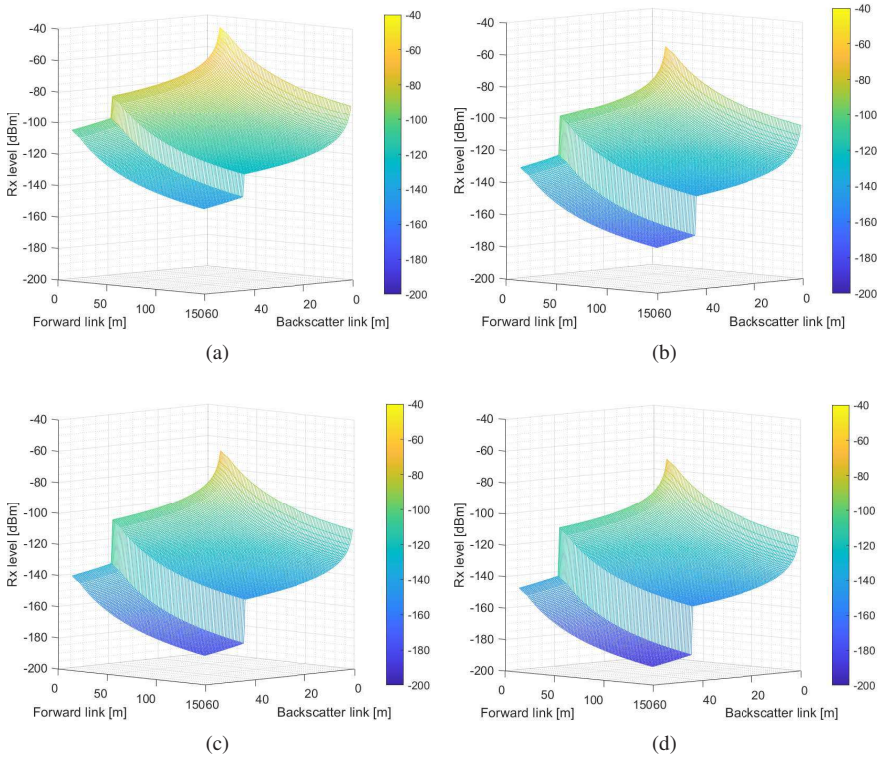

Fig. 2. Received power level at the receiver at, (a) 200 MHz, (b) 500 MHz, (c) 700 MHz, and (d) 900 MHz.

in the forward link can be extended to 150 m for backscatter link upto 45 m. It is observed from Fig. 2 that the signal strengths at the receiver decreases sharply when the receiver terminal is moved from the LOS to the NLOS region at all frequencies.

For higher frequencies i.e., for 500 MHz and 700 MHz, it can be observed in Fig. 2(b-c) that there is coverage in the LOS region when LoRa technology is considered. However, the coverage in the NLOS region is limited to short distances only. The maximum achievable distance is 62 m (forward link) and 44 m (backscatter link) at 500 MHz. At 700 MHz, the maximum achievable range in the NLOS region is 30 m in the forward link when the backscatter link is 60 m. Similarly, for NB-IoT technology, the maximum range of communication in the NLOS region at 500 MHz is 42 m (forward link) and 44 m (backscatter link), and at 700 MHz, the maximum range of communication in the NLOS range is 17 m in the forward link and 60 m in the backscatter link. From Fig. 2(d), it is clearly evident that the 900 MHz band is only feasible for short range communication and is unsuitable for long range IoT networks. These results shows the potential of using 200 MHz for IoT type of services, and signifies the importance of 200 MHz band for future smart city deployment, as long range coverage is a bottle neck even for technologies with very good receiver sensitivity level i.e., the LoRa backscatter and NB-IoT.

Fig. 3 shows the dynamic range of the bistatic backscatter system for four different considered frequencies. It can be observed from Fig. 3(a), that at the frequency of 200 MHz, the dynamic range of the signal varies between 14 dB and 47 dB in the LOS region. Whereas the dynamic range has values from 61.5 dB to 74 dB in the NLOS region. It is important to here re-call that in most of the practical AmBC systems the required dynamic range is below 30 dB as mentioned in the Section II-B, therefore the target is to achieve the dynamic range below the aforementioned threshold for correctly decoding the bits. By analyzing the results presented in Fig. 2(a) and Fig. 3(a) collectively, it can be said that at 200 MHz for IoT technologies like the LoRa backscatter and NB-IoT the limiting factor is not the coverage rather it is the dynamic range, and therefore interference suppression techniques mentioned in the Section II-B or any other means should be utilised to suppress the direct path. It is also revealed in Fig. 3(a-d) that the value of dynamic range increases with the increase in the frequency of operation, as in Fig. 3(b) the dynamic range has values between 22 dB and 55 dB in the LOS region, and similarly for other higher frequencies higher values of dynamic range were found.

VI. Conclusion

In this paper, we studied the coverage aspects of the bistatic BC mode at four targeted frequencies at sub-1GHz band in an urban microcellular environment through simulations. The received signal levels at the receiver were computed for different combinations of forward link and backscatter link distances, and it was found that at 200 MHz considering the LoRa receiver sensitivity level the reader should be able to

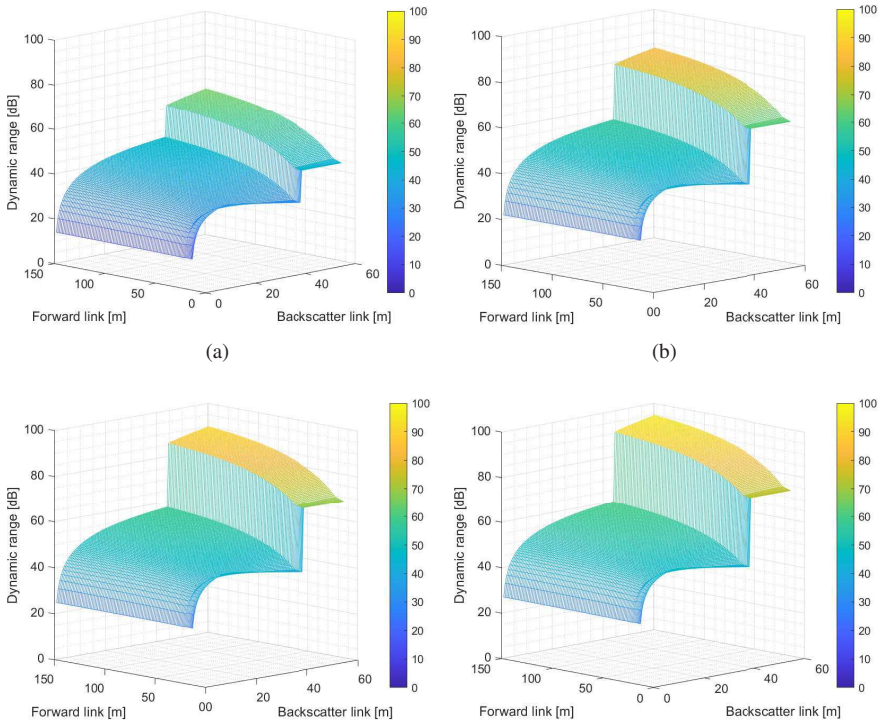

Fig. 3. Dynamic range at, (a) 200 MHz, (b) 500 MHz, (c) 700 MHz, and (d) 900 MHz.

hear the signal at $150\,\mathrm{m}$ for the forward link and $60\,\mathrm{m}$ for the backscatter link. Whereas, for NB-IoT signal technology, the coverage area shrinks to $115\,\mathrm{m}$ for the forward link and $60\,\mathrm{m}$ for the backscatter link. Even at 500 MHz it was hard to find long range coverage for both LoRa and NB-IoT in NLOS region. More interestingly, it was found that the limiting factor is not the coverage rather it is the dynamic range, as at 200 MHz frequency of operation for the considered distances the dynamic range of the signal varied between $14\,\mathrm{dB}$ and $47\,\mathrm{dB}$ in the LOS region, and in NLOS the value of dynamic range is even higher. These results signifies the importance of direct path interference suppression techniques, only migrating to a lower frequency band will not help in extending the coverage of the backscatter communication system unless the direct path interference is not properly mitigated.

References

[1] A. Al-Fuqaha, M. Guizani, M. Mohammadi, M. Aledhari, and M. Ayyash, "Internet of things: A survey on enabling technologies, protocols, and applications," *IEEE Communications Surveys Tutorials*, vol. 17, no. 4, pp. 2347–2376, 2015.

[2] W. Ayoub, A. E. Samhat, F. Nouvel, M. Mroue, and J. Prévotet, "Internet of mobile things: Overview of lorawan, dash7, and nb-iot in lpwans standards and supported mobility," *IEEE Communications Surveys Tutorials*, vol. 21, no. 2, pp. 1561–1581, 2019.

[3] N. Van Huynh, D. T. Hoang, X. Lu, D. Niyato, P. Wang, and D. I. Kim, "Ambient backscatter communications: A contemporary survey," *IEEE Communications Surveys Tutorials*, vol. 20, no. 4, pp. 2889–2922, 2018.

[4] V. Liu, A. Parks, V. Talla, S. Gollakota, D. Wetherall, and J. R. Smith, "Ambient backscatter: Wireless communication out of thin air," *SIGCOMM Comput. Commun. Rev.*, vol. 43, no. 4, pp. 39–50, Aug. 2013. [Online]. Available: http://doi.acm.org/10.1145/2534169.2486015

[5] M. U. Sheikh, R. Duan, and R. Jantti, "Validation of backscatter link budget simulations with measurements at 915 mhz and 2.4 ghz," in *2019 IEEE 89th Vehicular Technology Conference (VTC2019-Spring)*, 2019.

[6] J. D. Griffin and G. D. Durgin, "Complete link budgets for backscatter-radio and rfid systems," *IEEE Antennas and Propagation Magazine*, vol. 51, no. 2, pp. 11–25, April 2009.

[7] H. Guo, Y. Liang, R. Long, and Q. Zhang, "Cooperative ambient backscatter system: A symbiotic radio paradigm for passive iot," *IEEE Wireless Communications Letters*, vol. 8, no. 4, pp. 1191–1194, 2019.

[8] R. Tandra and A. Sahai, "Snr walls for signal detection," *IEEE Journal of Selected Topics in Signal Processing*, vol. 2, no. 1, pp. 4–17, 2008.

[9] R. Duan, E. Menta, H. Yigitler, R. Jantti, and Z. Han, "Hybrid beamformer design for high dynamic range ambient backscatter receivers," in *2019 IEEE International Conference on Communications Workshops (ICC Workshops)*, 2019, pp. 1–6.

[10] J. Lietzén, A. Liljemark, R. Duan, R. Jäntti, and V. Viikari, "Polarization conversion-based ambient backscatter system," *IEEE Access*, vol. 8, pp. 216 793–216 804, 2020.

[11] 3GPP, "Study on channel model for frequencies from 0.5 to 100 ghz," 3rd Generation Partnership Project (3GPP), Technical Report (TR) 38.901, 12 2017, version 14.3.0.

[12] ITU-R, "Propagation data and prediction methods for the planning of short-range outdoor radio communication systems and radio local area networks in the frequency range 300 mhz to 100 ghz," International Telecommunication Union (ITU), Recommendation ITU-R P.1411-10, 08 2009.

[13] V. Talla, M. Hessar, B. Kellogg, A. Najafi, J. R. Smith, and S. Gollakota, "LoRa backscatter: Enabling the vision of ubiquitous connectivity," in *Ubicomp*, Boston, MA, Mar. 2017, pp. 243–258.

[14] R. Ratasuk, N. Mangalvedhe, Y. Zhang, M. Robert, and J. Koskinen, "Overview of narrowband iot in lte rel-13," in *2016 IEEE Conference on Standards for Communications and Networking (CSCN)*, 2016, pp. 1–7.

PUBLICATION VII

Interference Analysis of Bi-static Backscatter Communication System: Two Backscatter Devices

Ritayan Biswas, Muhammad Usman Sheikh, Hüseyin Yiğitler, Jukka Lempiäinen, and Riku Jäntti

In: *2021 IEEE International Conference on RFID Technology and Applications (RFID-TA).* 2021, pp. 85–88
DOI: 10.1109/RFID-TA53372.2021.9617234

Interference Analysis of Bi-static Backscatter Communication System: Two Backscatter Devices

Ritayan Biswas*, Muhammad Usman Sheikh†, Hüseyin Yiğitler†, Jukka Lempiäinen*, and Riku Jäntti†
*Faculty of Information Technology and Communication Sciences (ITC), Tampere University, 33720 Tampere, Finland
Email: {ritayan.biswas, jukka.lempiainen}@tuni.fi
†Department of Communications and Networking, Aalto University, 02150 Espoo, Finland.
Email: {muhammad.sheikh, huseyin.yigitler, riku.jantti}@aalto.fi

***Abstract*—Ambient backscatter communication (AmBC) systems utilize existing ambient radio frequency (RF) signals to establish an indirect communication link between a transmitter (TX) and a receiver (RX). Backscatter devices (BDs) modulate their useful information on the incoming ambient signal emitted by the TX, as such their range is usually a very short event when only one BD is considered. This paper aims to analyze the impact of the interference generated due to the presence of another BD in a bi-static backscatter communication system. It is observed from the simulation results that the received signal degradation is mostly due to the cross interference of the other BD, which can be mitigated using successive interference cancellation (SIC) techniques. The level of both cross interference and self interference is significant when the interfering BD is located close to the target BD or the receiver. Therefore, AmBC systems can support more than one BD in an environment as long as the BDs are placed more than a wavelength apart from each other and RX.**

***Index Terms*—Successive Interference Cancellation, Backscatter communications, AmBC, SINR**

I. Introduction

Ambient backscattering communications (AmBC) is a niche wireless communication paradigm where sensors utilise ambient RF signals to establish communication with other sensors and user equipment (UE). These RF signals may be generated from a variety of sources such as cellular, WLAN, television broadcast and FM broadcast signals to name a few. The AmBC technology is based on scattering of electromagnetic waves, where a RF signal is reflected towards a receiver/reader for decoding [1]. The AmBC systems do not require a dedicated RF signal for their operation, and they enable ultra low-power sensing and monitoring applications, and paves the way toward development of battery-free and wireless communication capable sensor nodes. Therefore, AmBC devices can be deployed in remote locations or in places where regular maintenance is not possible.

Over the past few years there has been growing interest on AmBC systems, and the research activities in this field have gathered a significant momentum. The authors in [2] were the first to study the AmBC technology in the year 2013. The researchers were able to achieve communication distances of $45.7\,\mathrm{cm}$ and $76.7\,\mathrm{cm}$ utilising ambient television broadcast signals in indoor and outdoor environments, respectively. WiFi-based AmBC developed and investigated by the authors in [3] by decoding the BD information using the variations in the channel state information (CSI) and received signal strength indicator (RSSI) [3].

AmBC systems have generally been considered for short range communications due to the interference experienced by such systems. A major cause of interference is due to the direct path signal of the TX toward the receiver module. This interfering signal is more predominant due to the lower intensity of the backscattered signal. In [4], the interference suppression requirements for the direct path signal are studied. The possible methods to suppress the direct path interference is also stated in the article for a single backscatter device (BD). However, when another BD is introduced in the operating environment of AmBC, the scattered received signal properties changes. In this article, we investigate the impact of a second BD (BD_2), on the signal quality of a target BD (BD_1).

In this work, ambient signals from cellular base stations (operating at the $200\,\mathrm{MHz}$ carrier frequency) are considered. The signal to noise ratio (SNR) of the signal of BD_1 is used as a baseline for the analysis. Thereafter, BD_2 is introduced into the environment and the signal to interference plus noise ratio (SINR) is calculated after computing the interference due to the different signal paths between TX, BD_1, BD_2 and RX. It is observed that the most significant interference is caused by the signal travelling directly to the RX after impinging on the BD_2. Although, this interference component can be mitigated by utilising the successive interference cancellation, the other interference paths are only predominant when the BD_2 is placed close to the BD_1 or RX. Therefore, the effect of the interference caused by these paths can be mitigated by placing the BD_2 at shortest a wavelength meter away from the BD_1 and RX.

II. Backscatter communication

In backscatter communications, a RF wave transmitted from a particular source is reflected from an object (or, sensor/tag), towards a receiver for decoding. The backscatter technology generally has two modes of operation, namely monostatic and bistatic backscatter. In monostatic backscatter, the TX and RX antenna are located at the same site. However, in bistatic backscatter systems, the TX and RX are spatially separated and the signal is propagated forward towards the RX after impinging on the sensor.

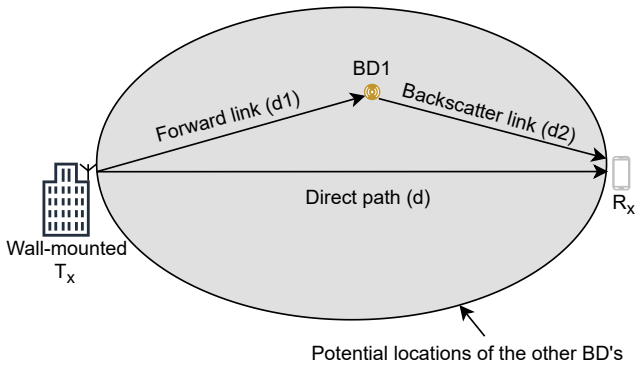

Fig. 1. Schematic diagram of the propagation environment.

A. Symbiotic Backscatter Communications

Ambient backscatter communications is a symbiotic backscatter communication technology. The AmBC system utilises ambient RF signals to establish communication without the necessity of active RF components. The communication system operates in the same spectrum as that of the transmitted signal [5]. However, the frequency of the backsacttered signal can be shifted to the adjacent non-overlapping frequency band to achieve better decoding at the receiver terminal [2]. Furthermore, AmBC systems aim to achieve better energy efficiency and also provide higher spectral efficiency [5].

The schematic diagram of the bi-static backscatter communication system in shown in Fig. 1. A major bottleneck of AmBC systems is the interference caused by the (legacy) signal following the direct path (d) between the TX and the RX. This is caused due to the the lower amplitude of the backscatter signal. Therefore, the design of the receiver for AmBC systems is challenging and the signal from the direct path needs to be suppressed in the analog domain before it reaches the automatic gain control unit (AGC) and the analog to digital converter (ADC). This needs to be done in order to avoid the backscattered signal from being shifted to the least significant bits [6].

The potential locations of the BD_2 is shown in Fig. 1. The presence of the BD_2 in the environment causes interference to the signal of interest at the RX. The interference causing signal can follow multiple paths after bouncing between the two BDs. However, the most significant interference is caused by the TX$\rightarrow$BD$_2\rightarrow$ RX signal path. However, by utilising a successive interference canceller (SIC) at the RX, the effect of this signal can be mitigated. SIC offers superior system efficiency and user fairness in comparison with orthogonal multiple access (OMA). The improvement provided by SIC is significant for non-orthogonally multiplexed users having different channel conditions [7].

III. Propagation models

A. 3GPP - Urban microcellular model

The propagation model developed by the 3GPP for urban microcellular environment [8] is utilised in calculating the propagation loss in the forward link ($d1$). This model is utilised to calculate the basic transmission loss in the link for LOS and NLOS regions. This propagation model is described in detail in [4].

B. ITU - Device to device (D2D) model

The international telecommunication union (ITU) developed a propagation model specifically for the communication between two devices located in an urban microcellular street canyon environment [9]. This model computes the basic transmission loss and also considers the location variability statistics for LOS and NLOS regions. This model is utilised to compute the backscatter link ($d2$). The detailed description of the model is provided in [4].

C. Multi-bounce phenomenon

Consider an ambient backscatter or symbiotic radio system, in which N backscatter tags share the spectrum with a downlink transmission from a base station. The backscatter devices uses non orthogonal multiple access (NOMA) to share the spectrum. The task of the receiver is to decode both the downlink transmission as well as the messages superimposed on it by the backscatter devices also known as tags.

We assume that both the base station and the receiver has a single antenna. The signal at the receiver antenna at time t can be written as

$$y[t] = \sum_{k=1}^{K} \tilde{h}_{d,k}\sqrt{P}x_0[t-\tau_{d,k}] \sum_{k=1}^{K} \tilde{h}_{r,k}\nu_k[t-\tau_{r,k}] + z[t] \quad (1)$$

where $x_0[t]$ denotes the signal transmitted by the base station, P is the transmit power, $z[t] \sim \mathcal{CN}(0,1)$ is the complex Gaussian received noise at time t, $\tilde{h}_{d,k}$ denotes the channel gain between the transmitter and $\tau_{d,k}$ is the associated propagation delay. Similarly receiver $\tilde{h}_{r,k}$ and $\tau_{r,k}$ denotes the channel gain between BD k ant the receiver and the delay between BD k and the receiver antenna, respectively. The signal scattered by the BD n at time t can be written as

$$\nu_n[t] = x_n[t]\left(\tilde{h}_{t,k}x_0[t-\tau_{t,k}] + \sum_{\substack{l=1 \\ l\neq n}}^{N} \tilde{g}_{nl}\nu_l[t-\tau_{nl}]\right) \quad (2)$$

where $x_k[t]$ denotes the symbol utilized by the BD device k at time t, $h_{t,k}$ is the channel gain from the transmitter to BD k and $\tau_{t,k}$ is the associated propagation delay, $\tilde{g}_{nl}$ denotes the channel gain between BD antenna l and k and τ_{nl} is the associated propagation delay.

Under the standard narrowband assumption that the BD and illumination signals would be constant over long period of time, we can rewrite the above in a vector form as

$$y = \sqrt{P}h_d x_0 + \boldsymbol{h}_r^H \boldsymbol{\nu} + z \quad (3)$$

$$\boldsymbol{\nu} = \boldsymbol{X}\left(\sqrt{P}\boldsymbol{h}_t x_0 + \boldsymbol{G}\boldsymbol{\nu}\right) \quad (4)$$

where h_d is the complex channel gain from transmitter to the receiver $\boldsymbol{X} = \mathsf{diag}\{x_n, n = 1, 2, \ldots, N\}$ is a diagonal matrix containing the BD symbols, $\boldsymbol{h}_t$ is the complex $N \times 1$ channel

TABLE I
SIMULATION PARAMETERS.

Parameters	Unit	Value
Frequency	MHz	200
TX power	dBm	33
TX antenna height	m	15
TX antenna gain	dBi	10
BD antenna gain	dBi	0
Slow fading margin	dB	15.2
Fast fading margin	dB	16
Polarization mismatch loss	dB	3
Modulation loss	dB	6

vector between the reader antennas and the BDs, $\boldsymbol{h}_r^T$ is the complex $1 \times N$ channel vector between BDs and the receiver, $\boldsymbol{G}$ is the $K \times N$ zero diagonal complex channel matrix between the BDs and z is the complex noise.

We assume that the receiver is not able to track the multi-bounce components and thus those components appear as channel uncertainty for the receiver. Thus we write

$$y = \sqrt{P}(h_d + \sum_{n=1}^{N} h_{r,n} h_{tn} x_k) x_0 + \sqrt{P}\boldsymbol{h}_r^T \boldsymbol{\varepsilon} + z \quad (5)$$

where

$$\boldsymbol{\varepsilon} = \boldsymbol{\nu} - \sqrt{P}\boldsymbol{X}\boldsymbol{h}_t x_0 \quad (6)$$

which can also be written as

$$\boldsymbol{\varepsilon} = \boldsymbol{X}\boldsymbol{G}\boldsymbol{\varepsilon} + \sqrt{P}\boldsymbol{X}\boldsymbol{G}\boldsymbol{X}\boldsymbol{h}_t x_0 \quad (7)$$

IV. SIMULATION SETUP AND PARAMETERS

A schematic diagram of the propagation environment is shown in Fig. 1. The TX antenna is wall-mounted on a building as in typical urban microcell deployments. The transmit power (or, P_{tx}) is $2\,\text{watts}$ or $33\,\text{dBm}$ and the carrier frequency is $200\,\text{MHz}$. The RX is located at a distance of about $150\,\text{m}$ or 100λ from the TX antenna. The BD_1 is the sensor of interest in this work and is located at a maximum distance of 10λ from the RX antenna. The thermal noise power (P_{n}) is $-133.97\,\text{dBm}$ and is computed utilising $10\,\text{kHz}$ bandwidth at room temperature ($290\,\text{K}$). The power level received at the RX (P_{rx}) is calculated using (8),

$$P_{\text{rx}}(\text{dBm}) = P_{\text{tx}} + G_{\text{t}} - (L_{\text{d1}} + L_{\text{d2}} + L_{\text{add}}), \quad (8)$$

where L_{d1} and L_{d2} are the basic transmission loss in the forward and the backscatter link, respectively. G_{t} represents the gain of the TX antenna. The additional losses (L_{add}) in the communication link is contributed by the slow fading (L_{SF}), fast fading (L_{FF}), polarization mismatch (L_{PM}) and modulation loss (L_{ML}), respectively. These values are obtained from [5] where a complete link budget is provided for backscatter systems and are summarized in Table I. L_{add} is calculated using (9),

$$L_{\text{add}} = L_{\text{SF}} + L_{\text{FF}} + L_{\text{PM}} + L_{\text{ML}}. \quad (9)$$

The signal to noise ratio (SNR) is computed the P_{rx} and P_{n} values. Subsequently, the second BD (or, BD_2) is introduced into the environment and placed in the shaded region represented in Fig. 1. The interference caused due to BD_2 can be due to different paths the signal travels and can be classified as self interference and cross interference. The three main interference causing signal paths can be identified as:

- TX $\rightarrow$ BD_2 $\rightarrow$ RX.
- TX $\rightarrow$ BD_2 $\rightarrow$ BD_1 $\rightarrow$ RX.
- TX $\rightarrow$ BD_1 $\rightarrow$ BD_2 $\rightarrow$ RX.

The first two paths contribute of the cross-interference and the third path causes self-interference to the received signal. The cross and self interference are calculated separately for the analysis. The total interference P_{i} caused due to the presence of the BD_2 is a sum of all these three paths. The SINR for any of the interference paths is computed utilising (10),

$$\text{SINR} = \frac{P_{\text{rx}}}{P_{\text{n}} + P_{\text{i}}}. \quad (10)$$

The signal can also follow a path where it ping-pongs between the two backscatter devices before reaching the RX. This also contributes to the total interference experienced at the RX. The ping-pong path can be represented by the path TX $\rightarrow$ BD_1 $\rightarrow$ BD_2 $\rightarrow$ BD_1 $\rightarrow$ RX. The interference caused by the signal following this path is also factored into the analysis.

V. RESULTS AND ANALYSIS

The SNR is calculated at the RX when only BD_1 is present in the simulation environment. It can be observed that the regions close to TX and RX antenna have better SNR values in comparison to other areas in the environment. Additionally, based on the applicable use cases it is required that the BD_1 and the RX are located relatively close to each other. Therefore, the location of the BD_1 was fixed at a maximum distance of 10λ or $15\,\text{m}$ from the RX. The SNR at this location was approximately observed to be $18.9\,\text{dB}$.

Subsequently, the BD_2 was introduced into the environment. As discussed in Section IV, the interference causing signal follows three different paths while travelling between the TX and the RX. The cross interference caused at the RX is due to the first two paths mentioned in Section IV. It was observed from Fig. 2 (a) that the SINR at the RX was less than $-10\,\text{dB}$. Similarly, it was also observed that the location very close to the transmitter also had a very low SINR. Therefore, due to the cross-interference, it was observed that when the BD_2 was located very close to the TX or RX, the signal strength is very poor. Therefore, in order to have proper communication, the BD_2 needs to be located away from the the TX/RX. However, the predominant cross-interference path TX $\rightarrow$ BD_2 $\rightarrow$ RX, can be suppressed by utilising SIC as stated in Section II-A. Fig. 2 (b) shows the SINR after SIC is performed. It was observed that after the SIC is considered, the cross-interference plays a role only when the BD_2 is located in the close proximity of BD_1.

The self-interference is caused by the signal path following TX $\rightarrow$ BD_1 $\rightarrow$ BD_2 $\rightarrow$ RX. It was observed that the SINR due

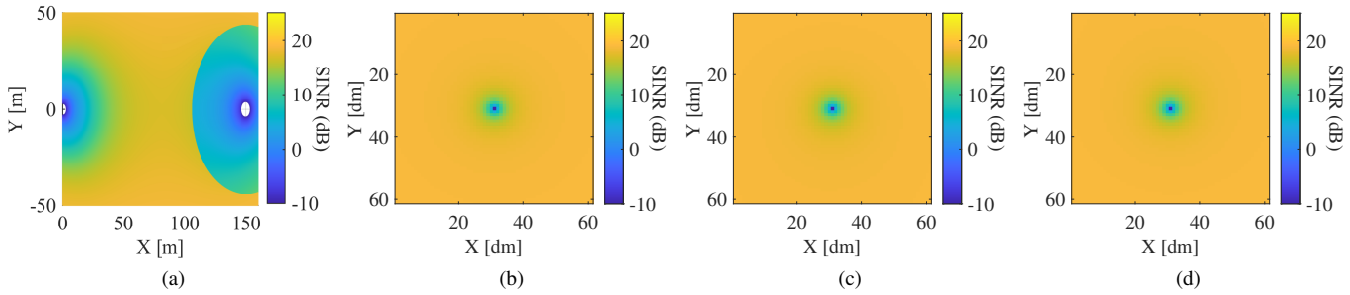

Fig. 2. Results for the variation of SINR with respect to the location of the BD_2 for different interference components. Fig. 2a illustrates the SINR for the total cross interference. In Fig. 2b, the SINR at BD_1 for the cross interference component after SIC is shown. Fig. 2c demonstrates the self interference component at BD_1. In Fig. 2d, the SINR for the self interference component at the RX is illustrated.

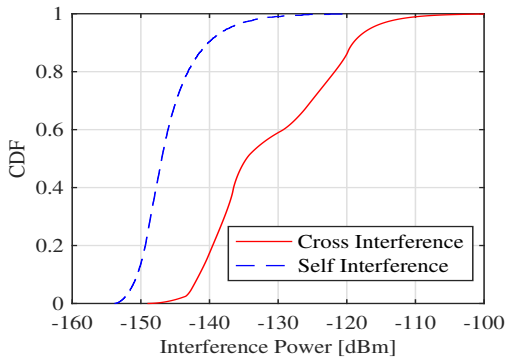

Fig. 3. Cumulative distribution function (CDF) of the cross and self interference power levels (in dBm) for the considered scenarios.

to the self interference was generally constant over the entire area except for the regions located in the close proximity of the BD_1/RX. It was observed from Fig. 2 (c-d) that the SINR due to the self interference only had a significant effect when the BD_2 is located very close to the BD_1/RX. Therefore, in order to have proper communication it is essential that the BD_2 is placed atleast 1λ meter away from the BD_1/RX.

The cumulative distribution function (CDF) of the interference power for the cross and self interference is illustrated in Fig. 3. The values for the cross interference power levels were computed over the entire area. The self interference power levels were computed only around the BD_1/RX. After computing both the interference power levels, it was clearly observed that the cross interference power levels were significantly stronger. Therefore, SIC is essential to mitigate the interference caused by the primary cross interference signal path.

VI. Conclusion

In this paper the interference caused due to the presence of a second BD in a bi-static backscatter environment was studied with the help of simulations. It was observed that the interference causing signal had three paths between the TX and the RX. The cross interference was primarily caused by the signal following the path TX$\rightarrow$BD$_2\rightarrow$ RX. However, by using SIC the impact of this interference could be mitigated. Consequently, it was observed that the cross interference caused by the path TX$\rightarrow$BD$_2\rightarrow$BD$_1\rightarrow$ RX is only predominant when the BD_2 is located close to the BD_1. Therefore, if the BD_2 is not located in the very close proximity of the BD_1 then the remaining cross interference could be mitigated. Furthermore, the self interference was caused by the path TX$\rightarrow$BD$_1\rightarrow$BD$_2\rightarrow$ RX. It was observed that the self interference was generally constant over the entire environment, but had an impact when the BD_2 was located close to the BD_1 or the RX. The impact of the self interference could be mitigated by placing the BD_2 about a wavelength meter away from the BD_1/RX. In conclusion, it can be stated that when a second BD is introduced into the network the effect of the self interference and the cross interference (after SIC) is negligible as long as the BD_2 is located one wavelength meter distance away from the BD_1 and the RX.

References

[1] H. Stockman, "Communication by means of reflected power," *Proceedings of the IRE*, vol. 36, no. 10, pp. 1196–1204, Oct 1948.

[2] V. Liu, A. Parks, V. Talla, S. Gollakota, D. Wetherall, and J. R. Smith, "Ambient backscatter: Wireless communication out of thin air," *SIGCOMM Comput. Commun. Rev.*, vol. 43, no. 4, pp. 39–50, Aug. 2013. [Online]. Available: http://doi.acm.org/10.1145/2534169.2486015

[3] B. Kellogg, A. Parks, S. Gollakota, J. R. Smith, and D. Wetherall, "Wi-fi backscatter: Internet connectivity for rf-powered devices," *SIGCOMM Comput. Commun. Rev.*, vol. 44, no. 4, pp. 607–618, Aug. 2014. [Online]. Available: http://doi.acm.org/10.1145/2740070.2626319

[4] R. Biswas, M. U. Sheikh, H. Yiğitler, J. Lempiäinen, and R. Jäntti, "Direct path interference suppression requirements for bistatic backscatter communication system," in *2021 IEEE 93rd Vehicular Technology Conference (VTC2021-Spring)*, 2021, pp. 1–5.

[5] J. D. Griffin and G. D. Durgin, "Complete link budgets for backscatter-radio and rfid systems," *IEEE Antennas and Propagation Magazine*, vol. 51, no. 2, pp. 11–25, April 2009.

[6] R. Tandra and A. Sahai, "Snr walls for signal detection," *IEEE Journal of Selected Topics in Signal Processing*, vol. 2, no. 1, pp. 4–17, 2008.

[7] K. HIGUCHI and A. BENJEBBOUR, "Non-orthogonal multiple access (noma) with successive interference cancellation for future radio access," *IEICE Transactions on Communications*, vol. E98.B, no. 3, pp. 403–414, 2015.

[8] 3GPP, "Study on channel model for frequencies from 0.5 to 100 ghz," 3rd Generation Partnership Project (3GPP), Technical Report (TR) 38.901, 12 2017, version 14.3.0.

[9] ITU-R, "Propagation data and prediction methods for the planning of short-range outdoor radio communication systems and radio local area networks in the frequency range 300 mhz to 100 ghz," International Telecommunication Union (ITU), Recommendation ITU-R P.1411-10, 08 2009.